Single molecule localisation microscopy by photoconversion and dynamic labelling using DNA-binding dyes resolves chromatin compaction in model ischemia

Dissertation

zur Erlangung des akademischen Grades

Doctor rerum naturalium (Dr. rer. nat)

im Fachbereich Biologie

eingereicht an der

Johannes-Gutenberg Universitat Mainz

Aleksander Szczurek

Geb. am 31. October 1989 in Krakau, Polen

Mainz, 20. December 2016,

Content

1. Abstract

Single molecule localisation microscopy (SMLM) is a method based on switching and subsequent nanometre-precision localisation of isolated fluorophore signals for super-resolution fluorescence microscopy. Thus far, this method has been successfully applied to imaging of various cellular structures including e.g. cytoskeleton, mitochondria, neuronal axons and many others, revealing manifold previously unknown cellulardetails. Strikingly, SMLM was applied to the DNA study only to a minor degree. Whereas a higher order DNA (chromatin) organisation in the cell nucleus still remainspuzzling, previous studies using SMLM focusedrather on imaging of isolated DNA molecules in vitro.

In this work novel solutions for super-resolution DNA imaging in eukaryotic cell nuclei were developed utilising SMLM principles. First approach relies on UV-induced photoconversion of DNA-binding Hoechst and DAPI dyes. By applying low intensity near-UV light a stochastic photoconversion of DNA-bound dyes occurs and single molecule signals can be discriminated based on spectral properties. Second approach utilises a previously developed dynamic DNA labelling (Binding Activated Localisation Microscopy) with directly binding dyes that upon transient association with the DNA become fluorescent. In turn, while dynamically dissociated are non-fluorescent. In this study different aspects of DNA chemistry andDNA-binding werestudied to enhance understanding of BALM mechanism and to facilitate applicationextensionto the nuclei of mammals and rodents. Both methods led to 3 – 5 fold improvement in resolution as compared to a conventional fluorescence imaging.

Chromatin, a complex of DNA and proteins, is known to directly respond and adapt to changes in environmental conditions just as temperature, ionic strength and many others. Currently among diseases involving such environmental balance disruptions, ischemia, a blood insufficiency,is1st(cardiovascular disease) and 2nd(stroke) cause of death worldwide according to the World Health Organisation.Knowing that epigenetic landscape in ischemia undergoes a massive remodelling e.g. involving a general deacetylation of chromatin, we anticipated that chromatin structure undergoes a change. We tested this hypothesis using aforementioned superresolution microscopy methodology. This approach revealed previously unknown chromatin condensation towards a nuclear periphery. In support we found that ischemic chromatin bore a decreased DNase Idigestion susceptibility and decreased linker histone H1dynamics. We hypothesise that thesource of chromatin condensation are polyamines and divalent cations otherwise complexed with ATP. Upon ATP depletion in ischemia they would relocate to the cell nucleus and bind to negatively charged DNA inducing its compaction.

The results presented in this dissertation have an impact on better understanding and interpretation of previous studies on ischemiaand may help to design a future therapy based on a novel aspect. The super-resolution methodologymay prove useful for studying effects of other environmental factorse.g. oxidative stress or to investigate chromatin texture in cancerous cells to assess their malignancy.

2. Zusammenfassung

Single Molecule Localization Mikroskopie (SMLM) basiert auf der Methode einzelne Fluorophore an- und auszuschalten und sie so nanometergenau zu lokalisieren. Diese Methode wurde bereits zur Untersuchung verschiedener biologischer Strukturen, wie z.B. dem Zytoskelett, Mitochondrien und neuronaler Axone verwendet und deckte bisher unbekannte molekulare Details auf. Obwohl die Organisation der DNA im Zellkern uns nach wie vor Rätsel aufgibt, wurde die DNA mittels SMLM nur wenig untersucht – überwiegend wurden isolierte DNA-Moleküle *in vitro* analysiert, nachdem sie mit DNA-bindenden Farbstoffen versetzt wurden.

In der vorliegenden Arbeit wurden SMLM-Prinzipien angewendet, um neue Ansätze für hochauflösende Aufnahmen der DNA in eukaryotischen Zellkernen zu erarbeiten. In dieser Studie wurden zwei Ansätze verfolgt, die auf verschiedenen physikalischen Prinzipien beruhen. Der erste Ansatz basiert auf UV-induzierter Photokonversion der DNA-Farbstoffe Hoechst und DAPI, die beide an die kleine Furche der DNA binden. Bestrahlt man die gefärbte DNA mit Licht von geringer Intensität nahe dem UV-Spektrum, findet eine stochastische Photokonvertierung des gebundendenen Farbstoffs statt und Signale einzelner Moleküle können mittels ihrer speziellen spektralen Eigenschaften unterschieden werden. Der zweite Ansatz macht sich eine bereits entwickelte Technik zu Nutze, bei der dynamisch bindende DNA-Farbstoffe verwendet werden, die nur im vorübergehenden gebundenen Zustand fluoreszieren. Diese Methode wird bindungsaktivierte Lokalisationsmikroskopie (BALM) genannt und wurde bisher noch nicht in eukaryotischen Zellkernen angewendet. In der vorliegenden Arbeit wurden verschiedene Aspekte der DNA-Chemie und Bindungsverhalten untersucht, um die zu Grunde liegenden Mechanismen von BALM aufzuklären und eine erweiterte Anwedung von BALM auf Strukturen des Chromatin im Zellkern zu vereinfachen. Beide Ansätze bewirkten eine verbesserte Auflösung in der Größenordnung 3 – 5, verglichen mit konventioneller Fluoreszenzmikroskopie der DNA.

Das Chromatin ist ein Komplex bestehend aus DNA und Proteinen und ist in der Lage, direkt auf Veränderungen der Umwelt reagiert, wie z.B. die Temperatur oder den Salzgehalt und sich den veränderten Bedingungen anpassen kann. Eine Ischämie bewirkt durch mangelnde Blutversorgung eine Änderung des Milieus und ist laut der Weltgesundheitsorganisation Todesursache Nummer eins und zwei und verantwortlich für 30% aller Todefälle weltweit.

Es wurde gezeigt, dass sich die epigenetische Landkarte während einer Ischämie massiv verändert und u.a. zu einer generellen Deacetylierung des Chromatins führt. Demnach ist es naheliegend anzunehmen, dass sich auch die Struktur des Chromatins unter diesen Umständen verändert. Um die Struktur der DNA während einer Ischämie in kultivierten Zellen näher zu untersuchen, wurde eine Methode zur Hochauflösungsmikroskopie entwickelt. Dieser Mikroskopieansatz zeigte eine bisher noch nicht beschriebene Kondensation des Chromatins an der nukleären Peripherie. Ein verminderter Verdau durch das Enzym DNase I und die Abnahme der Mobilität des Verbindungshistons H1 unterstützten diese Beobachtung. Wir stellten die Hypothese auf, dass der Grund für die Kondensierung des Chromatins Polyamine sind. Diese zweifach geladene Kationen sind unter normalen Umständen and ATP gebunden. Wird ATP nun während der Ischämie abgebaut, werden die freien Polyamine von der negativ geladenen DNA im Zellkern angezogen und ihre Bindung induziert das Verklumpen der DNA.

Die Ergebnisse dieser Arbeit tragen zum besseren Verständnis und zur Interpretation vorangehender molekularer Studien über Ischämie bei und basierend auf den beschriebenen

Konsequenzen können neuartige Therapien entwickelt werden. Die Methode der Hochauflösungsmikroskopie für DNA-Farbstoffe kann weiterhin verwendet werden, um den Effekt anderer Umweltfaktoren, ähnlich dem oxidativen Stress, zu analysieren oder die Struktur des Chromatins in Krebszellen zu untersuchen, um ihre Malignität zu bestimmen.

3. Introduction

In order to introduce a reader to the subject of chromatin super-resolution microscopy the introduction has been conceived as follows. First, a physicochemical concept of fluorescence is introduced. In the next step a reader is guided through the basics of conventional fluorescence microscopy andits resolution constraints. This is accompanied by single fluorescentobject localisation in space. Subsequently, reader is acquainted with photochemistry of single fluorophore switching between its non- and fluorescent states and the utility of this approach for achieving enhanced resolution. In the next steps, physical properties of DNA-binding fluorescent dyes of various binding modes are described together with their contemporary applications to super-resolution microscopy. As these molecules will be utilised to study chromatin throughout this work, in the following section an available knowledge on DNA and chromatin arrangement on various organisational levels is reviewed. This includes "beads-on-string" model, topologically associated chromatin domains and chromosome territories. Finally, an epigenetic background on chromatin biology in ischemic disease is highlighted with a particular emphasis on myocardial infarction as a main subject of the study.

3.1 Fluorescence emissionas a consequence of transition between electronic states

Fluorescent molecules (also termed fluorophores) that will be a subject to the discussion in this section bear typically aromatic structure ample with conjugated planar,linear,orring system of double covalent bonds between carbon atoms (2valence electrons per bond). Here, I introduce the basic principles underlying light absorption and fluorescence emission.

The electron (e^-) has a mass of 1/1836 of a mass of a proton and its position within chemical molecule cannot be estimated with an infinite precision(Heisenberg, 1927). As a solution to this issue a mathematical function has been proposed to approximate probability to find an electron in any specific location around the atom nucleus. This function is often termed as a molecular orbital, and as will become clear in few moments, describes features crucial for a description ofa chemical bond formation and an assembly of a fluorescent molecule.

In aromatic, conjugated systems such as fluorophores, one electron pair forms relatively strongσ-bond between carbon atoms (see benzene as an example, **Fig. 1B**). Creation of a secondanda third bond (e.g. π-bond) is also possible, but proceeds differently from the first one as each electron in the atom is described by a different molecular orbital and resides in a different quantum state. This complexity results invaryingproperties of electron pair involved in π-bond formation leading to so-called electron delocalisation. In conjugated systems just as fluorescent molecules, this electron delocalisation results ina formation of a common electronic cloud above and below the aromatic plane (**Fig. 1B**). This electronic conjunctionconstitutes basis for light absorption as delocalised electrons may absorb light of lower energy, equal to energy difference between highest occupied molecular orbital (HOMO) and lowest unoccupied molecular orbital (LUMO).This energy difference is smaller for delocalised electrons within π–bonds than for electrons in σ-bonds, and therefore visible light is of sufficient energy to induce this transition. Consequently, light absorption constitutes an inherent capability of conjugated atomic systems as fluorophores(Sauer et al., 2011).

In order to quantitatively describe the ability of a fluorescent molecule to absorb light extinction coefficient ε has been introduced. According to the Beer-Lamberts law,absorbance A can be expressed by the following simple equation:

$$A = \varepsilon cl$$

where *c* corresponds to the concentration of a fluorescent probe and *l* stands for light path'slength through the solution of the substance under investigation. Knowing the latter two, one is able to measure the absorbance and consequently further estimate the extinction coefficient of any substance. In biological research fluorescent compounds of higher extinction coefficient are desireddue to their ability to provide higher photon output as a result of an increased absorbtivity,altogether leading to a betterdetection sensitivity.

Once a fluorophore molecule underwent an excitation it bears higher energy that is stored in its electronic state. Thereafter, an internal conversion occurs (transitions from excited vibrational singlet states S_n (for $n > 1$) to lowest exited singlet state S_1) with a coincident heat dissipation. As a result of this process the electronic state loses a part of the energy that was originally absorbed and consequently fluorescent photon emitted will have a lower energy; therefore, emission wavelengths are longerthan the absorbed exciting wavelengths.

The fluorescence is not a sole mechanism of de-excitation to the ground state S_0 and many other processes should be taken into account. Among them are: solvent relaxation slightly decreasing the energy of S_1 state and dynamic (collisions) as well as static quenching via excited state interaction with other compounds present in the environment. These effects on fluorescent properties is easily measurable as it directly influences the energy gap between the excited S_1 state and a ground S^0 state what is commonly reflected in the alteration to the fluorescence emission spectrum (Lakowicz, 2006; Sauer et al., 2011).

Consequently, in order to investigate effects of other de-excitation processes another quantitative measure has been introduced tocharacterise quantitatively fluorophore ability to fluoresce. This normalised measure is termedas quantum yield and is equal to how many times a photon emission may occur per single absorption event. Anotherwords, it tells how susceptible a fluorophore in excited state is to other de-excitation processes than fluorescence. Among most pronounced ones are aforementioned quenching, solvent relaxation, or fluorescence resonance energy transfer (FRET). The design of novel fluorescent probes thus aims at elevating the quantum yield at a value near1.0.

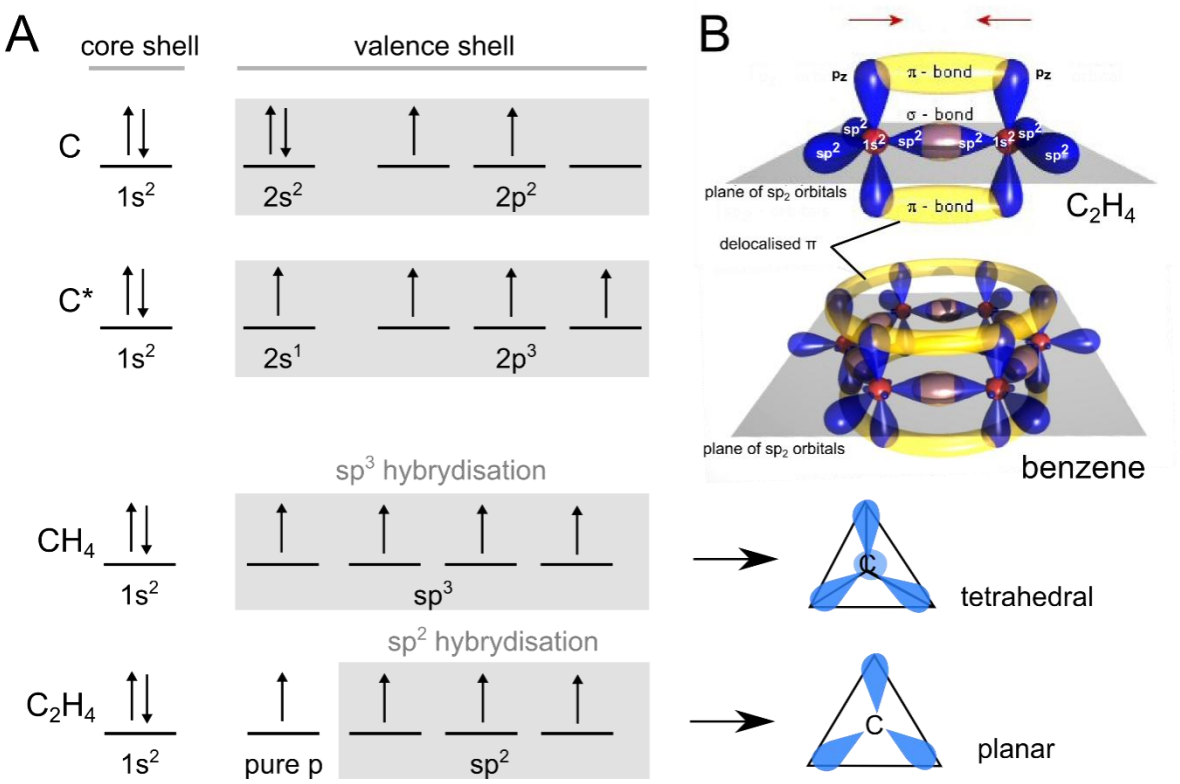

Figure 1.Hybridisation of molecular orbitals in a carbon atom and chemical bond formation in fluorescent probes.A) An example for an electron configuration of carbon in its ground state (C) and in its excited state (C*) where 4 e^- reside in a valence shell (each arrow represents 1 electron). Carbon excitation is promoted as it enables formation of more bonds leading to a decrease in total energy of the system.In the excited statean electronoriginating from 2s level underwent transient to 2p level giving a rise to 4 unpaired electrons constituting grounds for bond formation in methane (CH_4). Here, hybridisation results in formation of a tetrahedric sp^3 configuration. In turn, for ethene (CH_2=CH_2) hybridisation of a carbon atom proceeds differently, i.e. is valid only for one e^- from 2s level and for two e^- from 2p level that together contribute to $2p^2$ configuration. As a result anelectron distribution in space becomes planar and a single σ bond involving 2 e^- may be generatedbetween two carbon atoms in ethene (**B**, top image). The rest of $2p^2$ orbitals forms sigma bonds with hydrogen atoms (for clarity not shown). A remaining third e^- from $2p_z$ level (intact orbital) constitutes basis for a π bond located above and below the shortest distance spacing both carbon nuclei in ethene. In case of aromatic benzene ring (**B**, bottom image), due to sp^2 hybridisation and generation of 6 π-bonds, a delocalised cloud of electrons above and below a ring-plane is brought about (yellow). Such conjugated electronic configuration is typical for fluorescent molecules and is responsible for their ability to absorb exciting light. Pictures in (B) adapted from *www.iapp.de*

3.2 Fluorescence microscopy, diffraction limit, and resolution

This type of a light microscopy commonly used in cell biology takes advantage of fluorescence properties of an object, namely the light emission from the sample instead of using light reflection or absorption to study sample's structural features. Fluorescence microscopy is superior in terms of a contrast and specificity of labelling as compared to e.g. transmitted light or differential contrast microscopy, although several implementations have to be done in order to exploit it at its best.

Typically, all fluorescence microscopes are equipped with 3 crucial components. First among them is a special light source, e.g. a mercury lamp emitting light at broad range of wavelengths (**Fig. 2A**). A specific excitation range is selected by filtering out any excessive part of a source spectrum that does not suit fluorophore excitation maximum. This is done by insertion of an excitation filter. Before the exciting light arrives at the objective lens directly pointing at the sample to be imaged, the exciting light has to be reflected by a dichroic mirror (**Fig. 2B**). This mirror together with perpendicular configuration of a light source and objective lens ensures that the emitted fluorescent light of longer wavelengths will pass through and will be collected by a highly sensitive detector (perpendicular to the light source). Additionally a fluorescence emission filter is used to prevent the detector from unwanted illumination light. This turns out to be useful also in case when more than one fluorophore present in a sample undergoes excitation with selected part of the light source spectrum. Technically speaking, theseaccessories are implemented to the fluorescent microscope often using cubes containing excitation filter, dichroic mirror, and fluorescence filterintegrated at once (**Fig. 2B**).

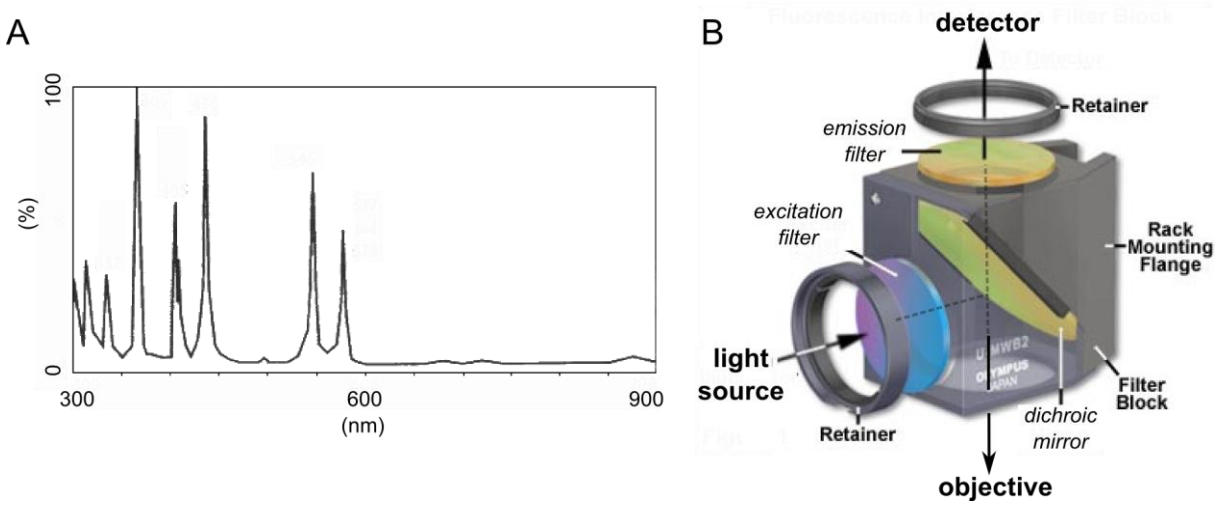

Figure 2.A) Mercury lamp spectrum with visible peaks (image obtained from *cair-research.co.uk*).**B**) A typical integrated filter cube with arrows indicating direction of light travel from the light source, after reflection by dichroic mirror towards an objective lens. After exciting fluorophores in a sample, fluorescent photons are transmitted through the dichroic mirror and arrive at the detector(image obtained from *olympus.micro.com*, altered).

Any optical microscopy, including its fluorescence-based derivative, suffers from a so called diffraction limit. Diffraction constitutes an innate feature of waves including electromagnetic ones

just as light.In the context of resolution limit diffraction was first described by Ernst Abbe in 1873(Abbe, 1873):

$$d = \frac{\lambda}{2nsin(\alpha)}$$

In this formula a resolution limit *d*or the minimal width of a resolvable structural feature is proportional to the wavelength λ collected for imaging and inversely proportional to refractive index *n* and the sine of an angle α corresponding to half angle of the acceptance cone of the light detectable by an objective lens (α characterises a sphere fragment). This equation determines the image obtained with an optical microscope. Therefore, an image of any point source of light (just as a fluorescent probe) will be convolved with so-called point spread function (PSF) of a microscope commonly termed as Airypattern (**Fig. 3A**). Depending on a fluorescence wavelength λ, PSF diameter increases linearly with a reasonable approximation. Since fluorescent light most often belongs to the visible part of a spectrum (~400 – 650 nm) the resolution limit amounts to minimum ≥200 nm.

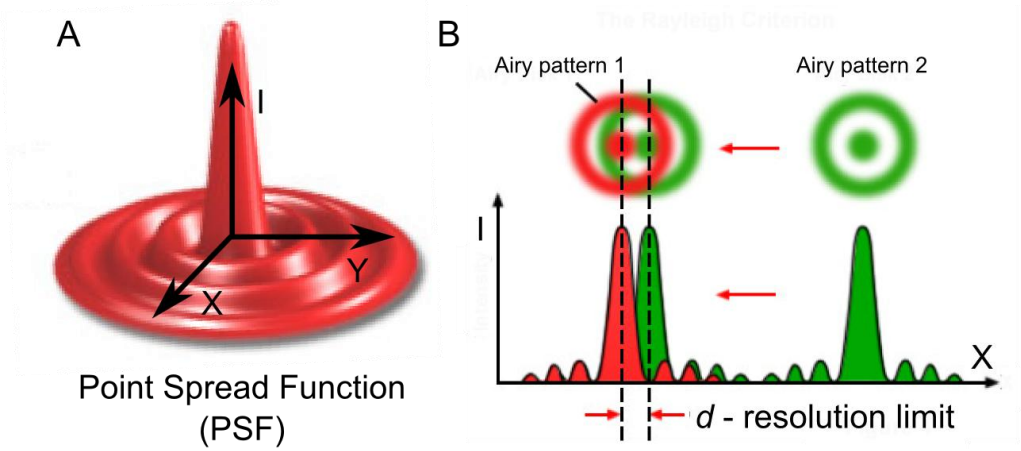

Figure 3. Diffraction limit of a fluorescent microscope.A) Theoretical point spread function ofa fluorescence microscope. Height corresponds to signal intensity (I) distributed over 2D space (x, y). **B**) Resolution limit depicted. Two infinitely small fluorescence sources (1 and 2) appear as Airy patterns. The (Rayleigh) diffraction limit *d*defines the shortest distance between two point light sources at which they are still resolved (image credit: *zeiss-campus.magnet.fsu.edu*).

3.3 Localisation of a single point-like light emitter

Localisation of a single light emitter has proven to be useful in such studies as single particle tracking (SPT) or single molecule localisation microscopy (SMLM, for details see next section). Consequently, localisation precision was necessary to be investigated as it reflects the precision of the measured features just as e.g. speed of molecular migration and diffusion (for SPT) or image resolution (in SMLM).

As mentioned in the previous section the resolution of a microscope is limited due to the diffraction of the light. Accordingly, fluorescing objects, evenif smaller than a diffraction limit, will always be convolved with a point spread function determining their minimal size in the fluorescent image to ~250-600 nm in a diameter depending on the fluorescence wavelength(**Fig.**

4D, left). In spite of the resolution limit that cannot be easily overcome without sophisticated equipment implementations (Hell and Wichmann, 1994; Gustafsson, 2000), these objects can be localised in space with a nanometre accuracy.

Few factorsneed to be taken into account for an appropriate description of localisation of a single point emitter. The term of localisation precision has been first introduced by(Bornfleth H. et al., 1998; Edelmann et al., 1998) and further extended by Thompson et al. (Thompson et al. 2002). For a single point-like light source emitting *N* photons an equation describing localisation precision (σ) has been derived:

$$\sigma^2 = \frac{s^2 + \frac{a^2}{12}}{N} + \frac{8\pi s^4 b^2}{a^2 N^2},$$

where a corresponds to the camera pixel size andsspread (variance) of a fluorescence spot (PSF) that can be assumed to have a normal distribution.

When looking at **Fig.4** it becomes clear that for ideally precise localisation ofa single light emitter, an infinite amount of photons *N*needs to be detected with simultaneous lack of any photonic background. This however is not realistic as typical commercially available fluorescent probes may emit only up to several thousands of photons per molecule in specifically designed chemical environment unless bleached (destroyed). Understandably, this poses a limitation to signal-to-noise ratio. Same holds true for the omnipresent background of a diverse origin. From the equation above it becomes understandable that the localisation precision falls as 1/N for a background noise level (second term) and as $1/\sqrt{N}$ for shot noise corresponding to a standard deviation of a Poisson photon distribution (first term). In addition an increased background may stem from out of focus signals of e.g. other emitters or sample contamination, CCD readout noise of the camera, dark current arising from the thermal lattice comprising a detector chip or pixelation noise (non-linear response of the CCD-pixel to a range of photons to be detected). All these factors restrict single molecule localisation precision in ordinary studies to about 5 - 20 nm (**Fig. 4D**).

Most commonly utilised approach of single molecule localisation takes advantage of 2D Gaussian that is least-square fitted to the distribution of the intensity extracted for each single molecule signal separately. Please note that 2D Gaussian function resembles the distribution of a point spread function of a typical microscope only to some extent and e.g. higherorder maxima of PSF are not approximated in this approach (concentric rings of the Airy pattern, **Fig. 3A**).In addition, itrelies on an unrealisticassumption that a single molecule of a fluorophoreemits light isotropicallywhich is unlikely for dipoles, i.e. molecules with uneven distribution of charge on the various atoms. Similar is true for fluorophores (this matters only in situation when molecular dynamics of a probe is negligibly small in comparison to the time-scale of fluorescence image acquisition).

Alternatively a model of a PSF accounting for fixed spatial orientation of the dipole with a theoretical approximation have been developed and used for a sake of maximum likelihood estimation (MLE) of single light emitter (Mortensen et al., 2010) This however, is computationally consuming and for a sake of SMLM typically its analytically derived expression well suited for isotropic emitters is used instead (MLE with 2D Gaussian fitting)(Mortensen et al., 2010; Sibarita and Heilemann, 2012):

$$\sigma^2 = \frac{\Delta^2}{N}\left(1 + 4\tau + \sqrt{\frac{2\tau}{1+4\tau}}\right),$$

where$\Delta = s + \frac{a^2}{12}and\tau = 2\pi\Delta^2 \mathrm{b}/\mathrm{N}a^2$.

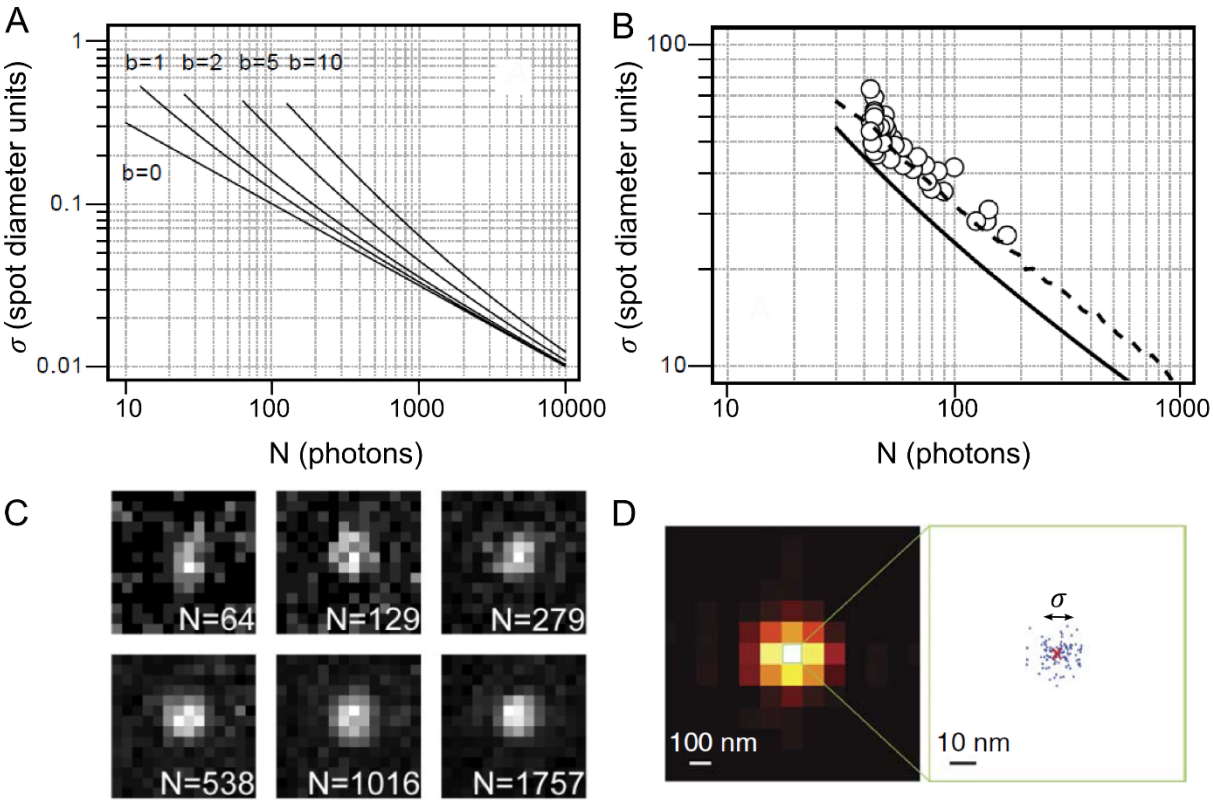

Figure 4. **Localisation of a single point-like light emitter in space.A**)Theoretical calculation of localisation precision depending on a number of photons obtained from a single emitter with constant background levels of 0 to 10 photons. Localisation precision is expressed in normalised point spread function full width at half maximum units. High background level hampers precise localisation of an object. **B**) Experimental measurements of localisation precision of 30 nm fluorescent beads with corresponding number of photons emitted (empty circles) as compared to theoretical prediction (solid line) and computer generated images (dashed line). **C**) Examples of diffraction-limited confocal images of fluorescent beads from (C) with a respective number of photons acquired. The number of photons acquired per bead influences the signal-to-noise ratio and localisation precision.**D**) An alternative method of localisation precision estimation. A localisation of a single light emitter is measured multiple times and σ is estimated from the normal distribution of measured values. Red cross designates mean position of the emitter.A-C adapted from(Thompson et al., 2002), D adapted from (Deschout et al., 2014).

3.4 Introduction to single molecule localisation microscopy

As mentioned in previous section, the resolution limit of a fluorescence microscope hampers observation of objects smaller than ~250 nm. This issue posesa great constraint on its practicalityin the molecular biological research as most biological machineries and protein interactions operate at the level of few nanometres. For instance a single nucleosome has a size of ~10 nm whereas a

cross section through a microtubule (cytoskeleton) is ~25 nm only.Noteworthy, these structures are from 1 to 2 orders of magnitude smaller than wavelength range of a visible light available for detection.

In order to overcome these limitations and enable real study of biological nano-structure, a whole family of methods has been developed including: structured illumination (SIM)(Heintzmann and Cremer, 1999; Gustafsson, 2000), stimulated emission depletion (STED)(Hell and Wichmann, 1994)and single molecule localisation microscopy (SMLM). In the following dissertation we shall focus in detail on the last one.

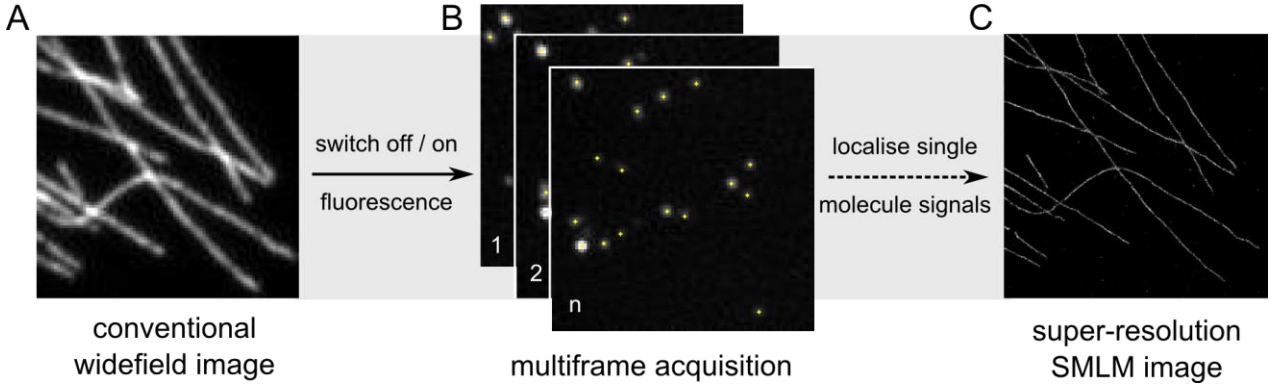

Figure 5. Concept of single molecule localisation microscopy. A) Conventional widefield image of a fluorescently labelled structure. Fluorescence is switched off and subsequently only few molecules are switched on at once with simultaneous image acquisition. Sophisticated software localises their position in space (indicated with yellow dots). This operation is repeated thousands of times unless a sufficient amount of single molecule signals is acquired (**B**). Based on localised positions a super-resolution reconstruction is generated (**C**). B-C comprises a common workflow for all of the single molecule localisation-based microscopy methodologies. Note that this method does not overcome the diffraction limit in a classical sense but rather extracts an information on fine details by separating individual positions convolved with a diffraction-limited point spread function of a microscope.

Even though the first theoretical concepts for SMLM have been developed already in early 90s of last century (reviewed in (Cremer and Masters, 2013)) it took almost a decade to develop a suitable experimental implementation for a single molecule localisation at high densities (average nearest-neighbour distance $<< \lambda/2$). In 2006 two novel independent approaches emerged, termed photoactivated localisation microscopy (PALM) using fluorescent proteins (Betzig et al., 2006; Hess et al., 2006) and stochastic optical reconstruction microscopy (STORM) utilising synthetic dyes(Rust et al., 2006). Since then many more have been developed among which the most important ones are: point accumulation for imaging in nanoscale topography (PAINT) (Sharonov and Hochstrasser, 2006), ground state depletion microscopy (GSDIM) (Fölling et al., 2008), direct stochastic optical reconstruction microscopy (dSTORM) (Heilemann et al., 2008), Spectral precision distance microscopy with physically modified fluorophores ($SPDM_{phymod}$) (Reymann et al., 2008), binding activated localisation microscopy (BALM) (Schoen et al., 2011) and many others.

The key to the single molecule microscopy is a controllable fluorescence switching mechanism. There are three primary mechanismsindicated as useful in SMLM: photoconversion (photoinduced shift in excitation and/or emission spectrum), photoactivation (photoinduced gain of fluorescent

properties to a non-fluorescent molecule), and photoswitching (photoinduced gain or loss of fluorescent properties by a molecule). Even though, the mechanisms of switching might be different for all of these methodologies they all bear a strong similarity in three key aspects: i) it is necessary to selectively capture the fluorescence from individual molecules from others in bulk, ii) the procedure has to be iterated many times in order to capture as many individuals as possible and iii) image reconstruction relies on nanometre-precision localisation of a molecule position using PSF fit function (Thompson et al., 2002) (**Fig. 4D, 5**).

In pursuance of better understanding of SMLM principles, PALM methodology will be explained in details. This method has been first described for photoactivatable fluorescent proteins (PA-FPs) expressed in live cell prior to a chemical fixation (Betzig et al., 2006). These fluorophores become photoactivated only upon illumination with UV or 405 nm light (Patterson and Lippincott-Schwartz, 2002). Initially, under exciting 488 nm illumination, sample is essentially non-fluorescent. However, followed by a moderate 405 nm light pulses, single molecules of PA-FP stochastically undergo a process of photoactivation, i.e. they gain fluorescent properties. As this process is stochastic, by fine adjustment of 405 nm light intensity only, one obtains sufficiently lowdensity of activated PA-FP molecules at once so that they are spaced by a distance much greater than their point spread function extent. By means of 488 nm light exposure they undergo excitation and can be detected as isolated, single molecule signals (**Fig. 5B**). The first fluorescent subset of PA-FPs is imaged until bleached and the procedure of 405 nm photoactivation is repeated again (ultimately thousands of times). Single molecule signals are localised in space with a sub-diffractional precision and their position estimates constitute basis for super-resolution reconstruction (**Fig. 5C**, for more details on signal localisation see previous section).

Since a SMLM image is reconstructed from discrete positions of localised fluorescent probesthe term of resolution necessitates redefinition as the classical Abbe formula is not applicable to this method any more. In SMLM the resolution R_{SMLM} is defined as follows:

$$R_{SMLM} = \sqrt{(2.35\sigma)^2 + \left(\frac{2}{(\varphi d)^{\frac{1}{N}}}\right)^2},$$

where σ corresponds to the localisation precision and the second part of the equation stands for a commonly termed Nyquist resolution associated with a sampling density d in 1,2,3,...,N dimensions. It has been proposed that this classical approach based on Nyquist sampling theorem is insufficient to properly describe a SMLM image resolution in particular when it amounts to 20 - 40 nm only. This is due to the fact that in SMLM structure “sampling” is stochastic unlike ina classical Nyquist sampling theorem where signal sampling (e.g. of radio waves) is rather of constant frequency. As the localisation precision in single molecule fluorescent measurements reaches easily a value of ~10 nm, rather the localisation density constitutes a bottleneckin high resolution SMLM imaging. Therefore, it has been experimentally demonstrated that an oversampling factor φ of at least ~5 with respect to the Nyquist sampling theorem is pivotal for proper SMLM resolution description (Legant et al., 2016). In classical SMLM approaches just as PALM and STORM these sampling densities are rather difficult to achieve due to standard labelling methodologies. Worth noticing is the existence of emerging SMLM methods based on transient binding of fluorescent probes to the binding sites just as PAINT (Sharonov and Hochstrasser, 2006) and BALM (Schoen et al., 2011). Here, the localisation density is rather unlimited and ideally only time constraint plays a role.

3.5 Switching mechanism in direct STORM and design of imaging media

In order to accurately localise single fluorescent probes the aforementioned optical isolation has to be provided. In other words, fluorescing molecules with overlapping light diffraction Airy patterns have to be switched off in vast majority of the cases so that only very few of them at oncemaintain their fluorescing capability. This manoeuvre enables their separation and localisation in space. The following section elaborates on the most feasible and most commonly applied methods of controlling the switching properties of single molecules of fluorophores.

An original single molecule fluorescence switching approach utilising excitation light and additional switching wavelength was further simplified and named direct stochastic optical reconstruction microscopy (dSTORM) - here the excitation wavelength alone is sufficient for exciting the fluorescent probes as well as to stochastically switch between them in order to localise them individually (Heilemann et al., 2005, 2008). Such switching occurs under high intensity exciting illumination and in a presence of specific environmental conditions; namely, specific compounds interacting with the excited fluorophore are responsible for induction of its transition to a non-emitting or more often to a non-absorbing state.

Switching of low-molecular weight synthetic fluorophores can be best explained by a single fluorophore spectroscopy (Vogelsang et al., 2008, 2010)on an example of a typical cyanine-derivated or rhodamine-derivated organic dyes (**Fig. 6A**). The conversion of these dyes into a non-emitting state takes place under exposure to exciting light and is facilitated by a presence of a primary thiol just as β-mercaptoethanol (BME) or β-mercaptoethylamine (MEA) in millimolar concentration range and in the abescence of a molecular oxygen. Primary thiolscompete witha molecular oxygen to quench a triplet state of a fluorophore ($T_{1\text{-}n}$, where n= 1,2,3,...,**Fig. 6C**) by its reduction. Thus, oxygen needs to be removed in order to facilitate interaction between the dye and a thiol (van de Linde et al., 2011). It has been proposed that in these casesa dye-thiol radical with a lifetime of minutes to hours is formed via transition through a fluorophore triplet state (Vogelsang et al., 2010). This compound lacks light absorbance in typical excitation range, hence it is not visible in fluorescent acquisitions (Dempsey et al., 2009).

A broader description of possible fluorescent transients of a single molecule of a fluorophore has been also proposed enabling a better control of its fluorescent properties depending on a demand(Vogelsang et al., 2008). Here not only a reductant in the environment of a fluorophoreis taken into account but also an oxidant. This counterintuitive approach becomes clear when looking at the energy diagram (**Fig. 6C**). The diagram demonstrates that upon excitation a molecule ofa fluorophore typically undergoes a transition from asinglet ground state (S_0) to one of the singlet excited states ($S_{1\text{-}n}$ with n = 1,2,3,...) with a rate k_{exc}.From there, after internal conversion resulting in an energy loss ΔE, it undergoes a highly probable de-excitation with simultaneous fluorescence emission (k_{FL}). A fluorescence molecule experiencing transitions between various singlet states, and thus capable of light absorption and fluorescence emission, is commonly termed as a molecule in an ‘ON-state’ or a ‘bright-state’ (white box in **Fig. 6C**). From this regime it may, however, transfer to a non-fluorescent triplet state ($T_{1\text{-}n}$) which opens a whole spectrum of opportunities.

In the presence of a reducing agent (just as ascorbic acid) and/or an oxidant (e.g. methyl viologen) a fluorophore molecule currently residing in a triplet state may further undergo an electron transfer resulting in formation of radicals lacking any fluorescence emission ability ('OFF-state', 'dark-state', grey frame in **Fig. 6C**). What becomes apparent for a reader here is that by a simple alteration of reductant/oxidant concentrations one may manipulate switching properties ofa fluorescence probe while exposed to the exciting light(Vogelsang et al., 2008). As already mentioned before, molecular oxygen serves as a triplet state quencher, hence, removal of oxygen is necessary to keep the triplet state abundant and promote further radical formation ($T_1 \rightarrow F^{\cdot +}$ or $T_1 \rightarrow F^{\cdot -}$ transitions).

In the presence of an oxidant or a reductant alone (aforementioned primary thiols like MEA are reductants), formation of a fluorophore radical is facilitated. Under the exposure to the exciting light, arapidlyincreasing number of molecules undergoes moderately probable $S_1 \rightarrow T_{1\text{-}n}$ transition followed by a transition to one of radical states. Worth mentioning here is the fact that both $T_{1\text{-}n}$ and radical states are rather long lived (seconds to minutes) as compared to a singlet excited state (lifetime of few nanoseconds) and an increasing number of molecules will sustaina retention in these states while constantly illuminated with high excitation intensity. This, if only well adjusted in the fluorescence microscopy measurements, typically results in observation of isolated single fluorophore molecules occupying the 'bright-state' regime with a concurrent retention of vast majority of molecules in the 'dark-state' regime. Additionally, under continuous light-exposure, fluorophore molecules may become reactivated from the 'dark-states' spontaneously or with a help of a UV-excitation, both leading to radical decay (Dempsey et al., 2009). This is desired in single molecule localisation microscopy where optical isolation and continuous turn-over between states is a key to the resolution enhancement (see **Fig. 5**).

In contrast, assuming the goal of the fluorescence experiment is to rather suppress any 'dark-states' and facilitate high fluorescence emission, an alternative approach can be adopted. Here in order to suppress the triplet and radical state formation ('dark-states'), oxygen removal and high concentration of both reductant and oxidant has to be applied at once. This way radical states will be formed very frequently, though they will be only very short-lived as an oxidant and reductant will immediately serve as a reciprocal radical scavenger ($F^{\cdot +} \rightarrow S_0$ and $F^{\cdot -} \rightarrow S_0$ transitions). This procedure results in a highest photon emission rate per time unit, useful for e.g. single molecule studies just as single molecule tracking or single molecule stepwise photobleaching (Froeh et al., 2015).

Lastly, an alternative approach for a 'dark-state' formation utilises phosphine (TCEP) to feasibly generate a covalent adduct even in the absence of the exciting light (Vaughan et al., 2013). In both of aforementioned cases additional 405 nm light of very low intensity (Dempsey et al., 2009) can be used for light-induced abstraction of the adduct or optionally oxygen reperfusion can be applied (van de Linde et al., 2011), both to recover fluorescent properties of a fluorescent molecule. It has been also demonstrated that by fine adjustment of the intensity of excitation or photoswitchingnear-UV light one can control the kinetics of formation and disintegration of non-emitting state. This is of high significance in single molecule localisation microscopy as by manipulating the light intensity of these excitations one can control the amount and frequency of single molecule signals appearing during an acquisition (van de Linde et al., 2011).

3.6 Design of an imaging environment for fluorophorephotoswitching based on non-emitting state formation

From the previous paragraph it becomes clear that to control various transients of a fluorophore is a key to single molecule localisation microscopy.One deduces a core assumption set for successful SMLM: i) necessity of formation of a very abundant non-fluorescent ‘dark-state’ with concomitant maintenance of very few individuals at the moment in a short-lived ‘bright-state’, ii) possibility of circulation between two states with a rate that suits the measurement time-scale and equipment capabilities.

In classical photoswitching experiments (Dempsey et al., 2009; Heilemann et al., 2005, 2008; Vogelsang et al., 2008) these requirements are usually controlled by a chemical environment surrounding the molecule, and technically speaking, the imaging cocktail needs to be thoroughly designed in order to fulfil SMLM requirements for the fluorescent label chosen. Following aspects have to be regarded as relevant:

- Molecular oxygen dissolved in a solvent (O_2) facilitates fluorophore photobleaching (irreversible loss of fluorescence properties) (Bernas et al., 2004)and also serves asa quencher of a triplet state bridging formation of a stable long-lived radical ‘dark-states’. To overcome these deleterious effects, oxygen can be removed by means of a commonly used enzymatic oxygen scavenging system: a mixture of glucose oxidase, catalase, and glucose. The first catalyses incorporation of the oxygen to the glucose with a concomitant generation of a hydrogen peroxide immediately disintegrated by catalase. As a side effect D-glucono-1.5-lactone is formed and rapidly hydrolised to a gluconic acid inevitably leading to a drop in environmental pH ($pK_a \sim 3.7$). Thus, it has been proposed to replace glucose oxidase with pyranose oxidase known for analogous oxygen-scavenging properties and pH preservation(Sari et al., 2012; Swoboda et al., 2012).

- Choice of a switching reagent should be justified by experimental trials and is usually dye and agent specific (MEA, BME, phosphine (TCEP), trolox (TX), ascorbic acid (AA) with methyl viologen (MV) etc.). Typical concentrations used fall in millimolar range. However, since the agent concentration has an effect on transient probability (e.g. radical formation), it needs to be experimentally adjusted as well.As an example, low concentration of a primary thiol (reducing agent)may lead to an insufficient abundance of a $T_1 \rightarrow F^{\cdot -}$transient (**Fig. 6C**), hampering spatial isolation of single fluorophore signals in a bulk fluorescencemicroscopy acquisition.

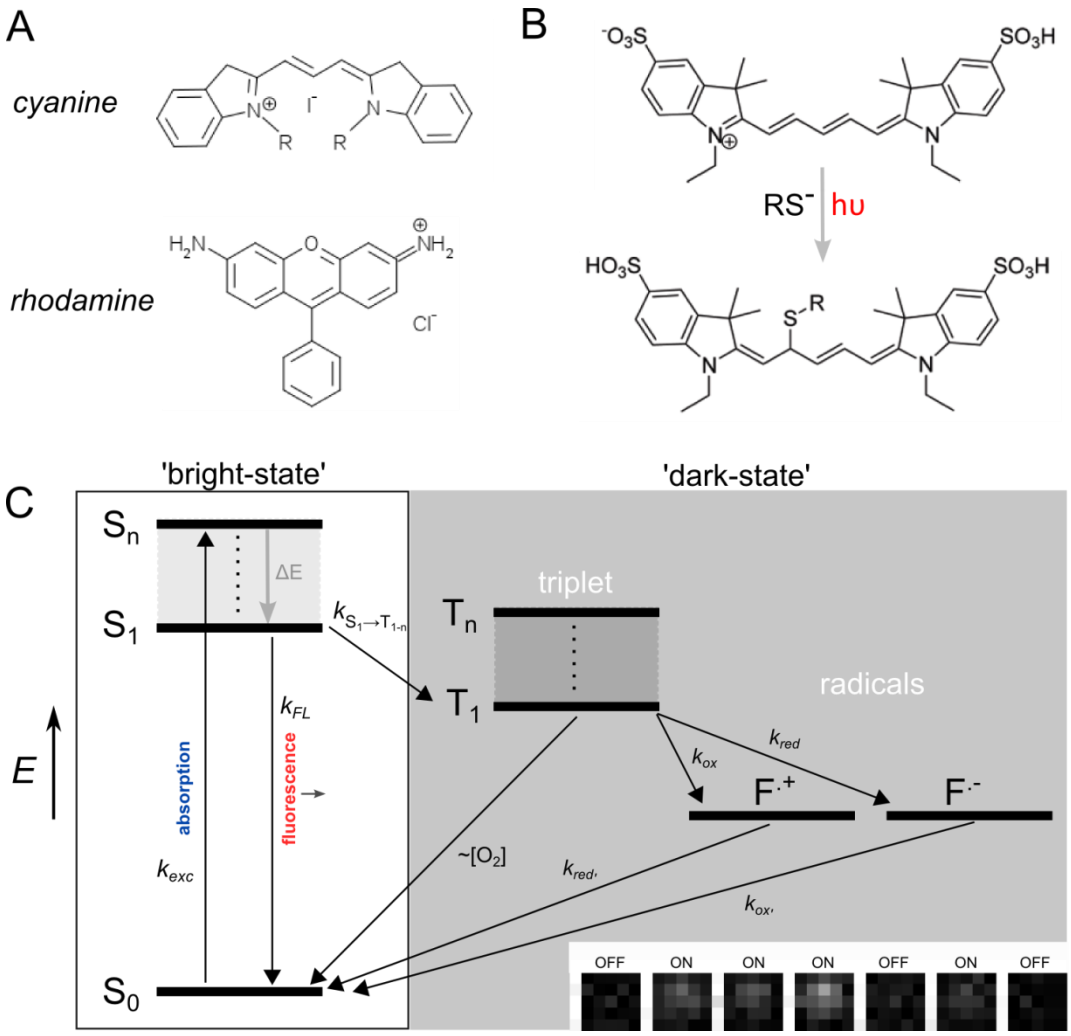

Figure6.**A**) Chemical structures of cyanine and rhodamine fluorescent probes. Most of commercially available fluorophores from Alexa and Atto families are derived from them.'R' corresponds to a chemical substitutes.**B**) Model of light induced formation of the dark (non-emitting) state in a presence of a primary thiol (RS^-). Under light exposure the dye undergoes a reduction and a non-fluorescent dye-thiol adduct is formed. It may recover to a previous state either spontaneously or by exposure to additional near-UV illumination. In the latter the backwards reaction is accelerated proportionally to the UV-light intensity. Adapted from(Dempsey et al., 2009). **C**) Jabłoński energy diagram for a fluorescent probe useful for SMLM. Black arrows designate transitions between corresponding states. White box corresponds to a 'bright-state' of a fluorophore capable of excitation and fluorescence emission whereas grey box signifies the non-fluorescent 'dark-states' of a fluorophore. Under the exposure to light a molecule of a fluorophore undergoes an excitation. Here, it may emit fluorescence ($S_1 \rightarrow S_0$ transient) or optionally, with a limited probability, it may further transfer to one of the triplet states ($T_{1\text{-}n}$). Triplet state might be effectively quenched by a molecular oxygen ($T_1 \rightarrow S_0$ transition) or optionally, in the presence of a reducing or an oxidising agent (e.g. ascorbic acid and methyl viologen respectively), it may continue the transient to a long-lived radical 'dark-state'.For clarity, a sequence of fluorescent images of a single 'blinking' molecule of anAlexa 647 fluorophore acquired every 25 ms are shown(right-bottom). For simplicity, an irreversibly photobleached state and non-radiative S_1 deexcitation processes just as energy transfer, quenching, and solvent relaxationhave been neglected in the graph.Please note that radical 'dark-states' prevent from irreversible photobleaching of a fluorophore as here it is not susceptible to a light absorption that may lead to a photolysis or reactive oxygen species formation. For more details see (Vogelsang et al., 2008).

- pH of the fluorophore's environment has been demonstrated to have an effect on fluorescent properties of fluorophores and hence should be carefully adjusted. It has been shown for Alexa 647 (cyanine-derivative) that in pH around 5 single fluorophore molecules emit fluorescence for longer, with higher integrated number of photons probably due to a decreased probability to interact with a switching agent (Olivier et al., 2013). Low pH (<6.5), hence, may constitute an issue when optical isolation of single fluorophores is required, whereas higher pH (~8) may be of choice when fast SMLM measurements are desired.

- Solvent used for fluorescent measurement may have an effect on fluorophore excited state deexcitation via direct interaction. It has been demonstrated that e.g. replacement of water with heavy water (D_2O) suppresses formation of transient hydrogen bonds between a fluorophore and a surrounding water, effectively increasing the quantum efficiency of a fluorescent probe (Klehs et al., 2014). In addition another factor that should be controlled is the viscosity of a buffer. For instance, glycerol is known to enhance fluorescent lifetime of a DNA binding PicoGreen ~180 fold as compared to water (Dragan et al., 2010). Thus, simple, partial or almost total replacement of water with glycerol might be expected to improve brightness of the fluorescent probes crucial for single molecule detection.

3.7 Fluorescent DNA-binding dyes

In optical microscopy, chromatin, a protein complex with DNA, yields poor contrast in standard transmitted light mode or even when differential interference microscopy applied. Hence, the necessity to label the DNA with fluorescent probes. In fluorescence microscopy, in order to do so*in vitro* or *in situ* in fixed samples, a number of dyes with nucleic acid affinity has been developed. These compounds, further abbreviated as DNA dyes, are typically positively charged promoting their close interaction with negatively charged nucleic acids (phosphate groups constituting nucleic acid backbone are responsible for negative total net of nucleic acids). Electrostatic attraction however is not a sole mechanism of interaction and is insufficient for a tight binding to the DNA (please see further paragraphs for more information). In the following section the complexities of these interactions will be covered. This will enable the reader to better understand the purpose and the coverage of the work performed for the sake of this dissertation.

The first type of binding mechanism is DNA intercalation (**Fig. 7B**, left). The term "intercalation" was first introduced by L. Lerman to describe the insertion of planar aromatic compounds between DNA base pairs of double stranded DNA(Lerman, 1961). Among the most commonly used intercalators in fluorescence microscopy are ethidium bromide, acridine orange, and cyanine based YOYO-1, TOTO-1 (bis-intercalators), YO-PRO-1 (mono-intercalator). Besides their outstanding fluorogenic properties (Table 1) they are known to have an effect on mechanistic nature of the dsDNA (Günther et al., 2010; Kundukad et al., 2014). For instance, a DNA dye YOYO-1, widely used in single DNA molecule biophysical studies (Reisner et al., 2010), in spite of having no effect on DNA persistence length (measure of a stiffness of a polymer), it induces an increase of up to 38% in DNA contour length (maximal physical extension of a polymer) at full saturation of 1 dye molecule per 4 DNA base pairs. This means that a single YOYO-1 molecule extends the DNA by approximately 0.5 nm (Kundukad et al., 2014). Using atomic force microscopy it has been also

found that in closed dsDNA molecules in vitro (DNA plasmids), YOYO-1 induces undertwisting and super-coiling (Kundukad et al., 2014). Abovementioned aspects make intercalating dyes impractical for live cell investigations highly desired in cell biology (Wojcik and Dobrucki, 2008). Nevertheless, they are still highly recommendable for in vitro experiments where high sensitivity in DNA detection is in demand (e.g. in DNA electrophoresis or polymerase chain reaction).

The second major binding mechanism is termed generally as DNA minor groove binding (**Fig. 7B,**right). This group of dyes is known for widely used benzimidazole-based Hoechst and DAPI dyes or cyanine-derived PicoGreen. Dyes capable to bind to the DNA this way turned out to have less deleterious effect on DNA double helix mechanistic features (Pigram et al., 1973) and proved to be less cytotoxic to living cells (Wojcik and Dobrucki, 2008). The binding mechanism of these compounds is however a bit more complex and can be best explained by means of an example.

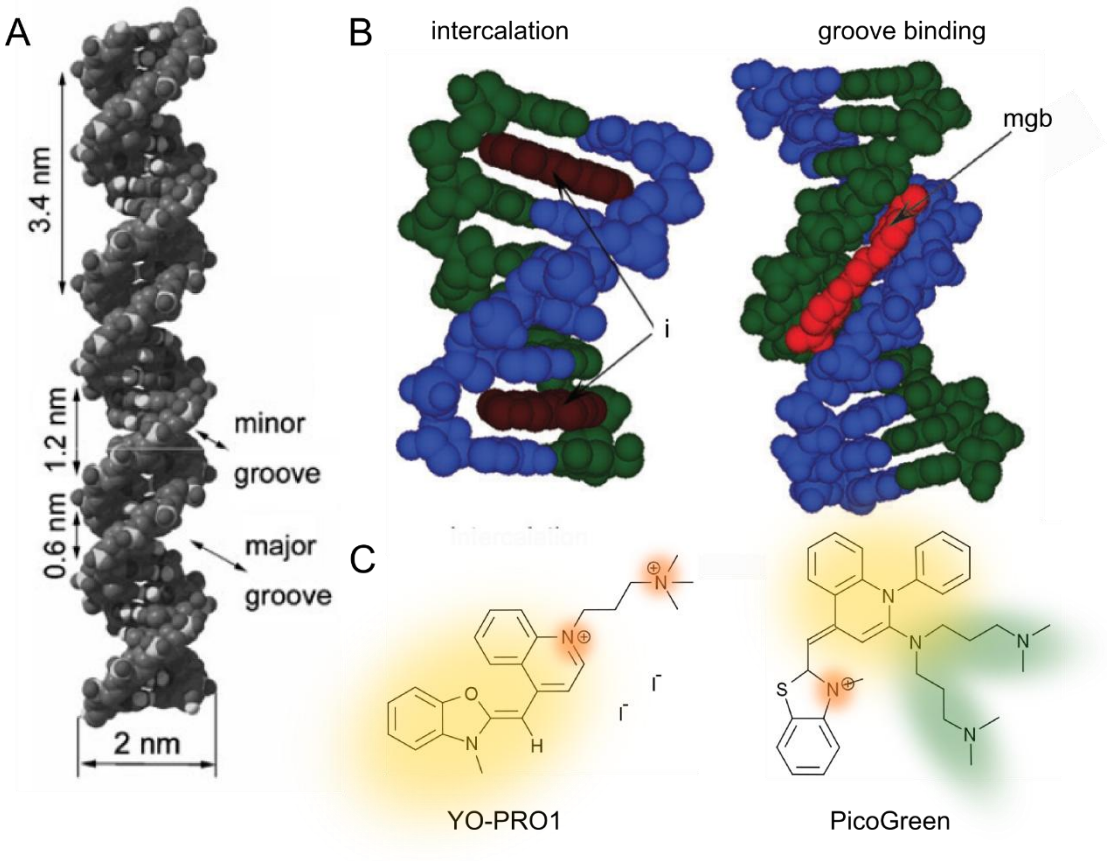

Figure 7.DNA binding mechanisms of low-molecular weight dyes.A) Double stranded DNA (dsDNA) structure. Minor and major grooves of dsDNA are indicated with arrows. **B**) Demonstration of possible DNA dye locations with respect to dsDNA double helix. Depending on their binding mechanism: intercalation between DNA base pairs (left), and minor groove binding (right). Abbreviations correspond to:*i* - an intercalating molecule (PDB ID: 1Z3F),*mgb*- a minor groove binder (PDB ID: 102D). Images were adopted from (Liu et al., 2008).**C**) Examples of intercalators (left) and minor groove binders (right). In orange a positive charge responsible for electrostatic interaction with the DNA is indicated. Yellow labels benzo thiazol/quinolinium group likely intercalating between DNA base pairs. Green designates parts believed to be responsible for interaction with dsDNA minor groove (Dragan et al. 2010).

Studies on PicoGreen dsDNA binding in an increasing salt concentrations revealed decreasing association strength as judged on fluorescence signal intensity. Such an effect is typically attributable to electrostatic interactions (Dragan et al. 2010). For instance it has been demonstrated that NaCl concentration of 100 mM escalatesPicoGreen dissociation constant ~10 fold.This means that most of the interaction forces that remain in this case are not electrostatic-related(Dragan et al., 2010). Therefore, one of the mechanisms of interaction of this molecule with dsDNA is purely electrostatic. The rest of the interaction with a DNA minor groove is likely shared among two aminopropyl groups having similar structure to AT-hooks known to have alone a DNA-affinity at the minor groove (indicated in green in **Fig. 7C**, left)(Dragan et al. 2003). Nonetheless, it is hard to encounter a pure interaction with the DNA minor groove. In case of the PicoGreen, its aromatic groups (yellow in **Fig. 7C**, left) are anticipated to intercalate to some extent between DNA base pairs. Therefore, this interaction mechanism is rather a mixture of minor groove insertion and intercalation.

DNA-binding dyes are essentially non-fluorescent in a solution (except a few cases such as e.g. DRAQ5 or DAPI, **Table 1**). However, upon binding (irrespective of the binding mechanism) DNA dyes experience great increase in their brightness, often exceeding even 10^3 fold. This increase in quantum efficiency provides an extreme contrast demanded in e.g. optical microscopy imaging. But what are the physical bases for this phenomenon? In order to explain this fluorescent enhancement it is best to review in detail an example of well studied PicoGreen - a cyanine-derived DNA dye (for details see previous paragraph). Fluorescent lifetime measurements of PicoGreen in a watery buffer revealed its value to amount ~4 ps, however, upon binding its value reaches ~4 ns (1000x fold increase). In order to decipher the underlying mechanism of quantum efficiency increase it is important to separately target different aspects of physical interactions of the dye with its environment. For instance, it hasbeen observed that alteration to the viscosity of environment increases fluorescent lifetime of this DNA dye by ~180 fold in the absence of DNA(Dragan et al., 2010). Such change of the fluorescence lifetime uponincreased viscosity constitutes a typical hallmark of affected intramolecular dynamic fluctuations of a molecule investigated.Therefore, the PicoGreen undergoes excited state energy dissipation while in a solvent, and as a consequenceits dramatically low quantum efficiency can be attributed to this process.In contrast, intramolecular dynamics is abolished while molecule of this DNA-binding dye is immobilised to the dsDNA, leading to a very high quantum efficiency and high probability of fluorescence emission.

	Extinction coefficient at exc. max. [$cm^{-1}M^{-1}$]	dsDNA binding constant [M^{-1}]	Quantum efficiency while bound to dsDNA	Peak absorption/ emission with dsDNA [nm]	Fluorescence enhancement and binding mechanism
Hoechst 33258	**47,000**	**10^6-10^7** (Drobyshev et al., 1999)	**0.42** (Cosa et al., 2001)	**349/466** (Cosa et al., 2001)	**13x**, **mgb** (Cosa et al., 2001)
DAPI	**27,000**	**10^5-10^6** (Manzini et al., 1985)	**0.34** (Cosa et al., 2001)	**358/456** (Cosa et al., 2001)	**18x**, **mgb** (Cosa et al., 2001)
YOYO-1	**98,900** (Benvin et al., 2008)	**10^{10}-10^{12}** (Glazer and Rye, 1992)	**0.38**	**458/489**(Rye et al., 1992)	**<1,000x** (Cosa et al., 2001; Rye et al., 1992), **i**
YO-PRO-1	**52,000**(Benvin et al., 2008)	**10^5-10^6** (Glazer and Rye, 1992; Joseph et al., 1998)	**0.44**	**475/486**(Rye et al., 1992)	**700x** (Rye et al., 1992), **i**
PicoGreen	**70,000**	**$5x10^9$** (Dragan et al., 2010)	**0.5**	**498/528**(Cosa et al., 2001)	**1,070x** (Cosa et al., 2001), **mgb**, **i**(Dragan et al., 2010)
Ethidium bromide	**~6,000**	**~10^5** (Alonso et al., 2006; Vardevanyan et al., 2003)	**0.35** (Cosa et al., 2001)	**520/610** (Rye et al., 1992)	**35x** (Rye et al., 1992), **i**
SybrGreen	**70,000**(Dragan et al., 2012)	**10^7** (Dragan et al., 2012)	**0.42** (Dragan et al., 2012)	**~500/525**	**>1000x**, **mgb**(Dragan et al., 2012)
DRAQ5	**20,949** (Smith et al., 2000)	**–**	**0.004** (Njoh et al., 2006)	**646/681** (Smith et al., 2000)	**~1x** (Njoh et al., 2006), **i** (Smith et al., 2000)
Sytox Orange	**79,000** (Yan et al., 2005)	**10^8** (Yan et al., 2005)	**0.9** (Yan et al., 2005)	**543/575** (Yan et al., 2005)	**~450x** (Yan et al., 2000), **i,** (Yan et al., 2005)

Table 1.Physicochemical properties of intercalating and minor groove binding DNA dyes. Fluorescence enhancement refers to a quantum efficiency increase upon binding to the DNA. Cyanine-derivated dyes (in particular YOYO-1, SytoxOrange, and PicoGreen) bear highest photon emission. Among dyes with high photon emissionlisted here,YO-PRO1 and SybrGreen bind to dsDNA weakest.SytoxOrange and YOYO-1 are the brightest among all DNA binding probes listed. Binding mechanism indicated as 'i' refers to dsDNA intercalation and 'mgb' to DNA minor groove binding. '–' – information not found.

3.8 DNAimaging with super-resolution microscopy

Since the very beginning of the super resolution microscopy, an imaging of the DNA constituted one of the key challenges (Rust et al., 2006)and the direct DNA labelling has been some solution to this problem at least to a moderate extent.

One of the first attempts comprised structured illumination microscopy (SIM) of the DNA labelled with DAPI minor groove binder (Schermelleh et al., 2008). The choice of DAPI was justified due to its spectral properties. In SIM the resolution enhancement is usually ~2x full width at half maximum of a point spread function of the wavelength emitted (λ_{em}). For DAPI λ_{em} is approximately 450 nm (blue) i.e. visible light of a shortest detectable wavelengths. This gives the highest achievable resolution of ~110 nm laterally (x, y) and ~300 nm axially (z) and has been successfully applied to imaging of a rodent and mammalian cell nuclei(Schermelleh et al., 2008). In spite of common image artefacts in SIM (Sahl et al., 2016), thanks to its versatility and ease of application, it soon emerged as a main tool for studying DNA/chromatin architecture in the cell nucleus (Markaki et al., 2010; Popken et al., 2014, 2015).

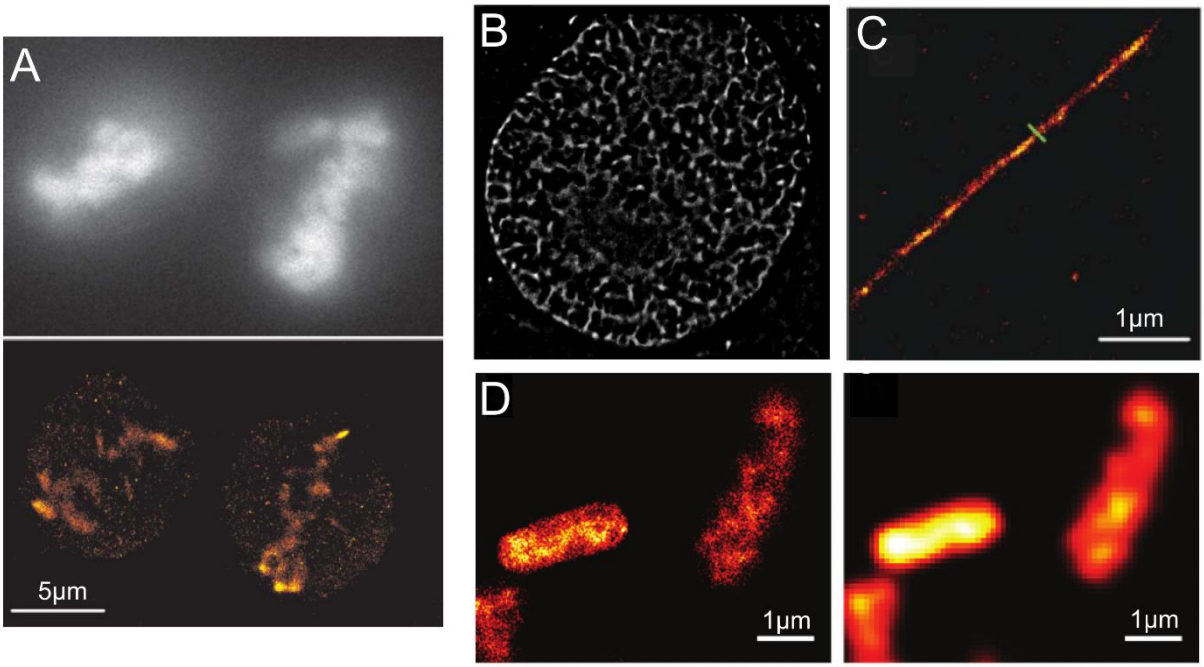

Figure 8.SMLM of directly binding DNA dyes.A) Fixed, mitotic chicken cells labelled with SYTO-13, widefield (top) and SMLM image (down). Image from (Flors, 2011). **B**) SMLM image of live U2OS cell stained with Picogreen. Adopted from (Benke and Manley, 2012). **C**) SMLM image of an isolated λ-phage DNA stained with YOYO-1 (Flors, 2010). **D**) Binding activated SMLM of fixed *E. Coli* bacteria using transient PicoGreen association, left super-resolution image, right conventional reconstruction. Adapted from (Schoen et al., 2011).

In parallel to SIM, stimulated emission and depletion (STED) microscopy has been first applied to the DNA study. Here the isolated and stretched λ-phage DNA was stained with YOYO-1 and exposed to two wavelengths: exciting and depleting. As a result, a resolution in the order of 50 nm has been achieved (Persson et al., 2011). Few years later STED microscopy was again applied to the subject of DNA imaging (Lukinavičius et al., 2015). This time living cells were labelled using

specifically designed DNA probe based on Hoechst backbone (Si-R Hoechst). Although, the authors claim the resolution in the order of 80 nm, they are unable to present an image of an entire cell nucleus. STED microscopy typically does not perform well on structured 3D samples due to a difficulty to maintain reciprocally aligned focussed light beams as the light refraction index varies throughout a sample's structure. Any follow-up study and application of this method to DNA imaging is presently missing.

Currently, a growing number of technical solutions has been put forward in a field of single molecule localisation microscopy of DNA. First studies involved imaging of isolated λ-phage DNA labelled with cyanine-derived dsDNA intercalators such as YOYO-1, YO-PRO-1 or TOTO-3 (Flors, 2010, 2011; Flors et al., 2009). In case of these studies the DNA was pre-stained and embedded in an imaging buffer devoid of oxygen containing 50 – 100 mM β-mercaptoethylamine (MEA). It has been postulated that this compound facilitates a photoinduced reduction of a dye leading to a formation of a reversible, non-emitting dark state(this term was introduced in the **section 3.5**)(Flors, 2010). These protocols were applied to imaging of isolated DNA (**Fig. 8C**) and cell nuclei (**Fig. 8A**). In case of the latter, with a moderate success due to limited single molecule localisation density reducing structural details in an image.The other research focused on live cell SMLM using a cyanine-derived minor-groove binder PicoGreen in a presence of 1 mM ascorbic acid (AA) and in the absence of oxygen (Benke and Manley, 2012) (**Fig. 8B**). The authors inferred that by using reducing (here AA) and oxidative agent (supposedly intracellular reactive oxygen species) both with an appropriate proportion, PicoGreen's fluorescence switching occurs as was previously demonstrated for other synthetic cyanine- and rhodamine- derived dyes (Vogelsang et al., 2008) (for more details see **section 3.6** and **Fig. 7**).

One of the very interesting approaches involving single molecule localisation termed Binding Activated Localisation Microscopy (BALM), relies on a transient binding of YOYO-1 and PicoGreen to the DNA in a specially designed buffer containing milimolar concentrations of methyl viologen and ascorbic acid with simultaneous oxygen deprivation (Schoen et al., 2011). Such chemical environment provided an increased dynamics of association and dissociation of DNA-binding dyes with/from dsDNA in isolated λ-phage DNA and in bacteria (**Fig. 8D**). The dye concentration was carefully adjusted so that only very few isolated dye molecules are bound to the DNA and fluoresce at the same time. Concurrently, the rest is not detectable as the emission rate of a DNA dye in a solvent is negligible (for details see **section 3.7**).In BALM the dye molecules associate with dsDNA only for few milliseconds enabling the detection of up to 2,000 photons per molecule and its precise localisation. This approach turned out to provide an excellent resolution of 10 – 20 nm for isolated DNA fibres. Interestingly however, BALM has not been applied to imaging of the nuclei yet.

Currently the switching mechanisms and dynamic binding in aforementioned methods have not been described in sufficient detail. Better understanding of switching properties of the DNA dyes as well as development of new DNA imaging techniques is presently highly demanded in the cell biology (see next section).

3.9 Photoconversion of benzimidazole-based DNA dyes and Vybrant Violet

Photoconversion is a process known best for photoconvertible fluorescent proteins e.g. mEos and Kaede (reviewed in (Shcherbakova et al., 2014)).Under the exposure to a specific light a molecule of a fluorescent probe changes its spectral properties.For instance, it might experience a change to

the excitation or emission spectrum or both at once. Most often a red-shift towards longer excitation and emission wavelengths occurs as a repercussion of a photoinduced cleavage in a structure of a fluorescent protein chromophore. Until recently the phenomenon of photoconversion was not known for any of the DNA-binding dyes.

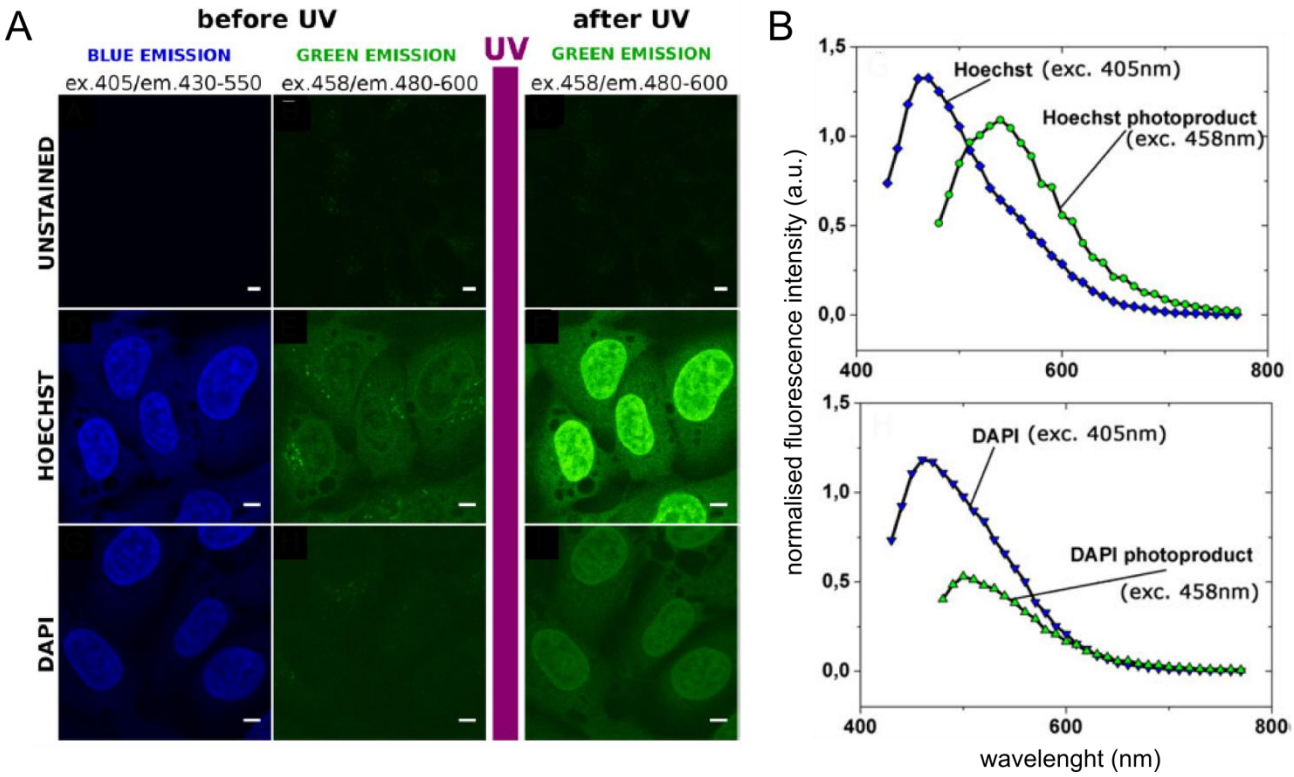

Figure 9. Confocal studies of the photoconversion of benzimidazole DNA dyes.A) Column 1 and 2 from the left present Hoechst 33258 and DAPI fluorescence once bound to cellular DNA. Blue fluorescence excited with 405 nm laser light presented in blue, faint green fluorescence excitable with 458 nm laser light presented in green. Column 3 demonstrates a spectral change to Hoechst (upper row) and DAPI (lower row) after exposure to UV light; here the green fluorescence originating from the cell nuclei becomes stronger suggesting that photoconversion occurred. Concomitantly, the fluorescence of a standard blue-emitting form undergoes strong reduction (not shown). **B**) Respective fluorescence spectra of UV-excited/blue emitting and blue-excited/green emitting forms of Hoechst (upper row) and DAPI (lower row) in a presence of a cellular DNA. Images from (Żurek-Biesiada et al., 2013).

Contemporary studies demonstrate that benzimidazole based dyes just as Hoechst 33258, Hoechst 33342, DAPI and VybrantDyeCycleViolet undergo a process of photoconversion upon illumination with UV or 405 nm laser light (Żurek-Biesiada et al., 2014, 2013). Mass spectrometry studies revealed that under such circumstances DAPI and Hoechst 33258 undergo additional protonation (Żurek-Biesiada et al., 2014). Whereas under standard conditions their excitation and emission maxima amount to around 360 nm and 460 nm respectively (see **Table 1**), after UV irradiation they become easily excitable with light from 458 – 488 nm range with their emission maxima shifted to 505 nm (DAPI) and 530 nm (Hoechst)(**Fig. 9A, B**). This has been indicated particularly hazardous in case of conventional fluorescence imaging of DNA labelled using these dyes together with other green emitting label just as GFP as both emission spectra would significantly overlap (Webster et al., 2013). Nevertheless, both DNA-binding dye's spectral forms,

can be easily separated using an appropriate filter set. Interestingly, any usefulness of these properties and similarity in behaviour to photoactivated localisation microscopy probes yet has not been recognised.

3.10 Review on chromatin organisation in the cell nucleus

The DNA is a polymer composed of a basic unit known as a nucleotide. There are four types of nucleotides depending on their composition. Typically they comprise phosphate, deoxyribose and either cytosine, guanine, adenosine, or thymine. One of the greatest breakthroughs in biology that revolutionised the world was the discovery of how do they form a polymer and transfer biological information brought to the world by Watson and Crick in 1953(Watson and Crick, 1953).This discovery alone, did not, however, explain how theDNA having a length of approximately ~2 m can folditself in order to fit into a cell nucleus of a diameter 5 order of magnitude smaller. In order for this to happen, formation of chromatin, a complex of DNA and proteins, is necessary. The DNA is wrapped around histone protein octamers termed nucleosomes, having on average 146 base pairs (bp), with a linker DNA ranging from 10 to 50 bp(**Fig. 10A**)(Jiang and Pugh, 2009). The linker part of the DNA is known to be a location to H1 histone dynamically supporting and determiningthis basic structure(Misteli et al., 2000). All together, this well established chromatin model assumes the existence of so called 'beads on the string' explaining chromatin organisation and initial length reduction at the level below 11 nm.

However, in spite of a great deal of an effort invested, the precise higher order spatial organisation of the chromatin is still a subject to an ongoing debate (Maeshima et al., 2010; Cremer et al. 2015). After mitosis condensed chromosomes undergo partial decondensation and align to the freshly formed nuclear periphery. Surprisingly, they do not mix with eachother but rather form distinct chromosome territories and typically maintain their radial position in the nucleus throughout a cell cycle(**Fig. 10B**)(Cremer and Cremer, 2001; Gao et al., 2016).Nonetheless, the chromatin architecture on a length-scale between a chromatin fibre and chromosome territory remains elusive (10 - 200 nm). Currently the most persuasive models have been derived using chromosome conformation capture methods (3C, 4C, 5C, and Hi-C, for example see (Dixon et al., 2012)). These methods rely on formaldehyde fixation of the chromatin in situ and together with a massive parallel sequencing revealDNA sequence-specific contact probability throughout a genome with a resolution of ~1 kb(Rao et al., 2014). Using this technology the existence of small self-interacting chromatin domains, denoted as "topologically associated chromatin domains" (TADs) was discovered(Dixon et al., 2012). TADs are genomic regions that undergo a high frequency of local contacts while interacting infrequently with sequences within adjacent TADs. Their size ranges from kilo- to mega- base-pairs (Dixon et al., 2012; Fraser et al., 2015) and they are believed to constitute a basic higher order chromatin organisation unit above the level of individual nucleosomes, e.g. in DNA replication (Pope et al., 2014).

Although, the existence of TADs and even so called "meta-TAD" arrays (Fraser et al., 2015) seems to be broadly accepted, their internal structure and mechanism of formation are now in the spot light. Currently, a variety of novel methodological approaches are aiming to unravel the basic information on TAD organisation. For instance, classical chromosome conformation capture methods rely on the proximity ligation via e.g. formaldehyde cross-linking of chromatin stretches occupying same neighbourhood.

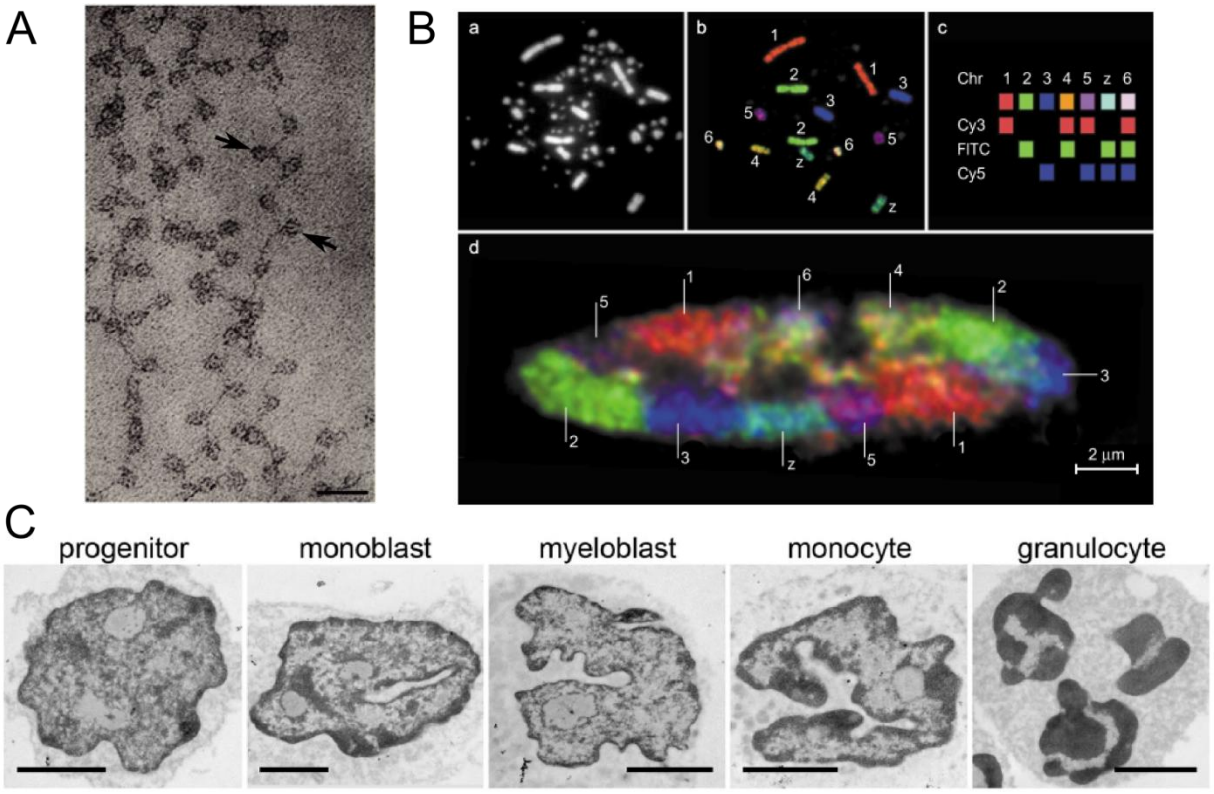

Figure 10. DNA arrangement at different organisational levels.A) An electron microscopy picture presentingthe basic chromatin unit – nucleosome, comprising DNA and histone proteins. So called "beads on a string" are indicated with arrows (image credit: (Olins and Olins, 2003)).**B**) A proof of concept experiment revealing the existence of chromosome territories in a chicken fibroblast.(a) Image of a DAPI- and (b) chromosome PAINT- stained metaphase spread by a combinatorial labelling with oestradiol, digoxigenin and biotin followed by a secondary labelling with three fluorescent labels: Cy3, FITC and Cy5 (source: (Cremer and Cremer, 2001)).**C**) A demonstration of changes in chromatin architecture throughout the time-course of myelopoiesis (from left to right)(Hübner et al., 2015). Chromatin structure changes as the cell commits to a specific function.

Other group of methods involving parallel massive sequencing, termed chromatin interaction analysis by pair-tag sequencing (ChIA-PET), was designed to detect genome wide interactions mediated by specific protein factors(Fullwood and Ruan, 2009). In a recent study ChIA-PET was applied to investigate CCCTC-binding factor (CTCF) and cohesin, i.e. proteins believed to tangle chromatin fibres and regulate loop formation (Tang et al., 2015). Thanks to an increased sequencing resolution of ChIA-PET reaching even 100bp (as compared with~few kb for HiC), it has been revealed that CTCF and cohesin, in 99% of cases, co-occupy same genomic loci that in addition correlate with a positioning of RNA Pol II factor responsible for gene transcription (Tang et al., 2015). Interestingly, previously it has been found that CTCF correlates with TAD boundaries (Rao et al., 2014). These evidences lead to a conclusion that chromatin loops are tangled with CTCF/cohesin at TAD boundaries where also RNA Pol II is enriched to serve transcription of active genes. Lately, it has been also hypothesised based on polymer simulations that an underlying principle of TAD formation is a dynamic loop extrusion(Fudenberg et al., 2016). Also experimental and modelling evidences are available suggesting that transient intra-chromatin interactions bridged by polycomb proteins lead to an increase in chromatin compaction in *Drosophila*cells (Boettiger et al., 2016).

Table 2	**Active Nuclear Compartment (ANC)**	**Inactive Nuclear Compartment (INC)**
factors	Transcriptionally competent chromatin And chromatin loops Transcription factors, RNA Pol II CTCF, cohesin Active histone marks: H3K9ac, H3K4me3 Replication factors (e.g. PCNA)	Compacted part of CDCs Repressive histone marks like H3K9me3, H3K27me3 DNA methylation Heterochromatic proteins, HP1

Table 2. Occupancy of protein factors in active and inactive nuclear compartments. Proteins transiently not associated with chromatin are believed to diffuse throughout the interchromatin compartment. For further details and depiction see **Fig. 11A**.

In line with biochemical studies, based on microscopic evidences, a new general model of chromatin organisation at the level of 100 – 1000 nm has been put forward (Cremer et al., 2015)(**Fig. 11A**). This model of the cell nucleus is based on two functionally distinct active and inactive nuclear compartments (ANC and INC, respectively). The ANC is built up of transcriptionally active peripheral part of chromatin domain clusters (CDCs) whose core comprises transcriptionally inactive, condensed chromatin of the INC. CDCs occupy roughly 50% of the total nuclear volume and are surrounded by interchromatin compartment (IC) providing a physical connection to the nuclear pores at the nuclear periphery. This major compartmentalisation of the nucleus leads to heterogeneity in local molecule concentration, crowding effects, and phase separation (Pederson, 2014;Hancock & Jeon, 2014; Woringer, Darzacq, & Izeddin, 2014).

Presently it is understood that the local environment determined by e.g. chromatin compaction state, the epigenetic landscape, or the distance to other neighbouring chromosomal all a critical role in regulation of both, individual genes as well as the entire cell fate (**Fig. 10C**)(Cremer et al., 2015; Ma et al., 2015). Thus, necessity to develop novel investigation methodologies, including microscopy, to visualise the internal structure of TADs, their dynamic nature and mechanism of formation, is highly desired.

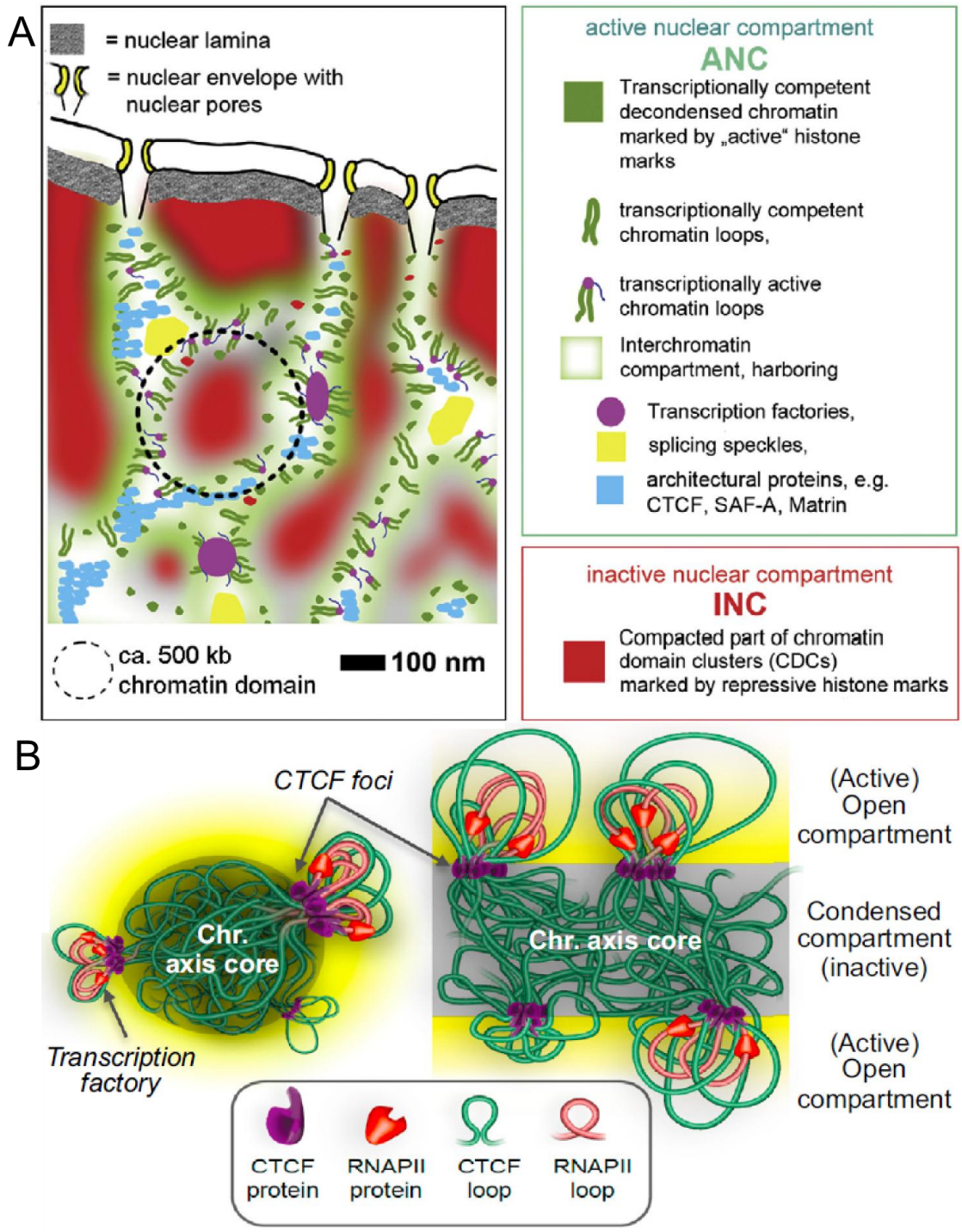

Figure 11. Chromatin organisation model in interphase cell nucleus based on spatially co-aligned functional zones.A) General model of active-/inactive- nuclear compartments derived from contemporary microscopic studies (Cremer et al., 2015). The core assumption of this model is that chromatin does occupy nuclear volume only to some extent and in vast majority of the cases remains inactive (in one moment, genes are dynamically expressed). Interchromatin compartment surrounds such chromatin islets and serves dynamic diffusion of nuclear factors throughout the cell nucleus. **B)** Model explaining active gene location in chromatin landscape (Tang et al., 2015). DNA transcription, and likely repair and replication, takes place in a vicinity of chromatin loops at TAD boundaries of decreased chromatin compaction. Images from (Cremer et al., 2015; Tang et al., 2015).

3.11 Microscopic methods to investigate chromatin organisation

In the following section I will briefly introduce several microscopy approaches commonly used to study the chromatin organisation.

3.11.1 Electron microscopy

Transmission electron microscopy (TEM) serves a gold standard for investigations of chromatin structure.It relies usually on few hundred nanometre-thick sections of a cell material.Typically Osmium ammine B is used to enhance chromatin contrast in electron density images. A very elegant example of TEM application to cell nuclei sections constitute cells undergoing myelopoiesis presented in **Fig. 10C**. In this case TEM revealed chromatin rearrangement of the chromatin from its initially diffused state to the dense layer at the nuclear periphery (Hübner et al., 2015).

3.11.2 Fluorescence microscopy image analysis

This simplest approach relies on fluorescent chromatin labelling, either via DNA binding dyes or histone proteins with e.g. GFP. Confocal microscopy is used to acquire high resolution images (ca. 250 nm resolution) and various image analysis tools can be applied e.g. based on dense cluster edge detection (Irianto et al., 2014) or on chromatin density classes distribution analysis (Popken et al., 2015). In addition through studying the distribution of chromatin associated proteins one can infer on chromatin state;following was demonstrated e.g. with a change to the distribution of histone H1 (Wojcik and Dobrucki, 2008) or redistribution of DNA-binding replication clamp (Trembecka-Lucas and Dobrucki, 2012). Examples are numerous.

3.11.3 Kinetics of DNase I chromatin digestion

Deoxyribonuclease I (DNase I) is a non-specific nuclease that cleaves DNA and releases di-, tri- and oligo- nucleotide products. Its molecular weight amounts to ~30 kDa. Thus it is plausible to assume that its penetration through chromatin will be rather limited (Bancaud et al., 2009). These two features of this enzyme have been decisive for its application in biochemical studies involving massive parallel sequencing (Boyle et al., 2008) as well as in microscopy of chromatin in situ in fixed cells with DNA labelled using a DNA-binding dye (Irianto et al., 2013). In case of the latter, DNase I of appropriately low concentration is added to the cells and DNA-bound dye signal is collected over time using a fluorescence microscope. Kinetics of the fluorescence signal decrease over time reflects chromatin compaction state; the more inclined the fluorescence decay is, the smaller compaction of chromatin can be expected.

3.11.4 Fluorescence recovery after photobleaching (FRAP) of chromatin associated proteins

FRAP is a technique based on fluorescence confocal microscopy platform. First, focused laser beam of high intensity is used to irreversibly bleach a small region of interest (ROI) of a fluorescently labelled sample of living cells (e.g. GFP). Subsequently, the signal intensity within ROI is monitored over a period of seconds to several minutes. If the molecule labelled is mobile and freely travel through the structure, fluorescence recovery within ROI will be very rapid and complete(as compared to the ROIs signal intensity prior the laser bleaching). However, if the molecule is immobile, e.g. at least permanently bound or trapped within a complex structure, the fluorescence recovery will proceed over a very long period of time and may be not fully accomplished. This versatile and fast technique was suggested to yield wealth of quantitative information on chromatin structure organisation in living cells with typically histone H3, H2B, H1

proteins and chromatin proteins just as HP1 or PCNA, all labelled using fluorescent proteins(Brown et al., 2006; Wojcik and Dobrucki, 2008;Trembecka-Lucas et al., 2013).

3.11.5 Fluorescence life time imaging of histone proteins

Fluorescence lifetime is a time needed for the number of excited fluorescence molecules to decay to 1/e of initial population number. Fluorescence lifetime can be affected by various factors including e.g. Foerster energy resonance transfer (FRET). Consequently measurement of fluorescence lifetime may serve to indirectly measure FRET. FRET relies on excited state energy transfer from a "donor" fluorophore to an"acceptor" fluorophore of another type in a proximity <10nm. Importantly an emission spectra of the first one needs to overlap with absorption spectra of the latter. This scheme was used to co-label the chromatin of living cells with genetically encoded histone H2B-EGFP, serving as a FRET donor, and H2B-mCherry as an acceptor (Llères et al., 2009). While chromatin is relaxed, these two species are randomly distributed along a chromatin fibre and FRET is unlikely to have a high efficiency. However, upon chromatin condensation, chromatin fibre undergoes compaction bringing two H2B species closer and, if only to the distance smaller than 10 nm, facilitating FRET. As a result fluorescence lifetime of a donor (H2B-EGFP) detectable with an appropriately equipped confocal microscope, undergoes a decrease.

3.11.6 Fluorescence correlation spectroscopy

The other useful biophysical tool to study the chromatin structure is called fluorescence correlation spectroscopy (abbreviated as FCS). It is based on a confocal microscopy platform and relies on measurements of fluorescence fluctuations over time collected from a diffraction limited spot where the excitation light is currently focused. Signal variation over time contains an information on the diffusing fluorescent probe that happened to localise to the excitation focus at the moment. Up to date FCS has been applied to a number of chromatin studies in living cells. For instance, it was used to study linker histone (H1-GFP) dynamics across a cell nucleus and revealed existence of subclasses of varied mobility (Bernas et al., 2014). The other elegant FCS-based study took advantage of a multi-scale fluorescence cross-correlation spectroscopy using line illuminating confocal microscope. In this study the authors demonstrated a varied mobility of inert GFP monomers (GFP_1), trimers (GFP_3) and pentamers (GFP_5) expressed intracellularlyin human U2OS cells(Baum et al., 2014).This study revealed that the chromatin constitutes a size-dependent barrier to intracellular factors and that this feature can be modulated using drugs such as trichostatin A.

3.12Introduction to ischemia

3.12.1 Ischemic disease

Blood is a fluid connective tissue and its fundamental role is to deliver nutrients and oxygen to other tissues of a body with simultaneous scavenging of metabolic by-products just as carbon dioxide or urea. Local tissueblood insufficiency, also termed as ischemia, leads to oxygen and nutrient deprivation and as a consequence may even result in death of an organism depending on type of affectedtissue. According to World Health Organisation ischemia is currently a leading cause of human death. Strikingly, its treatment strategy for all types of tissues remains still very deficient.

3.12.2 Specification of an injury in myocardial infarction

Among tissues that manifest the greatest treatment difficulties and most severe repercussions after ischemia, noteworthy,are the brain and the heart muscle (myocardium). Diseases associated with these two are called cerebrovascular accident (stroke) and myocardial infarction (heart attack) respectively. In most cases ischemia-related diseases develop as a result of a blood artery occlusion due to a retention of a so-called atherosclerotic plaques. In coronary heart disease (CHD, a most common among myocardial infarction) thisrelates to the blockade of coronary arteries responsible for blood delivery to the heart muscle.

An increased concentration of apolipoprotein B (a low-density lipoprotein, LDL) can be already a cause of atherosclerotic plaque formation leading to CHD. More often, however, the disease originates from multiple sources among which the most prevalent include smoking, diabetes mellitus, genetic background,andsex (predominance for males)(Bentzon et al., 2014). Noteworthy, individuals with very low LDL levels generally do not develop atherosclerosis irrespectively of the other factors(Steinberg et al., 2008). An initial disease mechanism brought about by LDL may involve other casual effects in later stages of the disease progression:macrophage foam cell formation, inflammatory cell recruitment, calcification, lipopoprotein recruitment, and thrombosis (thrombocyte deposits formation). Once a plaque detaches from the artery wall, it may block a lumen of smaller vessels therefore limiting the blood flow to the respective part of a muscle leading to e.g. myocardial infarction as a consequence of ischemia.

Myocardium is very susceptible to ischemia due to its profound oxygen and nutrient demand typical for metabolically active tissues. In the absence of oxygen an oxidative phosphorylation is terminated leading to mitochondrial membrane depolarisation, ATP depletion,and subsequently causes a myocard contraction halt(Hausenloy and Yellon, 2013). In the absence of oxygen, cellular metabolism switches to anaerobic glycolysis resulting in pH decrease due to lactate accumulation and in parallel Ca^{2+} overload as a consequence of losing a balance between action of various intracellular ion pumps(Hausenloy and Yellon, 2013). If ischemia prolonged, all these effects inevitably lead to cell death and impossibility to rapidly restore the contraction capability of constantly operating heart muscle.

While the concentration of oxygen in the air amounts to 21.1% (160 mmHg) in organs, it reaches a value several times smaller depending on oxygen consumption, e.g. only 3.8% (29 mmHg) in a muscle(Carreau et al., 2011). Upon blood insufficiency the level of oxygen becomes lower than aforementioned physiological concentration (hypoxia) and general hypoxic stress response is fired. This involves translocation of cytoplasmic HIF1α (hypoxia inducible factor) transcription factor to the cell nucleus followed by dimerisation with constitutively expressed nuclear HIF1β. Under normoxic conditions HIF-1α is hydroxylated on proline 402 and/or proline 564 residues by Prolyl hydroxylase domain that necessitates inter alia O_2 as a substrate. This modification facilitates HIF-1α ubiquitination and degradation by a proteosome (this in total involves the action of several factors). Under hypoxia this oxygen-dependent process is believed to be disabledthus increasing HIF1α stability and abundance of functionally active HIF-1 transcription factor (for review see (Semenza, 2009)). HIF-1 serves as an activator of genes involved in erythropoiesis (red blood cells formation), angiogenesis (blood vessel development), glucose transport, andglycolytic enzymes. All have a priority in expression over the other genes involving the active ATP consumption.

3.12.3 Reperfusionfollowing a myocardial infarction

Despite all processes involved in ischemic injury and active response to decreased oxygen level also the moment of blood restitution (reperfusion) needs to be taken into account in a therapy design as it may independently lead to death of cells that survived preceding ischemia.Hence, e.g. myocardial infarction should always be discussed in the context of ischemia-reperfusion (IR)events.

It has been shown that reperfusion alone may bear responsibility for up to 50% of the total myocardial infarct size (Yellon and Hausenloy, 2007), hence, it constitutes an important target for IR therapy. After an abrupt restoration of native conditions, the cell experiences detrimental effects of oxidative burstleading to e.g. lipid and protein peroxidation (Hausenloy and Yellon, 2013).Succinate has been identified as a metabolite likely driving ROS production during reperfusion (Chouchani et al., 2014).Furthermore, during reperfusion physiological pH in the muscle tissue undergoes a rapid restoration what has an effect on mitochondrial permeability transition pore (MPTP) opening(Lemasters et al., 1996). This in turn results in hypercontracture for first few minutes of reperfusion due to Ca^{2+} flux. Interestingly, in animal ischemic heart model, reperfusion with acidic buffers decreased infarct size (Qian et al., 1997).In addition, reperfusion of some tissue regions is impaired due to vessel obstruction as cardiomyocyte swell and capillary compression by endothelial cells. Currently there is no method available to treat the latter; however, a number of ideas to decrease the effect of reperfusion are existent.

3.12.4 Epigenetic contribution to ischemia-reperfusion in myocardial infarction

Hypoxia is known to activate specific histone modifications at gene promoters but in several instances was also shown to alter a global epigenetic landscape. Moreover, molecular oxygen is necessary for functioning of Jumonji dioxygenase domains crucial for operational status of histone demethylation. This in turn, is reflected in global increase in methylation of H3K4, H3K9, H3K27, and H3K36 histone residues (Shmakova et al., 2014). Moderate hypoxia is also known to decrease H3K9 acetylation and increase H3K9 dimethylation (Chen et al., 2006).

Interestingly, not only hypoxia but also reperfusion has a pronounced effect on epigenetic landscape alteration in myocardium. It has been reported that distinct genes experience changes in histone modifications (Webster et al., 2013). Also, an addition of histone deacetylase inhibitors just as trichostatin (TSA) at the onset of reperfusion has been proven to minimise infarct size by half and limit the induction of HIF1 (Granger et al., 2008). This altogether provides an incomprehensible picture of epigenetic component involved in IR pointing to a putative alteration to chromatin structure.

4. Objectives of the work presented in the thesis

In this work the following aims were indicated as crucial:

1) Advance single molecule localisation microscopy of the DNA. Test previously established methods anddevelop new techniques based on single molecule imaging of the DNA dyes directly binding to the chromatin of eukaryotic cells by:
    - applying a phenomenon of DNA-binding Hoechst,DAPI, and VybrantViolet UV-induced photoconversion to their green-fluorescent-emitting forms
    - investigating the mechanism of binding activated localisation microscopy (BALM) of DNA dyesvia studying various chemical conditions affecting the chemistry of the dyes, their interaction with the double stranded DNA as well as manipulate stability of DNA double-helix. Overarching goal here is to further extend BALM to imaging eukaryotic cell nuclei.

2) Challenge the validation of inactive-/active- nuclear compartment model of chromatin organisation by means of newly developed DNA super-resolution imaging methods (point 1).

3) Apply imaging techniques developed in point 1 to investigate the effect of an environment mimicking conditions of blood insufficiency on the chromatin structure in a mouse myocardiac cell model. Ascertain an effect of various compounds indicated as clinically promising on ischemic chromatin architecture.

The aims have been achieved in a series of 4 scientific publications that are included in the results section (not chronologically). In the **Section 11** all associated publications are listed.

5. Materials and Methods

5.1 Cell culture

For experiments on ischemia HL-1 cardiac muscle cell line was used: the first cardiac cell line able to maintain its differentiated phenotype over the serial passages(Claycomb et al., 1998). Among the features that HL-1 line retains are: the gene expression profile similar to that of adult atrial myocytes, the ability to contract in a cell culture, the distribution of the cardiac-specific markers just as desmin, sarcomeric myosin, and atrial nutriuretic factor, and confirmed existence of myofibrils in the cytoplasm (Claycomb et al., 1998). These cells are a kind gift from Prof. William Claycomb, LSU New Orleans School of Medicine, USA. HL-1 cells were cultured on tissue plates coated with 0.002% gelatine and 0.005mg/ml fibronectin (F-1141, Sigma-Aldrich) and in 37^{o}C / 5% CO_2 / 95% humidity in a Claycomb culture medium (51800C, Sigma-Aldrich) supplemented with 10% fetal bovine serum (FBS, F2442, Sigma-Aldrich), 2 mM L-glutamine (17-605E, Lonza) and 0.1 mM norepinephrine. Cells were passaged every 3 days once full confluency reached.

In order to influence chromatin structure while HL-1 cells in oxygen and nutrient deprivied conditions (OND), following pretreatments were used: i) 5 μM trichostatin A (HDAC inhibition) for 1h and ii) 100 or 200 μM difluoromethylornithine (ornithine decarboxylase inhibitor) for 48h, both prior to OND treatment.

To investigate DNA staining for super-resolution microscopy we used HeLa cervical cancer cells and VERO-B4African green monkey kidney fibroblast cultured in following media: Dulbecco's Modified Eagle's Medium (BE12-614F, Sigma-Aldrich) with phenol red (first) and RPMI w/o phenol red (32404-014, Gibco, latter), both supplemented with 10% FBS and 100 U/ml penicillin and 0.1 mg/ml streptomycin (Gibco). For cell passage 0.25% trypsin-EDTA (25200-056, Lifetechnologies, UK) was used. For HeLa cells stably transfected with H2B-mCherry (kindly provided by IMB-Mainz Core Facility Microscopy) and H1.1-GFP (obtained from Dr. Mirosław Zarębski, Jagiellonian University, Kraków) same culture conditions were used as for regular HeLa cells.

Hodgkin's lymphoma cell line HDLM-2 was prepared for microscopy as previously reported with few modifications (Righolt et al., 2014). After formaldehyde fixation cells were attached on poly-L-lysine coated coverslips, permeabilised with 0.1% TX-100 for 10 min, RNase treated in 37^{o}C overnight same as mentioned above. These cells were provided by Prof. Sabine Mai, University of Manitoba, Canada and Prof. Dr. Hans Knecht, Universite de Sherbrooke, Quebeck, Canada. Neuroblastoma Neu-2a (ATCC® CL-131™) cells (obtained from Dr. V. Tiwari, IMB Mainz, Germany) were cultured in 37^{o}C and high humidity in Dulbecco's modified Eagle medium supplemented with L-glutamine (Gibco), nonessential amino acids (11140050, Thermofisher), and 10% FBS (Gibco, Germany) and penicillin and streptomycin.

5.2 Oxygen and Nutrient Deprivation (OND) protocol for ischemia model

Living HL-1 cells were washed twice with phosphate-buffered saline (PBS, BE17-512F/12, Lonza) and placed in a hypoxia chamber (Whitley Hypoxystation H35) providing a following atmospheric conditions: 1 % O_2,5% CO_2, 94 % N_2 at 37 °C and 70–85 % humidity. In order to simulate the ischemic environment, cells were incubated in a medium containing 115 mM NaCl, 12 mM KCl,

1.2 mM $MgCl_2$, 2 mM $CaCl_2$, 25 mM HEPES (H3375, Sigma-Aldrich) and 5 mM 2-Deoxy-D-glucose (D8375, Sigma-Aldrich), all pre-equilibrated to 1 % O_2 for ~1h in hypoxia station (inspired by a recipe of (Vivar et al., 2012)). OND treatment lasted for 1 hour and was followed by a wash with PBS and return to the Claycomb medium under normoxic conditions. This continued for 0 (OND), 5, 15, 60 and 240 minutes following OND. Such an abrupt recovery was designed to mimic reperfusion after the ischemic event cessation as would happen in a medical treatment. Non-recovered OND-treated cells were harvested and fixed in a hypoxic atmosphere. Untreated cells were kept under normal culture conditions until fixation.

5.3 Immunofluorescent staining protocols

Cells were grown on gelatine / fibronetctin coated cover-slips inserted in six-well plates (2 ml of Claycomb or OND buffer was used). Cells were then washed twice with PBS, fixed in 1 ml ice cold methanol (8388.5, Carl Roth) for 10 min, washed with PBS and permeabilised with 1 ml PBS containing 0.3% Triton X-100 (T8787, Sigma-Aldrich) and 0.3% Tween-20 (P1379, Sigma Aldrich) for 10 minutes at room temperature (RT). This was followed by 1h incubation with 1 ml blocking buffer containing 5% bovine serum albumin (BSA) and 0.1% Tween-20, all in PBS, RT. Cells were then incubated with anti-H3 (ab1791, Abcam, 1 μg/ml), anti-H3K14ac (5275s, Cell Signalling, 1:500), anti-Lamin B1 (ab16048, Abcam, 1 μg/ml) antibodies overnight at 4 °C in 500 μl blocking buffer. Subsequently, samples were washed three times with 1 ml PBS containing 0.1% Tween-20 and incubated with Alexa 488 (A-11034, Invitrogen) or Alexa 647(A-21245, Invitrogen) conjugated secondary antibody (2 μg/ml) for 1 h in 1 mlPBS containing 0.1% Tween-20. Then, samples were washed trice using the same buffer.

5.4 Confocal microscopy

For fluorescence intensity measurements of dye DNA-association and DNA-unbinding over time in an entire cell nuclei we used an inverted Leica SP5 Confocal microscope equipped with 63x/1.4 NA objective lens and a Hybrid detector suited for photon counting (Leica Microsystems, Germany). The 488 nm line of an argon laser was used for excitation and fluorescence of DNA bound YOYO-1, YOPRO-1, and PicoGreen (all purchased from Lifetechnologies except PicoGreen which was a kind gift from Prof. Sabine Mai, Cancer Care Manitoba, Winnipeg, Canada) detected in the 490 - 560 nm emission range; 512 x 512 pixel images from 5 - 6 fields of view. The pixel size, object plane equivalent corresponded to 303 nm. Measurements were performed on 3.7% formaldehyde fixed (for 10 min) and 0.5% Triton X-100 (10 min) treated HeLa cells grown on 500 μl μ-slide 8-well chambers with a microscopic-glass bottom (IBIDI, Germany). All cells were treated with 0.5 U/ml RNase A and 20 U/ml RNase T1 (AM2286, Ambion, USA) in 37^{o}C overnight to diminish DNA non-related signal. For dye dissociation studies cells were stained with 12 nM YOYO-1 for 1h, 1:10,000 PicoGreen for 40 min, or 30 nM YO-PRO-1 for 40 min (500 μl volume). Cells were washed with PBS overnight to ensure lack of freely diffusing dye in the solution that could potentially bind to the chromatin due to e.g.possible enhanced chromatin permeability. For dye association studies, an initial 'background' image was acquired in 250 μl of PBS (Gibco) and this was followed by the addition of 250 μl of 2x concentrated dye solution. Images were acquired every 2 min. For the dye dissociation assay we used the same method with few exceptions: for studies on pH dependence, an initial image was performed in 100 μl distilled

water that wasthereafter replaced with a buffer of a given pH; these images were acquired every 4 min for 30 min.
To investigate achange to the overall chromatin structure inflicted by different SMLM-imaging media (**Publication 3**)we used 3D confocal microscopy followed by deconvolution (SVI 3D Huygens Deconvolution & Analysis Software, Scientific Volume Imaging B.V., Hilversum, Netherlands). HeLa cells were grown as indicated above on 8-well slides, incubated for 12 min with 10 μM 5-ethynyl-2'-deoxyuridine (EdU), and fixed with 3.7% formaldehyde followed by 0.5% TX-100. "Click-it" Alexa 555 fluorophore conjugation was performed according to manufacturer's instructions (Lifetechnologies). This approach enables the 3D imaging of chromatin-bound reference points before and after a hypothetical structural change inflicted by an imaging buffer. Confocal images were acquired with a voxel size of 60 nm in an object plane and with a z-stepof 130 nm. Next, using ImageJ plugin 3D Foci Picker calculating centres of fluorescence gravity maxima were found to identify the exact 3D position of these foci. Each data stack was separately evaluated and visually inspected for the quality of maxima hits. Further, the resulting list of foci coordinates was used to calculate nearest neighbour distances in MATLAB (Mathworks). 5 cells were evaluated per condition before and after subjecting them to the acidic treatment including following conditions: (i) 20 min of treatment with a buffer of pH=3.6, (ii) 4h incubation with 0.5 mg/ml glucose oxidase (GOX, G2133, Sigma-Aldrich), 40 μg/ml catalase (CAT, 850187, Sigma-Aldrich) and10 % (w/v) glucose prepared freshly, (iii) 20 min treatment with same GOX/CAT buffer prepared 7h before. In order to quantitatively express a change to chromatin structure we subtracted the mean value after treatment from the respective mean value of the same cell prior to the treatment. The outcome of a negative value reflects shrinking whereas the positive outcome reflects nuclear structure expansion. Nuclear volumein these 3D CLSM images was calculated by determination of a convex-hull using foci 3D coordinates in MATLAB. In order to calculate the change in the cell nuclear volume (Δ) a following formula was used: $\Delta=1-V_{before}/V_{after}$, where V corresponds to the estimated volume.

5.5 Fluorescence recovery after photobleaching (FRAP)

In order to infer on chromatin dynamics in live cells, FRAP experiments on H2B-mCherry and H1.1-GFP histones stably expressed in HeLa cervical cancer cells were performed (for other details on this methodology see **section 3.11.4**). Cells seeded at low confluency of ~15% were subjected to the OND and embedded in 200 μl of either OND buffer or original culture medium in case of untreated cells. Subsequently, coverslips were fixed to the glass slide with a cavity and sealed using a Picodent Twinsil fixative (1300 1000, Picodent) preventing from any further oxygenation. FRAP measurements were performed in 37°C for no longer than 1h 15min and this time was strictly monitored.

For mCherry FRAP acquisitions following settings were used: bleaching was carried out by one 256 x 256 pixel scan in 2 x 2 μm^2 ROI with 80% of 561 nm laser line, after bleaching images were acquired every 0.328 s with a resolution of 256 x 256 pixels (pixel size corresponding to 96.5 nm) with an excitation of 6% of 561 nm laser line, mCherry emission was collected between 602 – 711 nm and measured in 2 x 2 μm^2 ROI.

For GFP FRAP acquisitions following settings were used: point bleaching was carried out by parking the focused 488 nm laser line for 100 ms (80 % power), after bleaching images were acquired every 1 s with a resolution of 256 x 256 pixels (pixel size corresponding to 96.5 nm) with

an excitation of 13% of 488 nm laser line, mCherry emission was collected between 500 – 591 nm and measured in 1.5 μm in diameter circular ROI.

Three images were acquired prior bleaching. More than 10 cells were measured for each group. FRAP data processing was carried out as previously described in (Trembecka-Lucas et al., 2013) with a following modification: every individual measurement was further processed using ImageJ plugin StackReg, *http://bigwww.epfl.ch/thevenaz/stackreg/*(P. Thévenaz, U.E. Ruttimann, 1998). Rigid body function was used to correct for cell movement during the measurement with respect to the first frame. Curves were averaged and presented with a standard deviation as an error estimator.

5.6 DNase I digestion susceptibility assay

HL-1 cells were seeded in 8-well μ-slide (IBIDI) at the density of $0.01x10^6$ per well and grown for two days. They were then fixed using 4% PFA (16005, Sigma-Aldrich) on ice for 15 min, permeabilised with 0.3% TX-100 for 10min and 30 min stained using 5 μM DNA binding dye DRAQ5 (ab108410, eBioScience). Samples were mounted on to the confocal microscope stage (see **section 5.4**). Each well contained 250 μl respective DNase buffer and twice concentrated DNase I solution was added (M0303S, New England Biolabs, final solution 5 U/ml). Fluorescent signal of DRAQ5 was monitored over time with following parameters: 7% 633 nm HeNe laser excitation, fluorescent collection using HyD detector between 643 and 749 nm, 512 x 512 images were acquired with 600 Hz scanner speed, 2AU confocal pinhole width, pictures were taken every 4min. Fluorescent decays were analysed using ImageJ plugin Time Series Analyzer (*https://imagej.nih.gov/ij/plugins/time-series.html*). Fluorescent decays from separate cells in the field of view were averaged and presented with standard deviation.

5.7 Super-resolution single molecule localisation microscopy (SMLM)

5.7.1 SMLM sample preparation

In all cases the cells were grown on 20 x 20 x 0.017 mm^3 microscopy coverslips. After 8 min fixation with 4% formaldehyde and following permeabilisation using 1% Triton X-100 (5 minutes), the VERO-B4 cells were washed with PBS and incubated with a 1 ml 0.2 mg/ml, 37^{o}C RNase A for at least 1h. Next, the cells on cover-slips were stained for 30 min with 1 ml water solution of Vybrant®DyeCycle™ Violet (VdcV, V35003, LifeTechnologies) at the concentration range 10 nM - 5 μM. Subsequently, they were washed with PBS and embedded in an imaging buffer containing 90% glycerol (G5516, Sigma-Aldrich), 10% (w/v) glucose (G0350500, Sigma Aldrich), and0.5 mg/mlglucose oxidase (GOX) and 40 μg/ml catalase (CAT). Similar procedure was used for Hoechst 33342, Hoechst 33258, and DAPI staining in HeLa cells;concentrations used were as follows: 0.1 μg/ml, 0.2 μg/ml, and 0.1 μM, respectively. For chromosome spreads a mitotic block on HeLa cells was carried out with 126 μM vinblastine for 4 h followed by a wash with medium. Next, the medium containing mitotic cells was collected and spinned down (150 g, 5 min). The cell pellet was resuspended in 5 ml 75 mM KCl water solution for 10 min and subsequently, we added 5 ml fixative (3: 1 glacial acetic acid: methanol) and centrifuged them again (150 g, 5 min). Finally, the cells were re-suspended in ice cold fixative. This step was repeated at least 4 times. Such cell suspension with 6 ng/ml Hoechst 33258 was dropped on a

cover-slip in horizontal position and air-dried until the fixative evaporated. DNA fibre analysis was attempted utilising a previously published protocol of (Schwab and Niedzwiedz, 2011).

For DNA strucuture fluctuation assisted BALM (*f*BALM) cells were stained with 12 nM YOYO-1 (1ml) for ~1h followed by an extensive wash. PBS based imaging buffer was used and contained 0.5 mg/ml glucose oxidase, 40 µg/ml catalase and 10% (w/v) glucose with an initial pH=7.6 decreasing over time down to pH~3.7. As a control we used an enzymatic oxygen scavenging system that maintains a stable pH even over a period of several hours (Swoboda et al., 2012). It is based on 5 U/ml glucose pyranose, 57 µg/ml catalase, and 10% (w/v) glucose. A cover-slip was embedded in ~25 - 30 µl of the same imaging buffer and fixed to the glass slide using a Picodent Twinsil cement. For this study we chose methanol-based fixation, as previously the DNA was reported to be slightly more resistant to denaturation while formaldehyde used (Traganos et al., 1975).

For super-resolution imaging of replicated DNA HL-1 cells were treated for 10 min with 10 µM EdU and fixed with 3.7% formaldehyde. Then,conjugation by means of the "click-it" reaction with Alexa 488 was performed according to the protocol of the manufacturer (Life Technologies). Measurements were carried out in glycerol-based ProlongGold (Lifetechnologies) as a mounting medium, as in our hands this medium reduces the extent of multiple blinking and increases Alexa 488 photoncount. Immunofluorescence against histone H3(Alexa 647) was performed same as described in previous section (**section5.3**). In this case, an imaging buffer based on PBS, GOX, and CAT was used, and contained 50 mM MEA as a switching agent known to induce a formation of a non-fluorescent long-lived radical state under exposure to an exciting light (Dempsey et al., 2009; Vogelsang et al., 2008).

5.7.2 Measurements

Super-resolution experiments were performed on a custom built widefield microscope described in detail in supplementary materials to**Publication 1**. Briefly, the microscope was equipped with air-cooled 12 bit CCD camera (SensiCam QE, PCO imaging) and a 63x, 1.4 NA oil immersed objective. Pixel size object plane equivalentcorresponded to 102 nm. A 491 nm diode laser was used for excitation (Calypso 05 series, Cobolt, Sweden) with an intensity in the sample plane of 1 - 2 kW/cm^2. This was achieved through a collimation ofa laser beam. For Hoechst and DAPI an additional 405 nm illumination (~2 W/cm^2) was used to accelerate photoconversion to the green-emitting form.Fluorescence of Hoechst, VybrantViolet, and YOYO-1 was captured after passing through a 525/50 nm bandpass filter (Chroma Technology Corp.) and through 630(90) filter (FF01-630/92, Semrock) for Hoechst dyes only. 20,000 - 30,000 frames with an integration time of 20 ms (YOYO-1), 65 ms (Hoechst, DAPI), and 50 ms (VybrantViolet) were acquired and converted into 16-bit .tiff stacks. For conventional image of imaged structure, typically three images prior to a SMLM acquisition were acquired and averaged for a better quality. For EdU-Alexa 488 labelled cells, 3,000 - 5,000 frames with 50 ms camera integration time were acquired. For H3-Alexa 647 and Lamin B1-Alexa 647, 25,000 frames with 25 ms camera integration time were acquired; ~2 kW/cm^2 647 nm diode laser intensity was used for excitation (LuxX, Omicron, Germany).

5.7.3 Data analysis and visualisation

In order to reconstruct single molecule localisation images we used fastSPDM updated MATLAB-based software (*https://code.iri.uni-frankfurt.de/trac/microscopy*) (Gruell et al., 2011). We found that it performs better on noisy data with conceivable out-of-focus background and such a situation is usually encountered while SMLM of 3D intact cell nuclei is performed. Individual molecule signals of peak intensity exceeding 3x noise standard deviation were analysed (here a simplified Poisson noise distribution was assumed as a CCD camerawas used). Single molecule signals appearing in subsequent frames were merged if they were localised closer than 2x the average localisation precision (yielding 95.4% confidence assuming Gaussian localisation precision distribution). In order to eliminate overlapping signals and strong out-of-focus signals, both affecting adversely the final image resolution (Burgert et al., 2015), approximately 30% of single molecule localisations were removed based on their (large) point spread function width. Drift correction was implemented via a cross-correlation analysis between intermediate reconstructions from typically 1,000 frame samples. After interpolation of discrete values, the list of single molecule x and y positions was altered according to the frame index. As a result of correction, the standard deviation of less than 5 nm between sample images was obtainable for DNA-density images.

The structural resolution in the SMLM images as either estimated using a formulae by (Legant et al., 2016) introduced in a **section 3.4** or by a Fourier ring correlation (FRC) analysis using a custom written MATLAB program similar to the method described in (Banterle et al., 2013; Nieuwenhuizen et al., 2013). Single molecule localisation list was randomly split into halves and Fourier analysis was carried out for each separately. The correlation between their Fourier images was performed within concentric rings radially expanding from the 0^{th} frequency. A 1/7 experimental cut-off was used to read out the FRC resolution from the intersection with FRC polynomial fit (25^{th} order).

Chromatin density distribution analysis in our super-resolution images of DNA was done by binning the single molecule localisation data in a 60 x 60 nm^2 grid using a *hist3* MATLAB function. Histograms of the number of single molecules per square bin and their cumulative probability were calculated using Origin 8.6 software (OriginLab). We found that grid size of 20 to 100 nm yielded very similar results. For signal intensity periodicity in super-resolution images signal was measured using a line-intensity profiles followed by and autocorrelation analysis using`autocorr` MATLAB function.

Images of VybrantViolet and Hoechst were visualised using a gaussian blur with an average localisation precision (Vybrant) or respective localisation precision (Hoechst). However, gaussian rendering of SMLM data may lead to 1.41 loss in image resolution (Baddeley et al., 2010). In order to account for this downside, afollowing Matlab routine was implemented: it generates “Wigner-Seitz cells” for the DNA localisation map where “cell’s” signal intensity depends inversely on its area.Next, a random jittering of single molecule coordinates by 100 times within the respective localisation precision is carried out. Finally, all these images are jointly plotted in a final averaged reconstruction with a pixel size corresponding to 5 nm. This procedure slightly smoothens the image and hence helps to perceive structures. It is similar to a triangulation concept utilising rather triangles than Wigner-Seitz “cells”, it is not prone to generation of artefacts, and maintains linear proportion between image intensity and localisation density (Baddeley et al., 2010).

6. Results

The following section contains a series of publications published during the time-course of this work (not all that were published). First three comprise a general information on super-resolution DNA methodology development utilising the phenomenon of DNA-bound label photoconversion (**Publications 1 - 2**) as well as through studying the interaction of DNA-binding (intercalating) dyes with the DNA subject to structure instability in a presence of denaturing conditions (**Publication 3**). **Publication 4** elaborates on the effects of transient ischemia on chromatin architecture in mouse myocardiac HL-1 cells studied using aforementioned methodology as well as by a multiple other approaches. For a full list of publications of mine see **Section 11**, Associated publications.

6.1 Publication 1

Single molecule localization microscopy of the distribution of chromatin using Hoechst and DAPI fluorescent probes

Szczurek, Aleksander T.*, Prakash, Kirti*, Lee, Hyun-Keun*, Żurek-Biesiada, Dominika J., Best, Gerrit, Hagmann, Martin, Dobrucki, Jurek W., Cremer, Christoph, Birk, Udo
(*equal contribution)

Nucleus, 2014, Volume 5, Issue 4, DOI:10.4161/nucl.29564

Abstract:

Several approaches have been described to fluorescently label and image DNA and chromatin in situ on the single-molecule level. These superresolution microscopy techniques are based on detecting optically isolated, fluorescently tagged anti-histone antibodies, fluorescently labeled DNA precursor analogues, or fluorescent dyes bound to DNA. Presently they suffer from various drawbacks such as low labeling efficiency or interference with DNA structure. In this report, we demonstrate that DNA minor groove binding dyes, such as Hoechst 33258, Hoechst 33342, and DAPI, can be effectively employed in single molecule localization microscopy (SMLM) with high optical and structural resolution. Upon illumination with low intensity 405 nm light, a small subpopulation of these molecules stochastically undergoes photoconversion from the original blue-emitting form to a green-emitting form. Using a 491 nm laser excitation, fluorescence of these green-emitting, optically isolated molecules was registered until "bleached". This procedure facilitated substantially the optical isolation and localization of large numbers of individual dye molecules bound to DNA in situ, in nuclei of fixed mammalian cells, or in mitotic chromosomes, and enabled the reconstruction of high-quality DNA density maps. We anticipate that this approach will provide new insights into DNA replication, DNA repair, gene transcription, and other nuclear processes.

6.2 Publication 2

Localization microscopy of DNA in situ using Vybrant®DyeCycle™ Violet fluorescent probe: A new approach to study nuclear nanostructure at single molecule resolution.

Żurek-Biesiada, Dominika, **Szczurek, Aleksander T.**, Prakash, Kirti, Mohana, Giriram K., Lee, Hyun-Keun, Roignant, Jean-Yves, Birk, Udo J., Dobrucki, Jurek W., Cremer, Christoph

Experimental Cell Research, Volume 343, Issue 2, Pages 97-106, 2016,
DOI: 10.1016/j.yexcr.2015.08.020

Abstract:

Higher order chromatin structure is not only required to compact and spatially arrange long chromatids within a nucleus, but have also important functional roles, including control of gene expression and DNA processing. However, studies of chromatin nanostructures cannot be performed using conventional widefield and confocal microscopy because of the limited optical resolution. Various methods of superresolution microscopy have been described to overcome this difficulty, like structured illumination and single molecule localization microscopy. We report here that the standard DNA dye Vybrant®DyeCycle™ Violet can be used to provide single molecule localization microscopy (SMLM) images of DNA in nuclei of fixed mammalian cells. This SMLM method enabled optical isolation and localization of large numbers of DNA-bound molecules, usually in excess of 10^6 signals in one cell nucleus. The technique yielded high-quality images of nuclear DNA density, revealing subdiffraction chromatin structures of the size in the order of 100nm; the interchromatin compartment was visualized at unprecedented optical resolution. The approach offers several advantages over previously described high resolution DNA imaging methods, including high specificity, an ability to record images using a single wavelength excitation, and a higher density of single molecule signals than reported in previous SMLM studies. The method is compatible with DNA/multicolor SMLM imaging which employs simple staining methods suited also for conventional optical microscopy.

6.3 Publication 3

Imaging chromatin nanostructure with binding activated localisation microscopy using DNA structure fluctuations.

Szczurek, Aleksander T., Klewes, Ludger, Xing, Jun, Gourram, Amine, Birk, Udo, Knecht, Hans, Dobrucki, Jurek W., Mai, Sabine, Cremer, Christoph

Nucleic Acids Research, Accepted Manuscript, December, 2016

Abstract:

Advanced light microscopy is an important tool for nanostructure analysis of chromatin. In this report we present a general concept for Single Molecule Localisation Microscopy (SMLM) super-resolved imaging of DNA-binding dyes based on modifying the properties of DNA and the dye. By careful adjustment of the chemical environment leading to local, reversible DNA melting and hybridization, control over the fluorescence signal of the DNA-binding dye molecules can be introduced. We postulate a transient binding as the basis for our variation of binding-activated localisation microscopy (BALM). We demonstrate that several intercalating and minor-groove binding DNA dyes can be used to register (optically isolate) only a few DNA-binding dye signals at a time. To highlight this DNA single-to-double stranded structure fluctuation-assisted BALM (*f*BALM), we applied it to measure, for the first time, nanoscale differences in nuclear architecture in model ischemia with an anticipated structural resolution of approximately 50 nm. Our data suggest that this approach may open an avenue for the enhanced microscopic analysis of chromatin nano-architecture and hence the microscopic analysis of nuclear structure aberrations occurring in various pathological conditions. It may also become possible to analyse nuclear nanostructure differences in different cell types, stages of development, or environmental stress conditions.

6.4 Publication 4

A transient ischemic environment induces reversible compaction of chromatin.

Kirmes, Ina*, **Szczurek, Aleksander T.***, Prakash, Kirti, Charapitsa, Iryna, Heiser, Christina, Musheev, Michael, Schock, Florian, Fornalczyk, Karolina, Ma, Dongyu, Birk, Udo, Cremer, Christoph, Reid, George, (* equal contribution)

Genome Biology, 2015, Volume 16, Issue 1, Pages 246
DOI: 10.1186/s13059-015-0802-2

Abstract:

BACKGROUND: Cells detect and adapt to hypoxic and nutritional stress through immediate transcriptional, translational and metabolic responses. The environmental effects of ischemia on chromatin nanostructure were investigated using single molecule localization microscopy of DNA binding dyes and of acetylated histones, by the sensitivity of chromatin to digestion with DNAseI, and by fluorescence recovery after photobleaching (FRAP) of core and linker histones. RESULTS: Short-term oxygen and nutrient deprivation of the cardiomyocyte cell line HL-1 induces a previously undescribed chromatin architecture, consisting of large, chromatin-sparse voids interspersed between DNA-dense hollow helicoid structures 40-700 nm in dimension. The chromatin compaction is reversible, and upon restitution of normoxia and nutrients, chromatin transiently adopts a more open structure than in untreated cells. The compacted state of chromatin reduces transcription, while the open chromatin structure induced upon recovery provokes a transitory increase in transcription. Digestion of chromatin with DNAseI confirms that oxygen and nutrient deprivation induces compaction of chromatin. Chromatin compaction is associated with depletion of ATP and redistribution of the polyamine pool into the nucleus. FRAP demonstrates that core histones are not displaced from compacted chromatin; however, the mobility of linker histone H1 is considerably reduced, to an extent that far exceeds the difference in histone H1 mobility between heterochromatin and euchromatin. CONCLUSIONS: These studies exemplify the dynamic capacity of chromatin architecture to physically respond to environmental conditions, directly link cellular energy status to chromatin compaction and provide insight into the effect ischemia has on the nuclear architecture of cells.

6.5 Chromatin structure in OND can be affected

6.5.1 Histone dynamics in OND can be affected by inhibition of specific enzymes

In order to test the putative involvement of polyamines in chromatin compaction revealed by super-resolution microscopy of the DNA (**Publications3-4**), a following experimental design was conceived.

Ornithine decarboxylase (ODC) is an enzyme involved in polyamine metabolism; it catalyses decarboxylation of a product of urea cycle named ornithine to form putrescine (the shortest among polyamines). ODC inhibition can be performed using an ornithine analogue difluoromethylornithine (DFMO)(Raul, 2007): leading to an immediate decrease in putrescine and, after few hours, to a decrease in intracellular concentration of other polyamines just as sperimidine. Thus, we decided to treat HeLa cells stably expressing H1.1-GFP histone to study the effect of this inhibitor on chromatin dynamics using fluorescence recovery after photobleaching (FRAP).

Figure 12A demonstrates that the cells in OND suffer from decreased H1.1-GFP mobility as compared with untreated cells (in line with the results in **Publication 4**). Interestingly, DFMO treatment for 48h prior tothe OND treatment partially recovers the original mobile behaviour of histone H1.1-GFP and fully restores an immobile fraction in OND cells (final signal level for olive and orange curves). Whereas with FRAP the differences are clear, theconfocal microscopyimages alone are rather hard to interpret and provide very illusive hint to this chromatin change (data not shown).

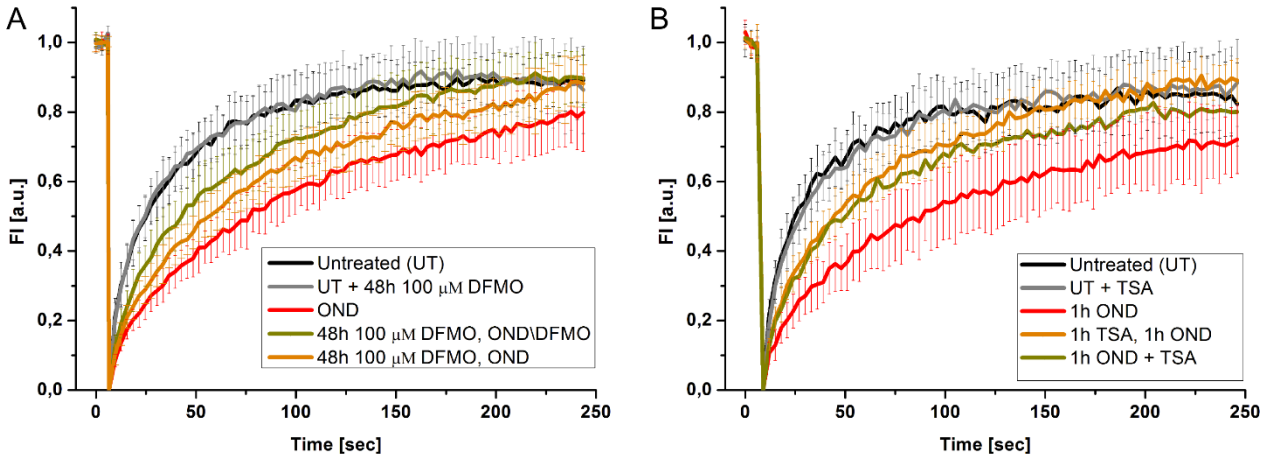

Figure 12. Inhibition of specific nuclear enzymes influences histone H1.1-GFP mobility in OND as revealed by FRAP analysis. Fluorescence recovery curves are presented. **A**) HeLa cells stably transfected with H1.1-GFP histone were subject to 48h 100 μM ornithine decarboxylase inhibitor difluoromethylornithine (DFMO) treatment and then to oxygen and nutrient deprivation protocol for 1h in the absence (orange) and presence (olive) of DFMO. For comparison fluorescence recovery curves for OND alone (red), untreated (black), and untreated with DFMO (grey) are presented.**B**) Fluorescence recovery curves for the cells subject to 1h treatment with 5 μM trichostatin A (TSA) inhibiting histone deacetylases prior to OND (orange), 1h prior and during OND (olive), OND (red), untreated (black), and the cells treated with TSA for 1h without OND (grey). Error bars, correspond to a standard deviation, more than 10 measurements per curve were carried out. FI – fluorescence intensity.

Chromatin structure is believed to be dependent on its epigenetic state and chromatin histone acetylation is considered as a permissive marker, i.e. histone deacetylase inhibition with a trichostatin A was demonstrated to increase penetration through the chromatin (Görisch et al., 2005) as well as to change its dynamics (Misteli et al., 2000). Consequently, we reasoned that it may constitute another degree of chromatin accessibility regulation that is potentially poly(cation)-independent thus constituting a potential tool to manipulate chromatin state in OND.

The 1h treatment with 5μM TSA turned out to have a strikingly similar effect to DFMO treatment; reduced dynamics of histone H1.1-GFP in OND was partially restored and immobile fraction reached the one of untreated cells (**Fig. 12B**). In turn, TSA treatment of cells not subject to OND did not significantly alter H1.1 mobility in our experimental setup.

In the next step we wondered if the effect of polyamine synthesis inhibition and the effect of chromatin hyperacetylation is additive, i.e. whether the effect can be strengthen when both DFMO and TSA applied simultaneously. We performed FRAP experiments in cells subject to DFMO treatment alone and DFMO treatment combined with TSA treatment same as described above. The result presented in **Figure 13** demonstrates that both treatments, independently of the presence of TSA, recover the chromatin dynamics to a very same extent (compare yellow and olive).This may suggestan action of both compounds on a similar chromatin feature that in both cases was addressed at its full capacity.

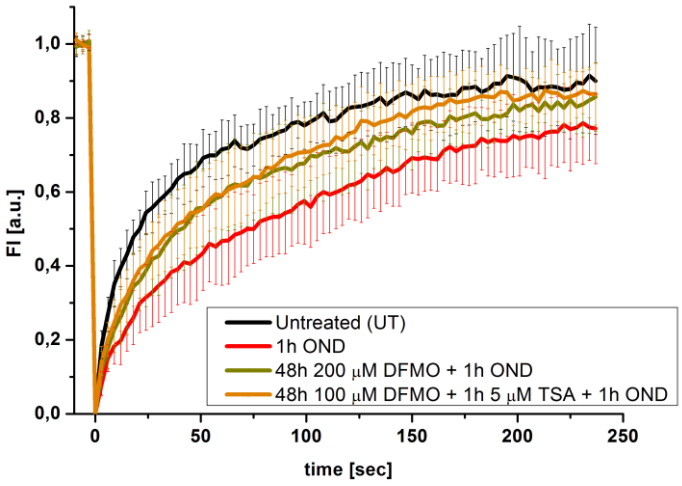

Figure 13. H1.1-GFP mobility in OND HeLa cells simultaneously treated with ornithine decarboxylase and histone deacetylase inhibitors.48h treatment with DFMO (olive) was combined with 1h treatment with TSA (yellow) and compared to untreated (black) and OND alone (red). Error bars, correspond to a standard deviation, more than 10 measurements per curve were carried out. FI - fluorescence intensity.

6.5.2 fBALM of cells treated with inhibitors of polyamine synthesis and histone deacetylation

FRAP experiments on H1.1-GFP provided feasibly quantitative information and helped in revealing a potentially preventive role of TSA and DFMO from OND-induced chromatin compaction. Nevertheless, histone H1.1 is only one of numerous proteins associated with chromatin and in principle its dynamic movement throughout the chromatin might be assumed to undergo an alteration upon change to the underlying chromatin structure (density). Therefore, we decided to investigate the latter by applying DNA structure fluctuation assisted binding activated localisation microscopy (*f*BALM) developed in the time-course of this work.

As expected, using *f*BALM high resolution imaging, chromatin condensation in OND became clearly seen; whereas untreated cells appear to have a sponge-like structure, the interchromatin compartment upon OND undergoes an expansion and integration (**Fig. 14**). In turn, in OND cells treated with TSA and DFMO, still the lion's share of chromatin remains in its compacted state. Although hard to judge, the overall impression suggests a slightly decreased compaction state. Confocal microscopy and cytometric analysis of immuno-labelled H3K14ac and H3K9ac confirmed hyperacetylated state of chromatin incells treated with OND and TSA (data not shown).

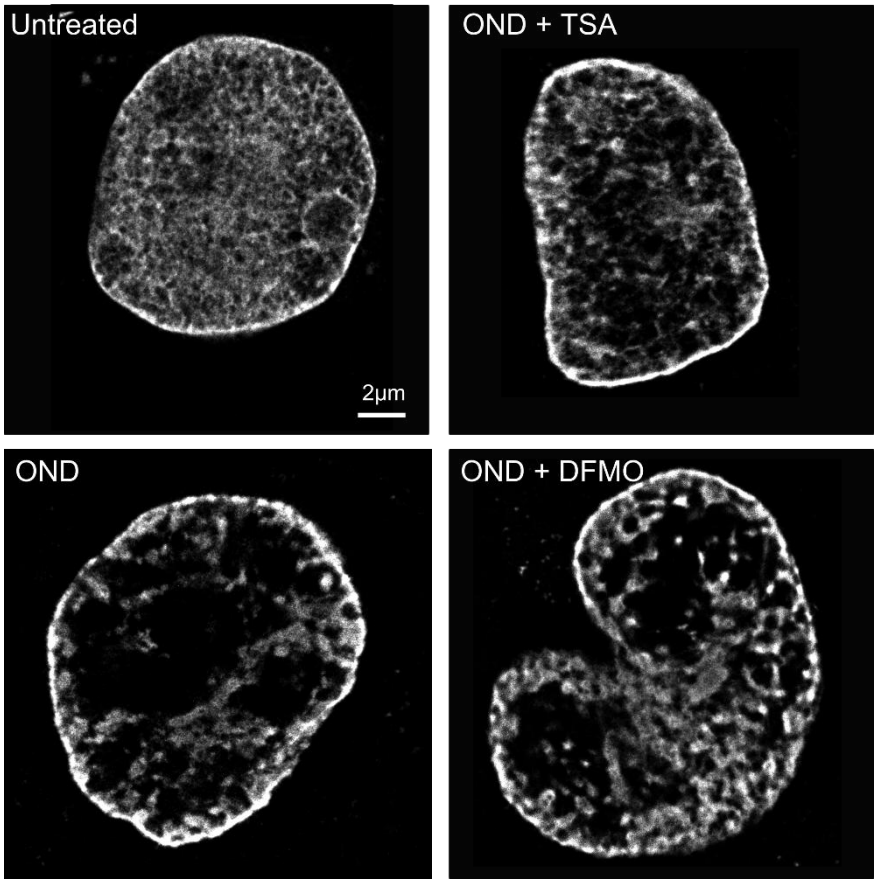

Figure 14. DNA structure fluctuation assisted binding activated localisation microscopy of HL-1 cells. The cells were a subject to oxygen and nutrient deprivation (OND) combined with 1h 5 µM trichostatin A (TSA) or 48h 100 µM difluoromethylornithine (DFMO) treatment. *f*BALM images demonstrate typical cell phenotypes. Scale bar corresponds to 2 µm.

7. Discussion

7.1 Methodological advancement of chromatin imaging using single molecule localisation microscopy

In this work two novel approaches to visualise chromatin at enhanced resolution were presented. Both rely onusage of directly binding DNA-dyes, single molecule fluorophore localisation, and non-classical mechanisms of fluorescence photoswitching involving no formation of a radical state of a fluorophore(Dempsey et al., 2009; Heilemann et al., 2008; Vogelsang et al., 2008; Dempsey et al., 2009). Both of these methodological advancements contribute substantially to broadening the knowledge on novel mechanisms of photoswitching and extend the application range of single molecule localisation microscopy to cell nucleus.

7.1.1 SMLM using photoconversion of Hoechst and VybrantViolet dyes to their green-emitting forms

From the methodological point of view this technique (**Publications 1** and **2**) bears a strong resemblance to photoactivated localisation microscopy (PALM)(Betzig et al., 2006)typically relying on photoactivatable or photoconvertible fluorescent proteins (FPs). In this approach, however, FPs were not used but instead low molecular weight dyes from (bis)benzimidazole family were chosen. Typical methodological scheme is based on light-induced (say "photoconverting" wavelength 1) conversion of very few, single molecules of a fluorophore to a distinct spectral state excitable witha separate wavelength(say "exciting" wavelength 2)and fluorescing in a distinct part of the spectrum. This way, by simultaneous or sequential illumination with wavelengths 1 and 2 along with insertion of an appropriate emission filter, one separates these few isolated signals of photoconverted form that can be localised in space using SMLM principles (for details see **section 3.4**).

In the approach presented in this work cellular DNA was labelled with DAPI or Hoechst dyes and subsequently exposed to a very low 405 nm illumination (I_p~ W/cm^2, "photoconverting") together with high intensity 491 nm illumination (I_e~ kW/cm^2, "exciting"). Whereas these dyes typically emit in blue range of the visible spectrum(approx. 450 – 500 nm), here the fluorescence was detected between 500 – 600 nm. This enabled spectral isolation of single fluorescing molecules of the green-emitting forms of these DNA-bound dyes. Constant "photoconverting" 405 nm illumination would enable continual replenishment of the green-emitting form that upon high "exciting" 491 nm illumination would fluoresce and subsequently undergo irreversible photobleaching (for further details see**Publication 1**).This technique was further simplified by using a VybrantViolet dye that would undergo aspontaneous photoconversionupon illumination with high intensity 491 nm light (see**Publication 2**).

Although, this approach was successfully applied to super-resolution imaging of cell nuclei as well as pachytene chromosomes (Prakash et al., 2015) with a resolution below 100 nm, one needs to be aware of two major limitations: (i) relatively high fluorescent background during the single molecule acquisition and (ii) rather faint single molecule Hoechst or VybrantViolet signals.

The first issue likely stems from the fact that 405 nm illumination excites also a native standard form that has a broad emission spectrum substantially overlapping with emission spectrum of the

green-emitting form (See **Publication 1** for more details). In addition epi-illumination used here results in excitation of the entire nuclear volume further increasing a background level. Approaches to decrease the fluorescent background and improve signal-to-noise ratio in measurements of 3D structures are existent and arethoroughly discussed in a following **section 7.1.2**. In case of photoconvertible DNA dyes, one idea is to decrease the staining concentration and simultaneously the number of signals appearing per measurement frame at the expense of a measurement time. This is rather impractical as this way the measurement time may exceed a practical range. Further study on the mechanism of photoconversion may however improve its efficiency and potentially maintain a decent single molecule signal number per frame despite of low DNA dye concentration used.

Low photon number emitted from single photoconvertible DNA dye molecules may be a result of only a moderate fluorescence extinction coefficient in particular low for DAPI (see **Table. 1, section 3.6** for details). This notion was reflected in SMLM images where DAPI signals were indeed the dimmest. These coefficient values however relate to the original, standard forms of these dyes and not the photoconverted ones. Nevertheless, Hoechst and DAPI dyes are known to have an increased quantum yield in low pH (Cosa et al., 2001) which simultaneously induces conversion to the green emitting form (Żurek-Biesiada et al., 2013, 2014) yielding a potential solution to the second issue.Although, this may elevate background originating from the standard forms. This has not been tested in this study.

Worth noticing is a remarkable role of glycerol in successful SMLM of photoconvertible DNA dyes (see supplementary materials to**Publication 1**). Importantly, it has been already used previously in DNA-dye study to account for extremely low quantum yield of PicoGreen in a solution (Dragan et al., 2010). Authors suggested a contribution of intramolecular dynamics to energy dissipation of the excited state of PicoGreen. It experiences 1070x quantum yield increase upon DNA binding and interestingly, for Hoechst and DAPI these values amount to only 13x and 18x respectively (see **Table 1**, **section 3.6**) suggesting either that these dyes have already a high quantum efficiency while in a solution (in fact it amounts to as much as~0.019, (Cosa et al., 2001)) or optionally that DNA alone does not protect Hoechst and DAPI well from non-radiative de-excitation. The latter speculation is supported by the fact that SMLM of DNA-bound Hoechst 33258 in glycerol alone gave 5x higher density of single molecule localisations than PBS (see supplementary materials to**Publication 1**). An addition of oxygen scavenging system to glycerol resulted in further 200x improvement.

Our preliminary experiments with single DNA fibres stained with Hoechst 33258 (data not shown) yielded rather poor linear localisation density suggesting that photoconversion constitutes rather relatively rare process and, as it is UV-induced, its efficacy is likely reduced by competing photobleaching of a standard form. Although disadvantageous in single DNA fibre analysis due to low specificity, this feature is quite useful to image overall DNA distribution in the cell nuclei as a single DNA-binding dye molecule can be discriminated from thousands to millions of others in this complex 3D arrangement. Fourier ring correlation analysis demonstrated that this group of nuclear chromatin imaging methods yields a resolution below 100 nm which constitutes roughly 2.5 fold improvement as compared with conventional fluorescence microscopy methods. Nevertheless, due to aforementioned issues with background and low brightness of Hoechst and VybrantViolet, an extension to 3D imaging e.g. based on astigmatism (Huang et al., 2008) seems unrealistic.

7.1.2DNA structure fluctuation assisted binding activated localisation microscopy (fBALM)

In this work a previous binding activated localisation microscopy (of isolated and bacterial DNA (Schoen et al., 2011)) was adapted for the first time to a nuclear chromatin imaging (see**Publication 3**). This *f*BALM methodology relies on moderate nuclear membrane permeabilisation followed by DNA-binding dye (YOYO-1) delivery inside the cell nucleus prior to a single molecule localisation measurement (for scheme see **Fig. 15**). Once cells are labelled, the pH is gradually decreased over couple of hours to slowly introduce instability to the dsDNA. This takes place with simultaneous maintenanceof native chromatin configuration. In this experimental setup pH eventually reaches a value of ~3.7, i.e. value that introduces reversible conformational changes to the dsDNA via ionisation of the bases (Courtois et al., 1968;Zimmer et al., 1968) but is moderate enough not to destroy irreversibly the DNA through depurination. This is performed in low ionic strength environment known to make the DNA structure more susceptible to changes (Sorokin et al., 1986). Due to a thus introduced instability of the double stranded DNA, the DNA intercalating dye can emit fluorescence from a local DNA sequence transiently as long as it is stable (note that dyeemission in the absence of a double stranded DNA is strongly reduced(Cosa et al., 2001)). Importantly, despite of nuclear membrane permeabilisation, the DNA-binding dye once dissociated from the DNA does not leave the cell nucleus immediately but rather undergoes retention in the complex nuclear structure for several hours. This limited YOYO-1 diffusionensures its sufficiently high concentration in a local vicinity of a nuclear DNA as it undergoes a transient between "denatured" and "renatured"(native) state (**Fig. 15B**). Transient stabilisation of the DNA in a presence of DNA-binding dye results in repetitive photon emission from a single binding site that appears in an image as a bright spot (even~2000 photons detected per signal on average)(Schoen et al., 2011). Photon emission continues until molecule photobleaches or DNA binding site occupied with a dye molecule undergoes denaturation again inevitably leading to a fluorescence emission halt e.g. via dye release (YOYO-1 is non-fluorescent in a solution, see **Table 1** in **section 3.7**). In support of at least partial dye release from the DNA is the occurance of commondye penetration artefacts, i.e. a preference for localising dye signals at the nuclear periphery (**Publication 3**, supplementary information).

To summarise, in low ionic strength environment with pH~3.7 the DNA spontaneously undergoes re-/de-naturation and binding sites become available locally throughout the time-course of the measurement. This enables sampling of numerous binding sites and forms basis for a versatile super-resolutionmicroscopy based on isolated signal localisation in the cell nucleus (termed by us *f*BALM). Note, that in this approach the primary role is played not by a chemical modification of a fluorescent probe leading to a non-emitting state formation, but rather by stochastic availability of binding sites due to the DNA nature in these specific chemical conditions. Nevertheless, YOYO-1 is known to have at least 4 protonation sites that in low pH may contribute to its conformation change as well as may influence DNA binding mechanism. In addition, molecule protonation is known to be responsible for a change in fluorescence emission for other DNA-binding probes such as Hoechst (Żurek-Biesiada et al., 2013, 2014). We anticipate that such a variety of effects may also play a role in*f*BALM.

In order to further improve super-resolution microscopy of the cell nucleus based on *f*BALM the following issues are necessary to be addressed: brightness of DNA-binding dyes, i.e. number of photons emitted per binding event (a result of susceptibility to absorption and quantum efficiency), fluorescent background during the measurement, dye diffusion, and density of single molecule localisations.

The number of photons per binding eventcan be addressed by further improvement to the imaging media recipe.This could be done by decreasing an effect of non-fluorescent de-excitation processes as well asof dark states unrelated to the dynamic labelling. It has been demonstrated for a carbocyanine-derivated PicoGreen that metal enhanced fluorescence effect may constitute a very promising approach to increase quantum efficiency of DNA-binding dyes (Dragan et al., 2012; Geddes and Lakowicz, 2002). Potentially this could be tested in SMLM approach advanced in this work. Additionally, it has been demonstrated for cyanine-derived dyes just as Cy3, Cy5 and Cy7 that heavy water (D_2O) increases their quantum efficiency and number of photons emitted per single molecule signal in dSTORM super-resolution microscopy by a factor of up to ~2(Klehs et al., 2014). This may lead to an increase in localisation precision by a factor of up to 1.4 when aqueous solution based on D_2O used. Lastly, the photon count per single molecule of the transiently bound DNA dye, theoretically, could be increased by co-staining with a second dye of a different binding mechanism and distinct spectral properties facilitating FRET. This, if only imaging conditions just as pH thoroughly adjusted, so that one type of a dye, e.g. YOYO-1, transiently binds in the presence of permanently bound Hoechst 33258, would lead to promotion of YOYO-1 fluorescence to a greater extent. This is, however, purely speculative.These aspects listed above were however not covered in the time-course of this study.

Although the *f*BALM labelling scheme presented here (**Fig. 15A**) helps to reduce DNA dye penetration artefacts as the DNA-binding dye is available in every part of a nucleus, there is still a room for an improvement (**Publication 3**). For instance, reversible nuclear membrane permeabilisation for the sake of DNA introduction to the nucleus would be desired: in such circumstances the DNA-binding dye would be uniformly dissolved inside the cell nucleus and would not leave from a pre-labelled cell. Nevertheless, as of now we are not familiar with such permeabilisation strategy for fixed cells. We anticipate that other ways of introducing the dye to the nuclei than ones based on permeabilisation should be successful as well (e.g. electroporation followed by cell fixation).

Further search for *f*BALM-applicable fluorophores, or ideally a chemical synthesis of specially designed probes, are highly welcome and constitute a future of this approach. In such case dyes of extremely high diffusion rates or very slow ones are highly welcome to either (i) undergo retention inside the nucleus or (ii) penetrate rapidly the cell nucleus when provided externally during the measurement. In case of the first group, definitely other bis-intercalating carbocyanine DNA-binding dyes can be taken into an account. In case of the latter, a promising approach is to check on cell nucleus penetration for a variety of DNA-binding probes of smaller weight than the ones used in this study. Certainly e.g. SybrGreen would constitute a good candidate. Its only difference, as compared withquite rapidly-diffusing PicoGreen, is a lack of one of dimethyloamino-groups with equally high fluorogenic properties (Dragan et al., 2012). Among other candidates here one should also mention DRAQ5 (molecular mass is even smaller and penetrates through live cell membranes). Moreover, in the time-course of this study we also found that SytoxOrange (monomeric cyanine DNA intercalator with highest quantum efficiency and extinction coefficient among DNA dyes commercially available(see **Table 1**, **section 3.7** for details) performs comparably well to YOYO-1 using a *f*BALM methodology.

Recently, similar attempts have been pursued to realise DNA imaging in single molecule localisation microscopy. For example, the dynamic labelling has been realised with specially designed Hoechst-JF_{646} that upon transient binding to the DNA can be imaged using point accumulation for imaging in nanoscale topography (PAINT) (Legant et al., 2016). In this approach fluorescent probe is composed of the DNA-binding Hoechst-backbone and conjugated rhodamine-

derived dyeJF_{646}. While in a solution it diffuses fast and is not well visible due to lower quantum efficacy and signal motion blur, upon binding its photon emission can be accumulated over hundreds of milliseconds from the location of a DNA-binding site well enough to provide single molecule isolation and to pursue SMLM. In combination with light sheet illumination (see next paragraphs for a discussion) even a 3D imaging of entire cell nuclei becomes possible. Nevertheless, due to an insufficient experimental details provided (no information on imaging environment or mechanism underlying transient association) this technique is less accessible than *f*BALM approach developed in this work.

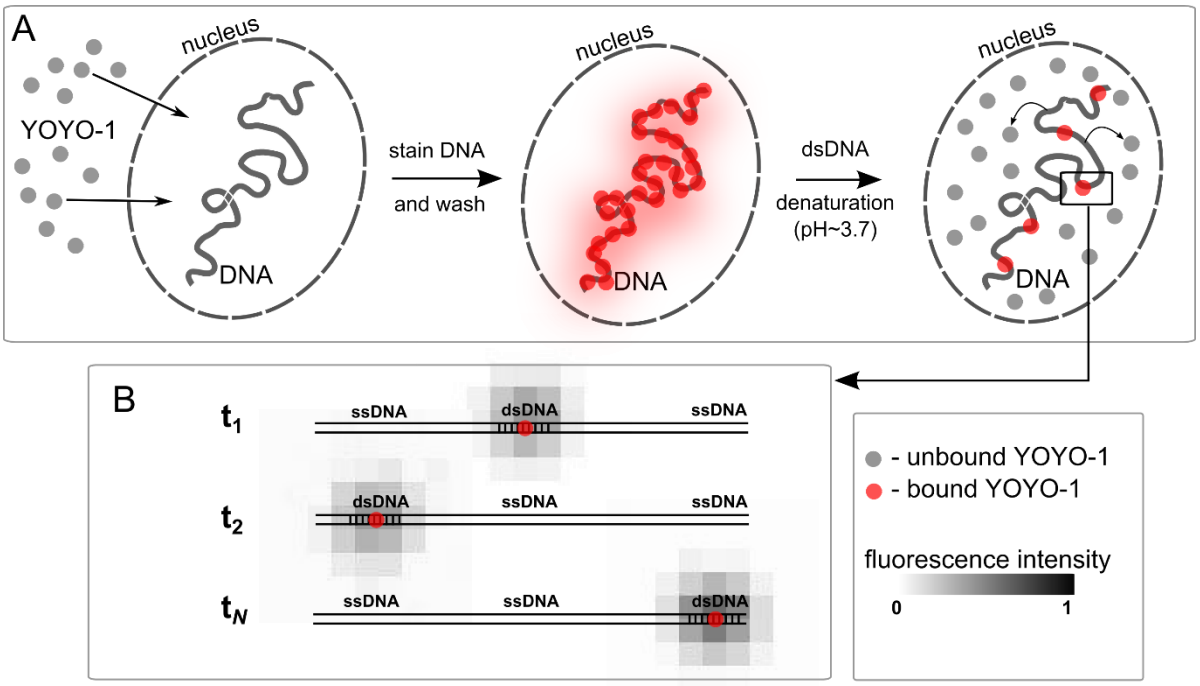

Figure 15. Outline of DNA structure fluctuation assisted BALM (*f*BALM) developed in this work.A)Fixed and permeabilised cells are first stained with YOYO-1 DNA-binding dye. This is followed by extensive washing. Subsequently, using an enzymatic oxygen scavenging system (glucose oxidase), pH is gradually decreased to a value of ~3.7. Once these conditions are reached the DNA-binding dye dissociates from the DNA but remains still trapped in the cell nucleus. **B**) The DNA is unstable in the conditions provided and local spontaneous renaturation (to dsDNA) and denaturation (to e.g. ssDNA) dynamically proceeds over time (t_1, t_2,...,t_N) enabling YOYO-1 transient fluorescence emission (depicted in red). This picture is somewhat simplified; note that YOYO-1 in a presence of ssDNA is also fluorescent to some degree (Cosa et al., 2001). In addition, both ssDNA and dsDNA undergo ionisation in low pH (Sorokin et al., 1986; Zimmer et al., 1968) further introducing a conformational change and likely affecting YOYO-1 DNA-binding as well as fluorescence emission. Therefore, designation 'ssDNA' in (B) refers to a variety of different denatured states rather than to ssDNA solely. Upon local stochastic stabilisationof dsDNA, single YOYO-1 becomes fluorescent, emits light, and thus can be localised in space using SMLM principles (shades of grey correspond to a fluorescent signal from a single binding site occupied with a DNA-binding YOYO-1).

While*f*BALM was proven here to be successful enough to image the chromatin in cell nuclei, the use of epi-illumination did not prevent from considerable fluorescent background. This phenomenon originates from the fact that in epi-illumination the entire volume of the cell nucleus (being a 3D structure) is illuminated and thus fluoresces. Such fluorescent background affects the effective localisation precision (see **Fig. 4** for more details), and hence the resolution. This problem can be solved by application of light sheet or lattice sheet illumination perpendicularly oriented to the direction of fluorescence collection. This advantage has been lately applied in other SMLM studies of the cell nucleus (Zhao et al., 2014; Legant et al., 2016). Furthermore, this approach would not only decrease the fluorescent background in *f*BALM but also would improve the dye availability within the volume imaged (only slice illuminated instead of entire nucleus). In such case dye molecules thattransiently bind to the DNA above and below illuminated volumewould not be a subject to irreversible photobleaching. This would also maintain YOYO-1 supply for longer measurements to capture greater number of signal localisations leading to an increase in their density in a final reconstruction (for an importance of single molecule density see **section 3.4**). It is reasonable to anticipate that such approach would enable more uniform penetration of YOYO-1 to the volume exclusively exposed to the exciting light (here a flat sheet through a nucleus). In addition, in such low-background circumstances, 3D *f*BALM based on astigmatism becomes manageable(Legant et al., 2016). Thus, we anticipate that using a light sheet illumination, the resolution can be further enhanced possibly down to 30 nm (x, y) and ~70 nm (z) range, with better uniformity throughout an image, eventually outperforming the capabilities of *f*BALM at its present state.

7.2 Chromatin labelling strategies for super-resolution single molecule localisation microscopy

The ideal chromatin labelling strategy for super-resolution studies should rely on following important principles: (i) needs to be asdirect as possible and (ii)should not be DNA sequence-specific or chromatin protein-specific, (iii) would not interfere with chromatin structure, (iv) has to be very sensitive as structures anticipated are rather small, (v) in case patients' samples are desired for investigation, a labelling strategy necessitatesno treatment prior to fixation (e.g. introduction of genetically encoded histone proteins is not an option), and lastly (vi) fluorescent properties have to be feasibly controllable.

Most of abovementioned requirements are well fulfilled by DNA binding dyes studied in this dissertation. Besides however other strategies are also present including: long-term DNA base analogue incorporation to the entire genomic DNA, followed by click-it reaction with photoswitchable fluorescent probes(Zessin et al., 2012), and antibody histone labelling (Ricci et al., 2015), or genetically encoded fluorescent proteins conjugated to the chromatin associated proteins (Markaki et al., 2010; Cremer et al., 2011; Ricci et al., 2015).

A big advantage of the approach utilising DNA base analogue incorporation is a direct labelling of the DNA of chromatin and possibility to introduce feasibly controllable fluorescent probes (e.g. Alexa 647). In turn, this approach is inapplicable to the human samples due to high toxicity of such treatment (Zhao et al., 2013), additionally triggering e.g. DNA damage signalling likely affecting local chromatin structure prior fixation(Burgess et al., 2014). Moreover, one can expect sequence specificity of such labelling as only one type of nucleotide is substituted.

In case of antibody histone labelling, again the ease to introduce favourite fluorescent probe is advantageous. On the other hand, it is expected that antibodies encounter a serious accessibility issues. While the size of an IgG molecule amounts to ~150 kDa, experiments with fluorescently labelled dextran of size of 25 kDa and more, injected to the nuclei of living cells, revealed signal depletion in DNA-rich zones suggesting limited chromatin penetration(Bancaud et al., 2009).In support, in our hands anti-histone antibody labelling failed in observation of condensed chromatin in ischemia (for further details see **Section 7.4**) In addition, once antibody recognises a histone protein, it locates a fluorescent label away from the target leading to a steric localisation error in the order of ~20 nm(Ries et al., 2012). Needless to say that histones occupy the DNA only every 146 bp + 10 to 50 bp (nucleosome + linker DNA) and in some circumstances the DNA is rather depleted of them (e.g. DNA repair, transcription, replication sites). Altogether, this chromatin labelling approach is a subject to strong limitationsin SMLM reaching a resolution of even 40 nm. It has been proposed that this method of chromatin labelling can be improved by replacing antibodies with nanobodies having smaller size (13 kDa), and effectively bringing a label closer to the target(Kaplan and Ewers, 2015; Ricci et al., 2015). Nonetheless, we demonstrate that limited anti-histone immuno-labelling can serve as a method to investigate chromatin compaction (for details see methodology developed in**Publication 4**).

In comparison to these methods highlighting the chromatin distribution in fluorescence microscopy using immunolabelling of chromatin-associated proteins, DNA-binding dyes have a molecular weight 100 to 200 times smaller than an antibody molecule, can label the DNA directly even every 3.2 bp (Günther et al., 2010), and are a subject to diffusion and penetration related constraints to much smaller extent (Bancaud et al., 2009).On the other hand, from the photophysics point of view, fluorescence switching for DNA dyes is still poorly understood, and explored thus far to a minor degree in only several research articles (Flors et al., 2009; Flors, 2010). Interestingly, dynamic labelling of the DNA with DNA-binding dyes, same as in BALM, opens a new avenue of opportunities to image chromatin at super-resolution as most binding mechanisms and NMR structures of DNA-dye complexes are well characterised (for example see (Dragan et al., 2010) and **Table 1**).

In DNA structure fluctuation assisted BALM presented in this work we took advantage of this wealth of available knowledge, consequently enabling imaging the chromatin in cell nuclei at so far unprecedented structural resolution. This DNA imaging approach, however, may suffer from a certain sequence bias as an underlying mechanism relies on transient localDNA denaturation ↔ renaturation transition. It is commonly acknowledged that DNA denaturation is sequence specific(Reisner et al., 2010), and that AT sequences (containing only 2 hydrogen bonds as opposed to GC having 3) are more prone to denaturation(Hermann and Fredericq, 1977). Thus, we reason that they may be overrepresented in *f*BALM.Interestingly, in previously published studies on BALM of isolated λ–phage DNA with YOYO-1 and in a presence of 10mM ascorbic acid (for relevant details see**Publication 3**), single molecule localisation density alonga DNA fibre appeared to be homogenous, suggesting only a minor sequence specificity in these settings. Similarly, a potential sequence-bias might hold true for photoconverting DNA-binding dyes presented in this work; Hoechst dyes (and likely its derivative VybrantViolet) are known to have a certain specificity to AT-rich sequences (Weisblum and Haenssler, 1974). In spite of these few potential limitations, DNA-binding dyes are superior to other chromatin labelling strategies for single molecule localisation microscopy.

7.3 Chromatin at super-resolution and compatibility of the results with existent data on chromatin structure

Model of functional nuclear organisation based on co-aligned active and inactive nuclear compartments (recently reviewed in (Cremer et al., 2015)) assumes great variability in nuclear chromatin density; nearly no chromatin can be found in the interchromatin compartment and high chromatin concentration can be found in gene-rich chromatin dense clusters. This basic notion that chromatin occupies the nuclear volume only partially could be confirmed by both DNA imaging methods developed in this study. For instance, *f*BALM revealed that DNA-associated signal may vary by more than two orders of magnitude with essentially no DNA-associated signal within interchromatin compartment. This also prompts us to reconsider a classical, old-fashioned model of nuclear chromatin, assuming low DNA density euchromatin and high DNA density heterochromatin – a model derived from diffraction limited fluorescence microscopy images of DNA. The results presented in this work demonstrate that this initial observation is rather a result of insufficient structural resolution, and that underlying nuclear organisation is way more complex (**Fig. 16A**). DNA structure fluctuation binding activated localisation microscopy (x,y resolution of ~50 nm, z resolution ~550 nm) revealed that DNA distribution in the nucleus is heterogeneousand occupies roughly 50% of the nuclear volume. It comprises various forms of domain-like structures, 350 - 500 nm in diameter, interconnected with each other via narrow chromatin bridges of ~50 - 200 nm thickness (**Fig. 16A**, dashed circle and square). In our 2D *f*BALM images it appears that each "domain" may be connected with 3 – 4 others; in reality this number however might turn out to be greater if studied in 3D. Interestingly, in parallel,single molecule localisation microscopy has been used to study well defined, distinct, epigenetic domains after fluorescent in situ hybridisation (FISH)(Boettiger et al., 2016). Strikingly, in this case super-resolution SMLM unravelled that chromatin domains of specific epigenetic signatures,different from neighbouring sequences (as assessed with massive parallel sequencing studies following ChIP), bear very similar structure to "domains" revealed in the study using *f*BALM (compare **Fig. 16A** and**B**). Namely,chromatin domains seem to be composed of a globular core branching and narrowing in several directions. Recently, similar has been demonstrated using computer simulation of polymer and Hi-C data (Gavrilov et al., 2016); also here chromatin domains were revealed to be spaced by thin and accessible fibre like "bridges".

Thus, we hypothesise here that chromatin is indeed organised in spatially resolvable 100 – 1000 kb "domains", constituting a basic regulatory units. The boundaries of these topologically associated domains were previously demonstrated to strongly correlate with replicating domains (Pope et al., 2014)(see **Fig. 16D**) and are enriched in chromatin-looping proteins and RNA Polymerase II (Tang et al., 2015). Hence, we anticipate them to physically localise to the boundaries of domains outlined in this work with the help of super-resolution microscopy. In support of this claim, our preliminary data on dual-colour SMLM of photoconvertible DNA dye in combination with immunofluroescently labelled H3K14ac suggests that this marker of gene regulatory elements including in- and active promoters (Karmodiya et al., 2012), is preferentially deposited to the boundary of DNA domains (**Fig. 16D**). Altogether, domain boundary is likely serving DNA information processing similarly as in previously proposed perichromatin concept assuming an existence of a thin layer of decondesed, transcriptionally active chromatin at the boundary of condensed chromatin (Cremer et al., 2015).

The piece of evidenceoutlined in the previous paragraph envisages chromatin organisation at a submicron level however at nanometre length scale the arrangement of chromatin fibres remains

unclear. As of now, none of the SMLM super-resolution techniques, including the ones developed in this study, enabled visualisation of chromatin loops. Their size can be approximated to few tens of nanometres only and, in order to pin point such small structures in a complex dense nucleus, a better contrast is highly desired (potentially achievable with e.g. light sheet illumination or appropriate astigmatism). Lately, it has been hypothesised that accessibility to a chromatin fibre is fine-regulated by so called "nucleosome clutches"; 2 – 8 nucleosome discrete assemblies interspersed with nucleosome depleted DNA (Ricci et al., 2015). Due to their small size, they could dynamically influence (e.g. via opening up) the local sequence read out by various factors. Interestingly, in our *f*BALM studies on ischemia, where chromatin condenses to a great extent (for more details see **Section 7.4**)providing an increased contrast, we found fibre-like structures protruding from and linking DNA domains containing periodically appearing DNA-signal clusters. These clusters are spaced by 65 – 80 nm and have ~50 nm in diameter. A single nucleosome has a diameter of ~11 nm and theoretically, while convolved with *f*BALM localisation precision of 20 nm, should appear in our images as a 30 nm spot. Clusters revealed by fBALM had 30 – 55 nm suggesting potential number of nucleosomes amounting to 2 – 8, depending on their reciprocal orientation withrespect to the imaging plane. Worth noticing here is the fact that theoretically YOYO-1 may have up to ~60 binding sites per nucleosome (Günther et al., 2010). In light of this information, these considerations seem plausible. Please note however, that in the *f*BALM the localisation precision amounts to ~20 nm and the theoretical resolution based on a normal distribution of measured light source would give 20 x 2.35 = 47 nm thus being very close to a cluster size (for extended discussion see supp. materials to **Publication 3**).

We took freedom to speculate even further and noticed that in *f*BALM images usually any chromatin domain is consolidated to 2 or more others (**Fig. 16A**, e.g. dashed circle). Chromosomal DNA is a single linear molecule and chromosomes are known to occupy distinct parts of the cell nucleus (Cremer and Cremer, 2001). In case of only 2 domains contacting each other, the chromatin fibre would first fold into one and then continue to form another one (as depicted in **Fig. 17A,** $D_1 \rightarrow D_2 \rightarrow D_3$). In such case the chromatin fibre forms one domain after another in a manner similar to a pearl-necklace. Such arrangement has been recently demonstrated using high resolution microscopy combined with FISH labelling of *HoxD* gene cluster flanked by two TADs (Fabre et al., 2015). In our *f*BALM images, however, we found that number of connections may apparently exceed even 4. The question of utmost importance arises here: in what manner is the DNA molecule arranged in these circumstances? Of relevance here is the fact that, different remote DNA sequences termed as enhancers and silencers may influence distal gene activity up to 1000 kb up- or down-stream within a DNA molecule (Shlyueva et al., 2014). Perhaps, additional (more than 2) neighbouring domains come from strong interaction between distal genomic loci D_n as depicted in**Fig. 17A**. Here the "necklace" of domains would bend towards itself to serve enhancers and/or silencers to the chromatin domain D_2 (**Fig. 17A**, DNA stretch indicated in cyan). Another idea explaining more than 2 neighbouring domains may assume that the chromatin fibre, after formation of one domain (e.g. D_2 in **Fig. 17B**), continues towards the next one (D_3) but subsequently travels back again to the previous one ($D_2 \rightarrow D_3 \rightarrow D_2$) either serving there enhancers /silencers or contributing further to its structure build-up. In support of this hypothetical configuration of regulatory elements is the fact that their marker, H3K14ac (Karmodiya et al., 2012), localises primarily to boundaries of chromatin domains as revealed in this study (**Fig. 16D**, **Publication 4**). In such case the reciprocal position of chromatin domains could be anticipated to be regulated not only by their linear sequence proximity but also the abundance of distal regulatory elements within other domains necessitating a physical interaction. In addition, it has been previously shown that

HoxD locus is regulated by enhancers originating from two flanking TADs 100 – 200 kb up- and down-stream (Montavon et al., 2011).

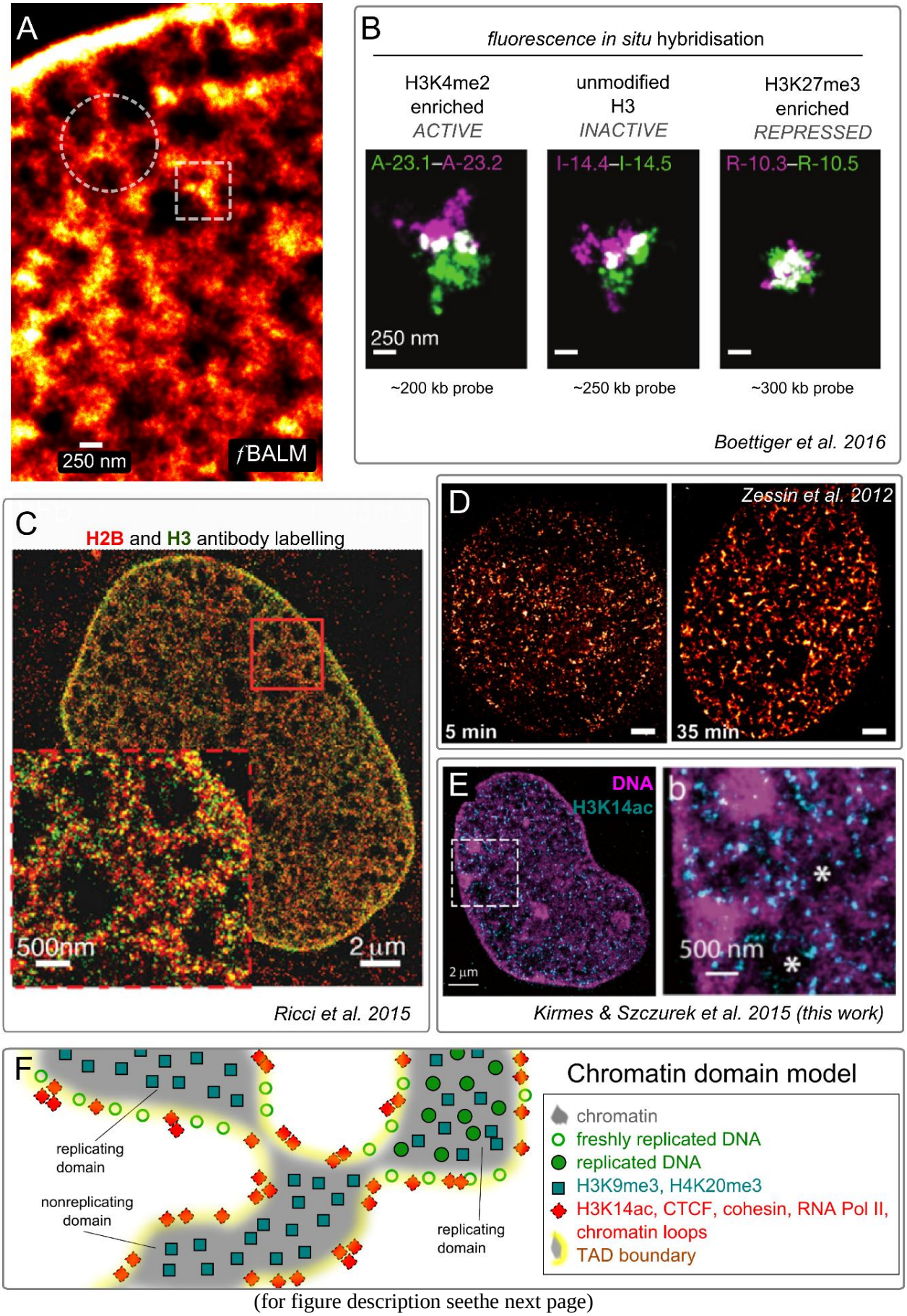

(for figure description seethe next page)

Figure 16. Single molecule localisation microscopy in eukaryotic cell nucleus suggests a model of chromatin organisation. In this figure contemporary SMLM results in the cell nucleus are compared. **A**) DNA structure fluctuation assisted binding activated localisation microscopy (*f*BALM) of DNA in mouse HL-1 cell nucleus demonstrates that chromatin is organised in a "sponge-like" manner: heterogeneity of DNA associated signal exceeds two orders of magnitude. Dashed circle and square demonstrate two domain-like structures at different compaction levels (**Publication 3**). Note that the *f*BALM image covers < 600 nm thick focal volume thus structures at various depth may overlap due to a projection to a 2D image.**B**) Super-resolution SMLM images of fluorescently labelled chromatin domains (Boettiger et al., 2016). Maximal projections of 3D SMLM data are shown. Distinct chromatin domains (~250 – 400 kb) were characterised by different occupancy of following histone marks: enrichment in H3K4me2 (termed active), lack of H3 modifications (inactive), and H3K27me3 enrichment (denoted as repressed). Subsequently, in situ hybridisation was carried out against these specific genomic loci using probes of length indicated in the picture. Image scale same as in (A) for better comparison. Note striking similarity between active domain and domain indicated ina circle in (A) and inactive domain and domain in square in (A). **C**) Super-resolution SMLM image of chromatin in primary human fibroblast labelled with anti-H2B and anti-H3 primary antibody followed by secondary antibody labelling (Ricci et al., 2015). In line with *f*BALM in (A) the chromatin appears to be arranged in a structure resembling a"sponge". Chromatin free regions of size up to 700 nm are clearly seen in an inset (red square, same scale as in A and B).**D**) Replicating cells incubated with DNA base analogue EdU (50 μM) for 5 and 35 min, followed by click-it reaction to couple Alexa fluorophore (image credit to(Zessin et al., 2012)). Short-term incubation with EdU results in small foci, whereasin the cells incubated with EdU for longer than 10 – 15 min, thedomain-like structures become apparent (compare 35 min EdU incubation with A, B, and C). Scale bar corresponds to 2 μm. We hypothesise that chromatin in S-phase undergoes a sequential replication at the boundaries of a specific TAD currentlyinitiated for a duplication: the longer the EdU incubation proceeds, the more chromatin in a vicinity of replication forks becomes labelled, ultimately resulting in labelling of entire chromatin domains for longer incubation times.**E**) Active H3K14ac (gene regulatory element marker (Karmodiya et al., 2012)) imaged at enhanced resolution together with chromatin (photoconversion of directly binding DNA dye Vybrant Violet). H3K14ac localises to the boundary of dense chromatin clusters. These fine details cannot be seen in diffraction-limited, conventional fluorescent microscopy image (bottom, right). **F**) Chromatin domain organisation model based on available single molecule localisation microscopy data andinferred based on available next generation sequencing data. Chromatin distribution as well as location of H3K14ac was revealed in this work. Location to the TAD boundary of chromatin tangle-proteins just as CTCF and cohesin was revealed previously using ChiA-PET (Tang et al., 2015). Replication domain boundaries have been demonstrated previously to perfectly correlate to TAD boundaries (Pope et al., 2014).We hypothesise that chromatin domains (likely TADs) are possiblyresolvable with the super-resolution SMLM *f*BALM approach.

Both models presented in **Fig. 17A** and **B**) would be further supported by an observation that domains of distinct epigenetic landscape, independently of their compaction state, were shown to physically overlap only marginally (Boettiger et al., 2016). Nevertheless, the divagations elaborated here have as of now a purely speculative character. We anticipate that in future, a combination of FISH super-resolution visualisation, chromosome conformation capture studies, chromatin immunoprecipitation, and *f*BALM super-resolution chromatin imaging may unravel the real domain arrangement. For instance a recommendable approach would involve genome-wide TAD identification followed by its specific labelling combined with total DNA labelling, both imaged at super-resolution. First successful attempts has been already published (Wang et al., 2016).

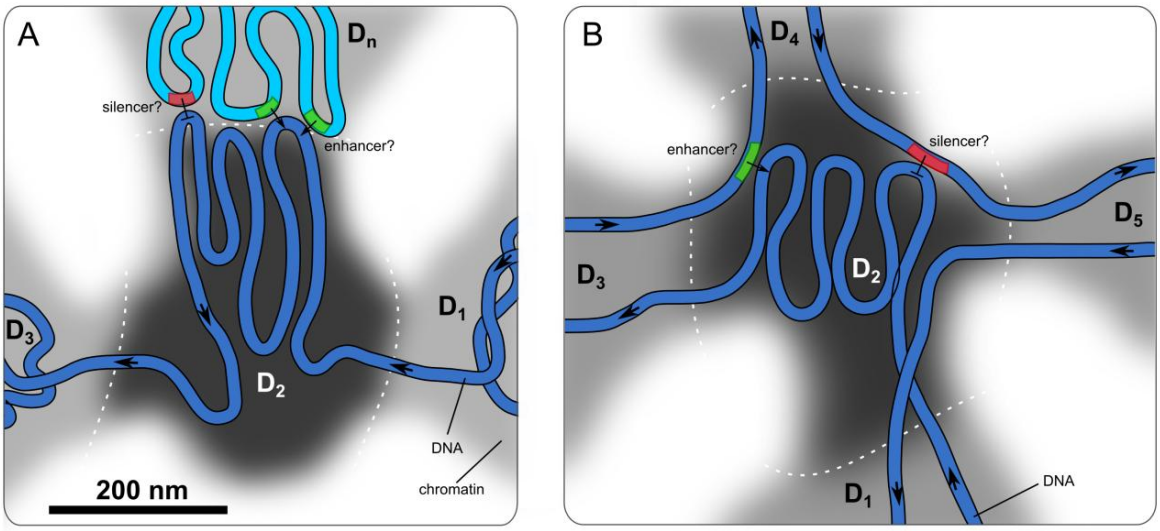

Figure 17. Hypothetical model of DNA arrangement in chromatin domains of a single chromosome. Compare to Fig. 16A demonstrating super-resolution images of chromatin.**A**)Linear domain organisation model. Black patch corresponds to a hypothetical domain D_2. In grey chromatin imaged with super-resolution microscopy, e.g. *f*BALM. The same DNA molecule, distal locus (D_n, cyan), may form a neighbouring domain that serves enhancers or silencers controlling transcription in D_2 domain, thus appearing in images as a contacting domain D_n. Such interaction usually does not exceed 1000 kb what would correspond to several chromatin domains/ TADs (Boettiger et al. 2016). **B**) Single DNA molecule (in blue) may form many chromatin domains that are not arranged linearly but instead may additionally interact with others in proximity (e.g. D_2 and D_4). This model potentially explains why enhancer/silencer sequences can lie only less than ~1 Mb away from the regulated sequence (length corresponding to ~1 – 5 domains assuming their size of several hundreds of kb (Boettiger et al., 2016)). Arrows depict DNA orientation, e.g. 5'→3'. White dashed lines separate chromatin domains. In both cases nucleosomal chromatin organisation was omitted for a sake of clarity.

7.4 Ischemia induces DNA compaction within minutes

In this work it is demonstrated using single molecule localisation of the DNA-binding dyes, that the nuclear architecture of immortal cardiomyocytes undergoes a compaction under experimental conditions (**publication 4**). DNA-dye photoconversion-based as well as DNA structure fluctuation assisted binding activated localisation microscopy revealed that chromatin compaction in this cell type may take place already in several minutes and similarly, is reversible already after minutes of reperfusion with regular, properly oxygenated medium containing all vital nutrients. The extent of compaction indicates that chromatin undergoes a phase transition: OND induces formation of previously unknown subnuclear configuration consisting of discrete atoll-like structures as well as rarely occurring chromatin double-layer at the nuclear boundary together with concomitant expansion of interchromatin (DNA-free) compartment by 250% as compared to the state before OND treatment. Hence, the DNA distribution in the cell nucleus changes significantly and this was captured with a dedicated quantitative analyses based on quantifying local densities or nearest neighbour analysis of DNA associated signals. Microscopic notion was further reinforced by a complementary super-resolution technique that does not rely on fluorophore photoswitching known as structured illumination microscopy(Heintzmann and Cremer, 1999; Gustafsson, 2000). Noteworthy, these changes to chromatin distribution take place with a simultaneouspreservation of nuclear volumeand shape (estimated by 3D confocal microscopy) as well as unaltered lamin A

mesh (as studied with SMLM, **Publication 4**) known to be responsible fora maintenance ofnuclear architecture at the nuclear periphery(Burke and Stewart, 2013).

Alternative analytical procedures have been employed to confirm the discovery made with novel super-resolution DNA imaging methods developed in this work. The chromatin in OND-subjected cells bore an increased DNase I-digestion susceptibility as revealed by time-course digestion assay with DRAQ5-labelled DNA. DNase I is a protein whose mass amounts to 39 kDa (approx. twice more than H1 molecule) and it can be anticipated that it does not penetrate throughout dense structuresthus serving as a molecular "probe" for DNA accessibility within nuclear chromatin.

Fluorescence recovery after photobleaching experiments on histone H1.1-GFP revealed its decreased mobility in live HeLa cells already after 10 min of OND-treatment. This histone variant is not a part of a nucleosome and is known to be rather not permanently bound to the chromatin as in case of core histones H2A, H2B, H3, and H4; on the contrary its dynamic interaction with the DNA is anticipated to regulate higher order chromatin structure(Corona et al., 2007; Wojcik and Dobrucki, 2008). In case of the OND, decreased fluorescence recovery in FRAP experiments with H1.1-GFP might be either a result of compacted chromatin (in such case H1.1-GFP molecules need more time to exchange in hardly accessible compacted chromatin regions) or a partial cause ofchromatin condensation via e.g. H1 phosphorylation affecting its interaction with chromatin(Zheng et al., 2010). The latter, however, has not been addressed in this work.

Change to the chromatin compaction status in OND has been further confirmed in cardiomyocyte cell line using light side-scattering in a flow cytometer typically providing an information about cellular granularity. This methodology was previously employed for chromatin condensation assessment(Smirnov et al., 1988)

Interestingly, it has been observed that immunolabelling of core histone H3 was significantly reduced in OND by 4.5 times as estimated using SMLM via comparison of densities of single molecule localisations. We attribute this difference to a decreased accessibility of antibody molecules to histones buried deeply in condensed chromatin. In support with this statement we failed to detect a decrease in H3 level using western blot analysis (data not shown). Also, previously it was suggested that histones may be expelled to the blood during cerebral stroke (Geiger et al., 2006; R. Chen, Kang, Fan, & Tang, 2014), however this was not observed in our experimental setup (validated with westernblot of culture medium, data not shown).These notions potentially suggest that previously reported increased histone levels in blood might have been rather a result of immunological reaction to inflammation known to accompany ischemic event (Jin et al., 2010).

On the other hand, previously published experiments with fluorescently labelled dextran of varying size (25 kDa and greater) injected into living cells revealed signal depletion in dense chromatin zones (Bancaud et al., 2009). In comparison, a typical IgG antibody molecule used for immunofluorescent labelling bears a molecular weight of ~150 kDa. In this study we also report on reduced DNA digestion by DNase I. This nuclease have a size several times smaller than an IgG molecule (39 kDa only) andcommonly serve as a "compaction-probe" in e.g. next-generation DNase I hypersensitive sites sequencing (Boyle et al., 2008). Consequently, we anticipate that anti H3 histone immunofluorescent labelling should be used carefully in super-resolution SMLM investigation of chromatin structure as reduced penetration of antibodies likely leads to labelling artefacts.

In these studies we investigated also H3 histone modifications and found a massive reduction of different “active” histone marks including pan-acetylated H3, H3K9ac, H3K14ac, H3K27ac, H3K4me3 with only minor reduction in “inactive” marks just as H3K9me3, H3K27me3, all studied with flow cytometry after immunofluorescence labelling. This behaviour has been, however, further confirmed with western blot analysisproving only minor antibody penetration artefacts in case of these histone modifications (experiments performed by Ina Kirmes). The opposite was found for unmodified H3 antibody staining that was reduced in contrast to westernblot contradicting this notion (H3 level unchanged). H3 histone is believed to be modified on its N-terminal “tail” exposed to the environment ~3 nm away from the nucleosome and, hence, it can be anticipated that modifications are more accessible to an antibody recognition. This would explain differences in results of immunofluorescence and Westernblot analyses between unmodified H3 and H3 modified on its tail. This knowledge prompts us also to hypothesise that anti-H3 staining can serve as a method to estimate chromatin condensation.

7.5 Dynamic chromatin structure in reperfusion

Aforementioned results from multiple-approaches suggest that chromatin undergoes a strong compaction during OND.Consequently, upon cessation of ischemic conditions, the nuclear structure of cardiomyocytes undergoes a rapid relaxation within minutes and reaches original status after approx. 60 min. In line with the results obtained with super-resolution microscopy, it has been found using immunofluorescent staining and Westernblot analysis that already after 10 min of reperfusion following OND treatment, active histone marks undergo upregulation as compared to the levels in OND (data not shown).

Moreover, several hours after a release from OND, chromatin adopts a more open configuration, as compared with untreated cells, likely being a consequence of epigenetic reprogramming of cells. This observation was further confirmed by a transcriptome analysis using next generation mRNA sequencing of myocardial infarction mouse tissues. These experiments revealed a considerable gene upregulation after 2, 4, and 24h (experiments performed by Ina Kirmes, not shown) which as a consequence may induce chromatin decondensation to increase accessibility of transcription factors to manifold genes necessary in reperfusion. To further strengthen this argument, we found that not only the number of genes undergo upregulation but also a total transcription rate increases by 40% already during 1h of reperfusion as shown using bromouridine incorporation assay followed by mass-spectrometry quantification.

7.6 Model of DNA compaction in ischemia

The results obtained in this study help to outline a model of action. OND leads to 10 fold ATP level reduction due to respiratory chain halt both as a result of hypoxia and insufficiency of nutrients. ATP occurs in cells predominantly as a complex with Mg^{2+} and as a consequence of ATP reduction in intracellular ATP levels, Mg^{2+} availability increases(Murphy et al., 1989). This might promote chromatin compaction as positively charged ions would easily relocate to the cell nucleus and bind to negatively charged DNA (depicted in **Fig. 18**). In fact, an increase to externally supplied Mg^{2+} in cell culture medium has been demonstrated before to provoke chromatin compaction as studied with fluorescent lifetime imaging of histones conjugated with fluorescent proteins (Visvanathan et al., 2013). The same would be applicable to naturally occurring,

intracellular polycationic spermidine and spermine innately complexed with ATP. Their liberation would lead to further chromatin compaction in case of OND. Along this line of argumentation it has been previously demonstrated that their addition to the cell culture in a presence of detergent permeabilised membranes has an effect analogous to the one inflicted by divalent cations, i.e. induce chromatin compaction(Visvanathan et al., 2013). In addition, according to our confocal microscopy experiments and anti-polyamine immunofluorescence labelling their nuclear signal is stronger in OND than in untreated cells (**Publication 4**). ATP-driven liberation of (poly)cations is further supported by our experiments on hypoxia and hypoglycemia applied to the cells for 1h separately. In both cases chromatin condensation occurred. Altogether, this suggests the model of "dormant"/"passive" chromatin availability regulation by means of ATP level change: in OND cells sense and respond to nutrient availability via (poly)cation liberation leading to chromatin condensation and transcription cessation.Such"passive" transcription halt would be more cost-effective than e.g. active enzymatic or epigenetic regulation of this process additionally consuming ATP.

In order to further validate this model, cells were treated with 2-difluoromethylornithine inhibitor (DFMO) – an inhibitor of polyamine biosynthesis interfering with ornithine decarboxylase. As long as *f*BALM super-resolution DNA imaging experiments together with DNA density distribution analysis have not been able to demonstrate convincingly an effect on OND-chromatin structure (**Fig. 14**), FRAP experiments on H1.1-GFP expressing HeLa cells revealed clearly that linker histone dynamics in OND increases while cells are pre-treated for 48h with DFMO prior to OND, reaching a level similar but still not fully recovered as compared with untreated cells (**Fig. 12**).Importantly, this treatment restored also mobile fraction of H1.1-GFP despite of OND treatment. This experiment further reinforces the validity of aforementioned model assuming an involvement of polyamines known already for long to interact with the DNA (reviewed in (Matthews, 1993)).

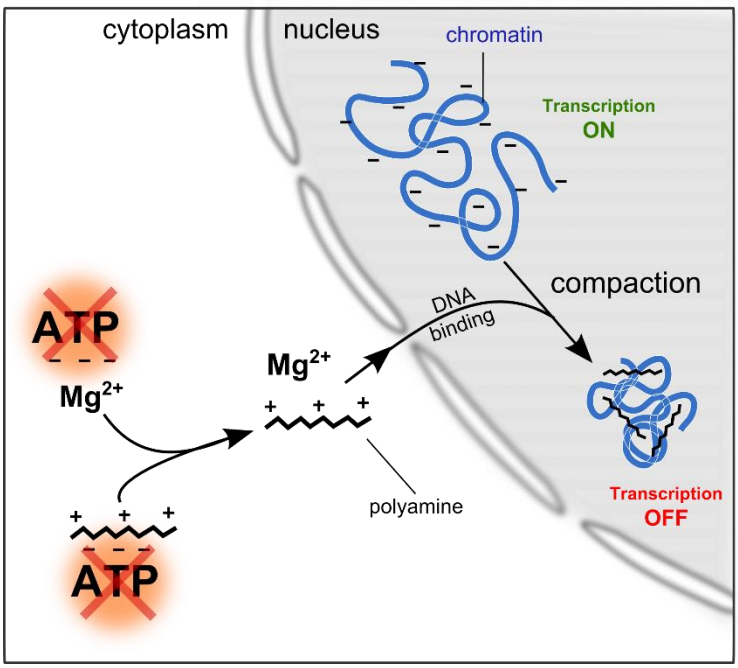

Figure 18. Model of chromatin compaction in ischemia. Upon adenosine triphosphate (ATP) depletion, (poly)cationic compounds undergo a release from this complex and relocate to the cell nucleus where they encounter negatively charged DNA. We hypothesise that such electrostatic interactions form basis for chromatin compaction and transcription halt as a negative chromatin charge is neutralised.

Noteworthy, chromatin of cells subject to ischemic treatment bears a decreased capability to associate with DNA dyes (**Publications 3, 4**). This result suggests either a reduced penetration of the DNA dye to the dense chromatin clusters or optionally highlights the lack of DNA-dye-binding sites due to polyamine and Mg^{2+} pre-occupation. Consequently, this would neutralise negative charge of the DNA and diminish the strength of electrostatic interaction between a DNA-binding dye and DNA (Dragan et al., 2010).

Question of utmost importance arises; whether this "passive" mechanism based on divalent cation and polyamine translocation to the nucleus is a sole instrument of chromatin compaction status control in ischemia. In order to address this point we set out to perform experiments in the same configuration as outlined above, i.e. *f*BALM DNA imaging and H1.1-GFP FRAP but for hyperacetylated chromatin after 1h treatment using trichostatin A – histone deacetylase (HDAC) class I and IIinhibitor, known to increase histone acetylation levels (Vanhaecke et al., 2004).Treatment with TSA in the context of ischemia has been previously reported as potentially therapeutically relevant for myocardial ischemia-reperfusion(Granger et al., 2008). Also HDAC pan-inhibition was formerly shown to have a positive effect in animal model of cerebral ischemia (Schweizer et al., 2013). In line with these observations, specific knockdown of HDAC3 and HDAC6 promotes survival in cortical neurons in a model ischemia involving both, oxygen and nutrient deprivation(Chen et al., 2012). In turn, the*f*BALM results have not revealed significant influence of TSA on decompaction of condensed chromatin. Whereas, super-resolution method failed to detect small differences, perhaps due to insufficiently precise analysis method, H1.1-GFP FRAP enabled discerning significant differences after 1h TSA pre-treatment of cells subject to OND. In this case H1.1-GFP mobility undergoes a partial restoration suggesting that hyperacetylated chromatin in OND has different physical properties from the one in OND alone.Our Western Blot and flow cytometry analysis combined with immunolabelling revealed indeed increased H3K14ac and H3K27ac levels for OND with TSA as compared with OND alone (experiments performed by Christina Heiser, not shown).

If (poly)cationic model of chromatin compaction is valid, it means that it is possible to affect chromatin condensation in an additional way even if it is already complexed with polyamines and Mg^{2+}, for instance using deacetylase inhibitors as demonstrated here.This is in line with previous findings that hyperacetylation of interphasic chromatin using TSA leads to an increase in chromatin accessibility (Görisch et al., 2005) and to an increase in mobility of chromatin associated proteins (Misteli et al., 2000).

Of importance here, however, is the fact that spermidine (a type of polyamine) can be acetylated by histone acetyltransferase that acetylates histone H4. This spermidine modification can alter its interaction with the DNA(Cullis et al., 1982). It has been even hypothesised that histone and spermine acetylation occurs in the same region of chromatin synergistically assisting in transcription (Matthews, 1993). Thus, any disruption of acetylation↔deacetylation balance in the cell nucleus is expected to have a profound effect on the chromatin organisation and functionality

in multitude of ways. Further studies are necessary to properly describe this multi-dimensional feature of chromatin structure.

7.7 Hypothetical role of chromatin compaction in ischemia

Polyamine are known to have a diverse role in cell differentiation, apoptosis, cell growth (Zhao et al., 2007). Thus, upon their depletion and potential translocation to the chromatin one might expect impairment in all of these processes at least as long as ischemia continues and shortly after. In line with the argument of necessity of constant polyamine availability, it has been found that in ischemia/reperfusion ornithine decarboxylase (ODC) and spermidine/spermine N^1-acetyltransferase (SSAT) activities were upregulated.This suggests a "counteraction" as the activity upregulation for polyamine synthesis enzymes occurred with simultaneous decrease in myocardiac polyamine pool(Zhao et al., 2007). Hence, it was reasoned to exogenously administer 1 mM spermine prior to ischemia and compensate for the deficit. Interestingly, this reduced myocyte necrosis and apoptosis as well as promoted the recovery of cardiac function after ischemia in rat heart (Zhao et al., 2007). In this case supplementation of spermine to the heart had a positive effect however the authors did not explain how polyactionic compound could penetrate through a cell membrane. Furthermore, this issue is a subject to an ongoing debate on polyamine transport system, reviewed in (Nowotarski et al., 2013). Nevertheless, if this happened, in light of our discovery, it would either lead to prolonged DNA condensation or replacement of cytoplasmatic pool of spermine or both simultaneously, having rather a protective effect as intracellular environment balance restoration would proceed slower. Another words, prolonged chromatin condensation would prevent from rapidly growing energy demand in context of chromatin transcription reactivation and associated dangerous oxidative stress at the onset of reperfusion. In addition to this hypothesis it has been demonstrated that polyamines may serve as free radical scavengers (Ha et al., 1998). Thus once complexed with DNA they could serve as its protectant.

Furthermore, our H1.1-GFP FRAP experiments suggest that inhibition of ODC for 48h prior to ischemic event (OND) helped to decrease the chromatin condensation (**section 6.5.1**). One could expect a decrease in spermine levels, however, an utmost care needs to be taken in interpretation of this result as the real polyamine levels have not been quantified by us in this case due to technical difficulties. Interestingly, results in other research groups suggested that the treatment with the same ODC inhibitor prolong life span of Drosophila subject to hypoxia (Vigne and Frelin, 2008).In case of our results in cell culture, however, 48h pre-treatment needs to be considered as quite long thus potentially also having an effect on cell cycle distribution leading to e.g. overrepresentation of measurements in cells in one particular sub-phase. This effect has not been tested though.

Similarly, a trichostatin A (TSA) treatment has been shown to decrease the infarct size in mouse ischemia model (Granger et al., 2008). In turn, in our hands TSA administration 1h prior to or during OND seemingly resulted in chromatin compaction to a lesser degree than in OND conditions alone (as revealed by H1.1-GFP FRAP). Based on the positive effects of TSA on viability reported in the literature one may infer that chromatin condensation is an undesirable phenomenon during ischemia and any potential therapy should focus on its prevention. Nevertheless, this process seems to be much more complex and still more work has to be done in order to situate (poly)cationic-induced chromatin condensation in novel strategies of stroke and heart attack treatment.

To summarise, two abovementioned examples seem to contradict each other:(i) addition of polyamines to the ischemic rat heart (Zhao et al., 2007)and (ii) reduction of polyamines by their synthase inhibition in hypoxic *Drosophila*(Vigne and Frelin, 2008)both led to a positive outcome. This altogether may suggest that cell and tissue viability is not dependent on polyamine-induced chromatin condensation alone but rather on the dynamics of this process and on dynamics of decondensation at the onset of reperfusion. In particular the speed of latter can be assumed to modulate a pace of transcription restoration and simultaneous energy demand decrease in short time after normoglycemia and normoxia restoration. While massive DNA transcription re-established fast (in our studies in < 1h of reperfusion), mitochondria are a subject to considerable stress associated with e.g. colossaloxidative damage inflicted at once in reperfusion. However, if oxidative damage burst distributed over longer period of time, it could be more bearable for a cell.This could be investigated in future using lipid peroxidation fluorescence-based kits specific to mitochondria (MitoPerOx).

7.8 Potential chromatin condensation in starvation and in tumour

Chromatin condensation upon oxygen and nutrient deprivation studied in this work may prove to be important in various different contexts besides ischemic diseases. For example, our results are also of relevance in investigations of starvation-induced effects on resistance against various factors. Short term starvation in a cell culture as well as in mice model has been proposed as a method to increase protection of normal cells against chemotherapy and oxidative stress.This methodology has been termed starvation dependent differential stress-resistance(Raffaghello et al., 2008). For instance, primary rat glial cells had an increased survival rate against hydrogen peroxide or cyclophosphamide treatment when additionally pretreated for 24h with a low-glucose media. On the contrary rat glioma, human glioma, and human neuroblastoma starvation did not change their relatively poor resistance to both types of treatment (Raffaghello et al., 2008). Additionally, very similar effect against etoposide have been discovered in mouse model after inoculation of tumour cells; mice subject to starvation prior to treatment had a prolonged lifespan whereas cancerous cells would not. Settlingpotential chromatin condensation to this broader context seems to be of importance in data interpretation.

Besides, it is widely accepted that advanced solid tumours, regularlysuffer from local ischemia and hypoxia, due to reduced angiogenesis and high nutrient consumption rate(Carreau et al., 2011;Weis and Cheresh, 2011). Thus, understandably,chromatin condensation may occur there similarly as discovered in this study using a cell ischemic model. Pursuing investigations in this direction may help in better characterisation and understanding of a tumour development.For instance, it has been previously hypothesised that chronic hypoxia in tumour may lead to selection of cancer cells of stronger malignant phenotype (Carreau et al., 2011). Furthermore, ischemic tumour cells may be a subject to a local inflammationtriggering pro-angiogenesis signalling (reviewed extensively in(Weis and Cheresh, 2011)). Affecting potential chromatin condensation of these cancerous cells could result in an increased harshness of oxidative stress effects or would constitute an interesting approach to investigatedevelopment rate of new vessels, crucial for further cancer growth and metastasis.Moreover, it is known that chromatin compaction has a preventive role protecting from ionising radiation (Takata et al., 2013) and tumour hypoxia negatively impacts radiotherapy (Moeller et al., 2007). Thus, plausible to hypothesise that potential chromatin condensation in tumour suffering from ischemia could be targeted in order to optimise its radiation therapy.Consequently, we anticipate that hypothetical chromatin condensation in solid tumours,

even though not proven directly yet, may contribute to a better understanding of a cancer functioning and may constitute a promising aspectto further boostexistinganti-cancer therapies.

The role of ischemia in tumour functioning is one important aspect. On the other hand, knowing deleterious effect of IR event, one would wonder how an artificial ischemic treatment could be employed to treat a cancer. Indeed, it has been previously recommended that ischemic treatment of a tumourcan constitute a very promising approach when combined with high-glucose reperfusion (Duan and Yang, 2012). This way, the ischemic event followed by reperfusion would induce stark oxidative stress interfering with tumour viability (Duan and Yang, 2012). The effectiveness of such ischemia, and in particular subsequent reperfusion in tumour treatment, has already been successfully recognised in experimental settings mimicking an anti-cancer therapy proving a robust contribution of oxidative stress in tumour suppression(Parkins et al., 1995). Regulation of putative chromatin condensation discovered in this work may turn out to be helpful in further optimisation of this treatment methodology.

In light of our discoveries it is important to mind a potential chromatin condensation in these circumstances and its putative protective role against oxidative stress, anti-cancer drugs, or rapid metabolism triggering.One can imagine that starvation-induced condensed chromatin is better protected against reactive oxygen species (ROS) of relatively short lifetime or DNA-binding cancer drugs (e.g. daunomycin (Wójcik et al., 2013)). In support of this claim, as revealed in this study, the condensed chromatin is rather transcriptionally inactive, decreasing cell energy demand and metabolism while nutrients unavailable, consequently preventing from ineffective energy production via anaerobic respiration.

7.9 Potential experimental issues

One last question remains unanswered in this work: is the chromatin organisation affected in a living organism suffering from ischemia? This has not been successfully investigated due to particular technical difficulties of microscopic approaches adopted. Anyhow, there is a fundamental difference between tissue culture model and a living organism: in case of the first the oxygen level has been artificially decreased from its basal level in well oxygenated culture mediumin flat culture plate to 1% but in reality full oxygenation in tissue is not realistic and spansrather between 4 - 8% only(Carreau et al., 2011). This means that the severity and abruptness of ischemia-induced changes in a cardiac muscle might be different than in thecell culture model used in this work. In turn, oxygenation levels in tumours may be even 10x lower than in healthy tissue. These values amount to 160 mmHg in the air, 100 mmHg in arterial blood, 29 mmHg in the healthy muscle and down to <2.5 – 13 mmHg in tumour (Carreau et al., 2011) meaning that oxygen level may drop in affected tissue as low as 0.2%. Likely similar values can be expected in metabolically active restless myocardium subjected to an artery occlusion. Importantly, it is interesting to know if chromatin condensation is e.g. proportional to decreased oxygen and nutrient concentration levels (ischemia severity) or chromatin condensation proceeds in a binary manner i.e. is triggered once total ATP pool is fully depleted. Future studies targeting different ischemic preparation protocols should be performed in this direction to broaden our understanding on how chromatin undergoes a regulation in the “passive” mode put forward in this work.

8. Conclusions

- Labelling constitutes currently one of the major obstacles preventing from real super-resolution fluorescent microscopy. In particular, chromatin labelling for super-resolution studies of eukaryotic cell nuclei necessitates an extreme care and existing methods suffer from major limitations

- Single molecule localisation microscopy of the chromatin in cell nuclei of mammals and mice using directly binding DNA dyes is feasible and was realised via:

  - Photoconversion of DNA-bound benzimidazole and VybrantViolet dyes enabling a structural resolution < 100 nm.

  - Transient fluorescence emission fromDNA-binding probes in a presence of nuclear DNA undergoing structure fluctuations in decreased pH. This method is further termed *DNA structure fluctuation assisted binding activated localisation microscopy* (*f*BALM) and constitutes a methodological advancement of previously existing BALM. This involved unravelling the mechanism of action and helped to extend application range to eukaryotic cell nuclei. *f*BALM yielded a structural resolution of approx. 50 nm.

- Super-resolution microscopy study presented in this work suggests a domain-like, hierarchical organisation of chromatin and in line with active-/inactive- nuclear compartment model, confirms existence of DNA-depleted regions in eukaryotic cell nuclei.

- Novel super-resolution methodologies developed in this work reveal so far unknown chromatin compaction induced by an ischemic treatment.

- The process of chromatin condensationprovoked by ischemia potentially depends on poly(cationic) compounds naturally associated with ATP. Upon ATP depletion in prolonged ischemia, they likely relocate and bind to negatively charged nuclear DNA inducing chromatin condensation.

- Dynamics of chromatin compaction and its decompaction could be targeted in order to neutralise deleterious effects of ischemia-reperfusion in such diseasesas cerebral stroke and myocardial infarction. This could potentially be realised via poly(cation) scavenger administration or interference with their synthesis.

- We recognise this so far unreported chromatin condensation upon ischemic treatment as relevant to other eventsinvolving ischemia just ascerebral stroke, tumour development,tumour angiogenesis and metastasis.

9. References

Abbe, E., 1873. Beiträge zur Theorie des Mikroskops und der mikroskopischen Wahrnehmung.

Alonso, A., Almendral, M.J., Curto, Y., Criado, J.J., Rodriguez, E., Manzano, J.L., 2006. Determination of the DNA-binding characteristics of ethidium bromide, proflavine, and cisplatin by flow injection analysis: Usefulness in studies on antitumor drugs. Anal. Biochem. 355, 157–164. doi:10.1016/j.ab.2006.06.004

Baddeley, D., Cannell, M.B., Soeller, C., 2010. Visualization of localization microscopy data. Microsc. Microanal. 16, 64–72. doi:10.1017/S143192760999122X

Bancaud, A., Huet, S., Daigle, N., Mozziconacci, J., Beaudouin, J., Ellenberg, J., 2009. Molecular crowding affects diffusion and binding of nuclear proteins in heterochromatin and reveals the fractal organization of chromatin. EMBO J. 28, 3785–98. doi:10.1038/emboj.2009.340

Banterle, N., Bui, K.H., Lemke, E.A., Beck, M., 2013. Fourier ring correlation as a resolution criterion for super-resolution microscopy. J. Struct. Biol. 183, 363–7. doi:10.1016/j.jsb.2013.05.004

Baum, M., Erdel, F., Wachsmuth, M., Rippe, K., 2014. Retrieving the intracellular topology from multi-scale protein mobility mapping in living cells. Nat. Commun. 5, 4494. doi:10.1038/ncomms5494

Benke, A., Manley, S., 2012. Live-Cell dSTORM of Cellular DNA Based on Direct DNA Labeling. ChemBioChem 13, 298–301. doi:10.1002/cbic.201100679

Bentzon, J.F., Otsuka, F., Virmani, R., Falk, E., 2014. Mechanisms of plaque formation and rupture. Circ. Res. 114, 1852–1866. doi:10.1161/CIRCRESAHA.114.302721

Benvin, A.L., Creeger, Y., Fisher, G.W., Ballou, B., Alan, S., Armitage, B. a, 2008. NIH Public Access 129, 2025–2034. doi:10.1021/ja066354t.Fluorescent

Bernas, T., Zarebski, M., Cook, P.R., Dobrucki, J.W., 2004. Minimizing photobleaching during confocal microscopy of fluorescent probes bound to chromatin: role of anoxia and photon flux. J. Microsc. 215, 281–96. doi:10.1111/j.0022-2720.2004.01377.x

Betzig, E., Patterson, G.H., Sougrat, R., Lindwasser, O.W., Olenych, S., Bonifacino, J.S., Davidson, M.W., Lippincott-Schwartz, J., Hess, H.F., 2006. Imaging intracellular fluorescent proteins at nanometer resolution. Science 313, 1642–5. doi:10.1126/science.1127344

Boettiger, A.N., Bintu, B., Moffitt, J.R., Wang, S., Beliveau, B.J., Fudenberg, G., Imakaev, M., Mirny, L.A., Wu, C., Zhuang, X., 2016. Chromatin Folding for Different Epigenetic States. Nature 1–15. doi:10.1038/nature16496

Bornfleth H., Satzler K., Eils R., Cremer C., 1998. High-precision distance measurements and volume-conserving segmentation of objects near and below the resolution limit in three-dimensional confocal fluorescence microscopy. J. Microsc. 189, 118–136. doi:10.1046/j.1365-2818.1998.00276.x

Boyle, A.P., Davis, S., Shulha, H.P., Meltzer, P., Margulies, E.H., Weng, Z., Furey, T.S., Crawford, G.E., 2008. High-Resolution Mapping and Characterization of Open Chromatin across the Genome. Cell 132, 311–322. doi:10.1016/j.cell.2007.12.014

Brown, D.T., Izard, T., Misteli, T., 2006. Mapping the interaction surface of linker histone H1(0) with the nucleosome of native chromatin in vivo. Nat. Struct. Mol. Biol. 13, 250–255. doi:10.1038/nsmb1050

Burgert, A., Letschert, S., Doose, S., Sauer, M., 2015. Artifacts in single-molecule localization microscopy. Histochem. Cell Biol. 144, 123–31. doi:10.1007/s00418-015-1340-4

Burgess, R.C., Burman, B., Kruhlak, M.J., Misteli, T., 2014. Activation of DNA Damage Response Signaling by Condensed Chromatin. Cell Rep. 9, 1703–1718. doi:10.1016/j.celrep.2014.10.060

Burke, B., Stewart, C.L., 2013. The nuclear lamins: flexibility in function. Nat Rev Mol Cell Biol 14, 13–24.

Carreau, A., Hafny-Rahbi, B. El, Matejuk, A., Grillon, C., Kieda, C., 2011. Why is the partial oxygen pressure of human tissues a crucial parameter? Small molecules and hypoxia. J. Cell. Mol. Med. 15, 1239–1253. doi:10.1111/j.1582-4934.2011.01258.x

Chen, H., Yan, Y., Davidson, T.L., Shinkai, Y., Costa, M., 2006. Hypoxic stress induces dimethylated histone H3 lysine 9 through histone methyltransferase G9a in mammalian cells. Cancer Res. 66, 9009–16. doi:10.1158/0008-5472.CAN-06-0101

Chen, R., Kang, R., Fan, X.-G., Tang, D., 2014. Release and activity of histone in diseases. Cell Death Dis. 5, e1370. doi:10.1038/cddis.2014.337

Chen, Y.-T., Zang, X.-F., Pan, J., Zhu, X.-L., Chen, F., Chen, Z.-B., Xu, Y., 2012. Expression patterns of histone deacetylases in experimental stroke and potential targets for neuroprotection. Clin. Exp. Pharmacol. Physiol. 39, 751–8. doi:10.1111/j.1440-1681.2012.05729.x

Chouchani, E.T., Pell, V.R., Gaude, E., Aksentijević, D., Sundier, S.Y., Robb, E.L., Logan, A., Nadtochiy, S.M., Ord, E.N.J., Smith, A.C., Eyassu, F., Shirley, R., Hu, C., Dare, A.J., James, A.M., Rogatti, S., Hartley, R.C., Eaton, S., Costa, A.S.H., Brookes, P.S., Davidson, S.M., Duchen, M.R., Saeb-Parsy, K., Shattock, M.J., Robinson, A.J., Work, L.M., Frezza, C., Krieg, T., Murphy, M.P., 2014. Ischaemic accumulation of succinate controls reperfusion injury through mitochondrial ROS. Nature 515, 431–435. doi:10.1038/nature13909

Claycomb, W.C., Lanson, N.A., Stallworth, B.S., Egeland, D.B., Delcarpio, J.B., Bahinski, A., Izzo, N.J., 1998. HL-1 cells: a cardiac muscle cell line that contracts and retains phenotypic characteristics of the adult cardiomyocyte. Proc. Natl. Acad. Sci. U. S. A. 95, 2979–2984. doi:10.1073/pnas.95.6.2979

Corona, D.F. V, Siriaco, G., Armstrong, J.A., Snarskaya, N., McClymont, S.A., Scott, M.P., Tamkun, J.W., 2007. ISWI Regulates Higher-Order Chromatin Structure and Histone H1 Assembly In Vivo. PLoS Biol 5, e232.

Cosa, G., Focsaneanu, K.S., McLean, J.R., McNamee, J.P., Scaiano, J.C., 2001. Photophysical properties of fluorescent DNA-dyes bound to single- and double-stranded DNA in aqueous buffered solution. Photochem. Photobiol. 73, 585–99.

Courtois, Y., Fromageot, P., Guschlbauer, W., 1968. Protonated polynucleotide structures. 3. An optical rotatory dispersion study of the protonation of DNA. Eur. J. Biochem. 6, 493–501.

Cremer, C., Kaufmann, R., Gunkel, M., Pres, S., Weiland, Y., Müller, P., Ruckelshausen, T., Lemmer, P., Geiger, F., Degenhard, S., Wege, C., Lemmermann, N. a W., Holtappels, R., Strickfaden, H., Hausmann, M., 2011. Superresolution imaging of biological nanostructures by spectral precision distance microscopy. Biotechnol. J. 6, 1037–51. doi:10.1002/biot.201100031

Cremer, C., Masters, B.R., 2013. Resolution enhancement techniques in microscopy. Eur. Phys. J. H 38, 281–344. doi:10.1140/epjh/e2012-20060-1

Cremer, T., Cremer, C., 2001. Chromosome territories, nuclear architecture and gene regulation in mammalian cells. Nat. Rev. Genet. 2, 292–301. doi:10.1038/35066075

Cremer, T., Cremer, M., Hübner, B., Strickfaden, H., Smeets, D., Popken, J., Sterr, M., Markaki, Y., Rippe, K., Cremer, C., 2015. The 4D nucleome: Evidence for a dynamic nuclear landscape based on co-aligned active and inactive nuclear compartments. FEBS Lett. 589, 2931–2943. doi:10.1016/j.febslet.2015.05.037

Cullis, P.M., Wolfenden, R., Cousens, L.S., Alberts, B.M., 1982. Inhibition of histone acetylation by N-[2-(S-coenzyme A)acetyl] spermidine amide, a multisubstrate analog. J. Biol. Chem. 257, 12165–12169.

Dempsey, G.T., Bates, M., Kowtoniuk, W.E., Liu, D.R., Tsien, R.Y., Zhuang, X., 2009. Photoswitching mechanism of cyanine dyes. J. Am. Chem. Soc. 131, 18192–3. doi:10.1021/ja904588g

Deschout, H., Cella Zanacchi, F., Mlodzianoski, M., Diaspro, A., Bewersdorf, J., Hess, S.T., Braeckmans, K., 2014. Precisely and accurately localizing single emitters in fluorescence microscopy. Nat. Methods 11, 253–66. doi:10.1038/nmeth.2843

Dixon, J.R., Selvaraj, S., Yue, F., Kim, A., Li, Y., Shen, Y., Hu, M., Liu, J.S., Ren, B., 2012. Topological domains in mammalian genomes identified by analysis of chromatin interactions. Nature 485, 376–380. doi:10.1038/nature11082

Dragan, A.I., Casas-Finet, J.R., Bishop, E.S., Strouse, R.J., Schenerman, M.A., Geddes, C.D., 2010. Characterization of PicoGreen interaction with dsDNA and the origin of its fluorescence enhancement upon binding. Biophys. J. 99, 3010–3019. doi:10.1016/j.bpj.2010.09.012

Dragan, A.I., Pavlovic, R., McGivney, J.B., Casas-Finet, J.R., Bishop, E.S., Strouse, R.J., Schenerman, M.A., Geddes, C.D., 2012. SYBR Green I: Fluorescence properties and interaction with DNA. J. Fluoresc. 22, 1189–1199. doi:10.1007/s10895-012-1059-8

Drobyshev, A.L., Zasedatelev, A.S., Yershov, G.M., Mirzabekov, A.D., 1999. Massive parallel analysis of DNA-Hoechst 33258 binding specificity with a generic oligodeoxyribonucleotide microchip. Nucleic Acids Res. 27, 4100–4105. doi:10.1093/nar/27.20.4100

Duan, Q., Yang, T., 2012. Ischaemia reperfusion may be a new approach in cancer interventional therapy. J. Med. Hypotheses Ideas 6, 50–52. doi:10.1016/j.jmhi.2012.03.003

Edelmann, P., Esa, A., Bomfleth, H., Heintzmann, R., Hausmann, M., Cremer, C., 1998. Correlation of chromatic shifts and focal depth in Spectral Precision Distance Microscopy measured by Micro Axial Tomography., in: Conference on Optical Biopsies and Microscopic Techniques III. Stockholm, pp. 89–95.

Fabre, P.J., Benke, A., Joye, E., Nguyen Huynh, T.H., Manley, S., Duboule, D., 2015. Nanoscale spatial organization of the HoxD gene cluster in distinct transcriptional states. Proc. Natl. Acad. Sci. U. S. A. 112, 13964–9. doi:10.1073/pnas.1517972112

Flors, C., 2011. DNA and chromatin imaging with super-resolution fluorescence microscopy based on single-molecule localization. Biopolymers 95, 290–7. doi:10.1002/bip.21574

Flors, C., 2010. Photoswitching of monomeric and dimeric DNA-intercalating cyanine dyes for super-resolution microscopy applications. Photochem. Photobiol. Sci. 9, 643–8. doi:10.1039/b9pp00119k

Flors, C., Ravarani, C.N.J., Dryden, D.T.F., 2009. Super-resolution imaging of DNA labelled with intercalating dyes. Chemphyschem 10, 2201–4. doi:10.1002/cphc.200900384

Fölling, J., Bossi, M., Bock, H., Medda, R., Wurm, C.A., Hein, B., Jakobs, S., Eggeling, C., Hell, S.W., 2008. Fluorescence nanoscopy by ground-state depletion and single-molecule return 5, 943–945. doi:10.1038/NMETH.1257

Fraser, J., Ferrai, C., Chiariello, A.M., Schueler, M., Rito, T., Laudanno, G., Barbieri, M., Moore, B.L., Kraemer, D.C., Aitken, S., Xie, S.Q., Morris, K.J., Itoh, M., Kawaji, H., Jaeger, I., Hayashizaki, Y., Carninci, P., Forrest, A.R., Dostie, J., Pombo, A., Nicodemi, M., 2015. Hierarchical folding and reorganization of chromosomes are linked to transcriptional changes in cellular differentiation. Mol Syst Biol 11, 1–14. doi:10.15252/msb

Fudenberg, G., Imakaev, M., Lu, C., Goloborodko, A., Abdennur, N., Mirny, L.A., 2016. Formation of Chromosomal Domains by Loop Extrusion. Cell Rep. 15, 2038–49. doi:10.1016/j.celrep.2016.04.085

Fullwood, M.J., Ruan, Y., 2009. ChIP-based methods for the identification of long-range chromatin interactions. J. Cell. Biochem. 107, 30–39. doi:10.1002/jcb.22116

Gao, J., Yang, X., Djekidel, M.N., Wang, Y., Xi, P., Zhang, M.Q., 2016. Developing bioimaging and quantitative methods to study 3D genome. Quant. Biol. 4, 129–147. doi:10.1007/s40484-016-0065-2

Gavrilov, A.A., Shevelyov, Y.Y., Ulianov, S. V., Khrameeva, E.E., Kos, P., Chertovich, A., Razin, S. V., 2016. Unraveling the mechanisms of chromatin fibril packaging. Nucleus 7, 319–24. doi:10.1080/19491034.2016.1190896

Geddes, C.D., Lakowicz, J.R., 2002. Metal-Enhanced Fluorescence. J. Fluoresc. 12, 121–129. doi:10.1023/A:1016875709579

Geiger, S., Holdenrieder, S., Stieber, P., Hamann, G.F., Bruening, R., Ma, J., Nagel, D., Seidel, D., 2006. Nucleosomes in serum of patients with early cerebral stroke. Cerebrovasc. Dis. 21, 32–37. doi:10.1159/000089591

Glazer, A.N., Rye, H.S., 1992. Stable dye-DNA intercalation complexes as reagents for high-sensitivity fluorescence detection. Nature 359, 859–61. doi:10.1038/359859a0

Görisch, S.M., Wachsmuth, M., Tóth, K.F., Lichter, P., Rippe, K., 2005. Histone acetylation increases chromatin accessibility. J. Cell Sci. 118, 5825–5834. doi:10.1242/jcs.02689

Granger, A., Abdullah, I., Huebner, F., Stout, A., Wang, T., Huebner, T., Epstein, J. a, Gruber, P.J., 2008. Histone deacetylase inhibition reduces myocardial ischemia-reperfusion injury in mice. FASEB J. 22, 3549–60. doi:10.1096/fj.08-108548

Gruell, F., Kirchgessner, M., Kaufmann, R., Hausmann, M., Kebschull, U., 2011. Accelerating Image Analysis for Localization Microscopy with FPGAs, in: 2011 21st International Conference on Field Programmable Logic and Applications. IEEE, pp. 1–5. doi:10.1109/FPL.2011.11

Günther, K., Mertig, M., Seidel, R., 2010. Mechanical and structural properties of YOYO-1 complexed DNA. Nucleic Acids Res. 38, 6526–6532. doi:10.1093/nar/gkq434

Gustafsson, M.G.L., 2000. Surpassing the lateral resolution limit by a factor of two using structured illumination microscopy. J. Microsc. 198, 82–87. doi:10.1046/j.1365-2818.2000.00710.x

Ha, H.C., Sirisoma, N.S., Kuppusamy, P., Zweier, J.L., Woster, P.M., Casero, R.A.J., 1998. The natural polyamine spermine functions directly as a free radical scavenger. Proc. Natl. Acad. Sci. U. S. A. 95, 11140–11145.

Hancock, R., Jeon, K.W., 2014. Preface, in: Biology, R.H. and K.W.J.B.T.-I.R. of C. and M. (Ed.), New Models of the Cell Nucleus: Crowding, Entropic Forces, Phase Separation, and Fractals. Academic Press, p. xiii. doi:http://dx.doi.org/10.1016/B978-0-12-800046-5.10000-1

Hausenloy, D., Yellon, D., 2013. Myocardial ischemia-reperfusion injury: a neglected therapeutic target. J Clin Invest 123, 92–100. doi:10.1172/JCI62874.92

Heilemann, M., Margeat, E., Kasper, R., Sauer, M., Tinnefeld, P., 2005. Carbocyanine dyes as efficient reversible single-molecule optical switch. J. Am. Chem. Soc. 127, 3801–3806. doi:10.1021/ja044686x

Heilemann, M., van de Linde, S., Schüttpelz, M., Kasper, R., Seefeldt, B., Mukherjee, A., Tinnefeld, P., Sauer, M., 2008. Subdiffraction-resolution fluorescence imaging with conventional fluorescent probes. Angew. Chem. Int. Ed. Engl. 47, 6172–6. doi:10.1002/anie.200802376

Heintzmann, R., Cremer, C.G., 1999. Laterally modulated excitation microscopy: improvement of resolution by using a diffraction grating. pp. 185–196.

Heisenberg, W., 1927. Über den anschaulichen Inhalt der quantentheoretischen Kinematik und Mechanik. Zeitschrift für Phys. 43, 172–198. doi:10.1007/BF01397280

Hell, S.W., Wichmann, J., 1994. Breaking the diffraction resolution limit by stimulated emission: stimulated-emission-depletion fluorescence microscopy. Opt. Lett. 19, 780–782.

Hermann, P., Fredericq, E., 1977. The role of the AT pairs in the acid denaturation of DNA. Nucleic Acids Res. 4, 2939–2947. doi:10.1093/nar/4.8.2939

Hess, S.T., Girirajan, T.P.K., Mason, M.D., 2006. Ultra-high resolution imaging by fluorescence photoactivation localization microscopy. Biophys. J. 91, 4258–72. doi:10.1529/biophysj.106.091116

Huang, B., Wang, W., Bates, M., Zhuang, X., 2008. Three-dimensional super-resolution imaging by stochastic optical reconstruction microscopy. Science 319, 810–3. doi:10.1126/science.1153529

Hübner, B., Lomiento, M., Mammoli, F., Illner, D., Markaki, Y., Ferrari, S., Cremer, M., Cremer, T., 2015. Remodeling of nuclear landscapes during human myelopoietic cell differentiation maintains co-aligned active and inactive nuclear compartments. Epigenetics Chromatin 8, 47. doi:10.1186/s13072-015-

0038-0

Irianto, J., Lee, D.A., Knight, M.M., 2014. Quantification of chromatin condensation level by image processing. Med. Eng. Phys. 36, 412–417. doi:10.1016/j.medengphy.2013.09.006

Irianto, J., Swift, J., Martins, R.P., McPhail, G.D., Knight, M.M., Discher, D.E., Lee, D.A., 2013. Osmotic challenge drives rapid and reversible chromatin condensation in chondrocytes. Biophys. J. 104, 759–769. doi:10.1016/j.bpj.2013.01.006

Jiang, C., Pugh, B.F., 2009. Nucleosome positioning and gene regulation: advances through genomics. Nat. Rev. Genet. 10, 161–72. doi:10.1038/nrg2522

Jin, R., Yang, G., Li, G., 2010. Inflammatory mechanisms in ischemic stroke: role of inflammatory cells. J. Leukoc. Biol. 87, 779–789. doi:10.1189/jlb.1109766

Joseph, M.J., Taylor, J.C., McGown, L.B., Pitner, J.B., Linn, C.P., 1998. Spectroscopic studies of YO and YOYO fluorescent dyes in a thrombin-binding DNA ligand. Biospectroscopy 2, 173–183. doi:10.1002/(SICI)1520-6343(1996)2:3<173::AID-BSPY4>3.0.CO;2-9

Kaplan, C., Ewers, H., 2015. Optimized sample preparation for single-molecule localization-based superresolution microscopy in yeast. Nat. Protoc. 10, 1007–21. doi:10.1038/nprot.2015.060

Karmodiya, K., Krebs, A.R., Oulad-Abdelghani, M., Kimura, H., Tora, L., 2012. H3K9 and H3K14 acetylation co-occur at many gene regulatory elements, while H3K14ac marks a subset of inactive inducible promoters in mouse embryonic stem cells. BMC Genomics 13, 1–18. doi:10.1186/1471-2164-13-424

Klehs, K., Spahn, C., Endesfelder, U., Lee, S.F., Fuerstenberg, A., Heilemann, M., 2014. Increasing the brightness of cyanine fluorophores for single-molecule and superresolution imaging. ChemPhysChem 15, 637–641. doi:10.1002/cphc.201300874

Kundukad, B., Yan, J., Doyle, P.S., 2014. Effect of YOYO-1 on the mechanical properties of DNA. Soft Matter 9721–9728. doi:10.1039/c4sm02025a

Lakowicz, J.R., 2006. Principles of Fluorescence Spectroscopy, Principles of fluorescence spectroscopy, Springer, New York, USA, 3rd edn, 2006. Springer US, Boston, MA. doi:10.1007/978-0-387-46312-4

Legant, W.R., Shao, L., Grimm, J.B., Brown, T.A., Milkie, D.E., Avants, B.B., Lavis, L.D., Betzig, E., 2016. High-density three-dimensional localization microscopy across large volumes. Nat. Methods 1–9. doi:10.1038/nmeth.3797

Lemasters, J.J., Bond, J.M., Chacon, E., Harper, I.S., Kaplan, S.H., Ohata, H., Trollinger, D.R., Herman, B., Cascio, W.E., 1996. The pH paradox in ischemia-reperfusion injury to cardiac myocytes. EXS 76, 99–114.

Lerman, L.S., 1961. Structural considerations in the interaction of DNA and acridines. J. Mol. Biol. 3, 18–30.

Liu, X., Diao, H., Nishi, N., 2008. Applied chemistry of natural DNA. Chem. Soc. Rev. 37, 2745–2757. doi:10.1039/b801433g

Llères, D., James, J., Swift, S., Norman, D.G., Lamond, A.I., 2009. Quantitative analysis of chromatin compaction in living cells using FLIM-FRET. J. Cell Biol. 187, 481–96. doi:10.1083/jcb.200907029

Lukinavičius, G., Blaukopf, C., Pershagen, E., Schena, A., Reymond, L., Derivery, E., Gonzalez-Gaitan, M., D'Este, E., Hell, S.W., Gerlich, D.W., Johnsson, K., 2015. SiR-Hoechst is a far-red DNA stain for live-cell nanoscopy. Nat. Commun. 6, 8497. doi:10.1038/ncomms9497

Ma, Y., Kanakousaki, K., Buttitta, L., 2015. How the cell cycle impacts chromatin architecture and influences cell fate. Front. Genet. 5, 1–18. doi:10.3389/fgene.2015.00019

Maeshima, K., Hihara, S., Eltsov, M., 2010. Chromatin structure: Does the 30-nm fibre exist in vivo? Curr. Opin. Cell Biol. 22, 291–297. doi:10.1016/j.ceb.2010.03.001

Manzini, G., Xodo, L., Barcellona, M.L., Quadrifoglio, F., 1985. Interaction of DAPI with double-stranded ribonucleic acids. Nucleic Acids Res. 13, 8955–8967. doi:10.1093/nar/13.24.8955

Markaki, Y., Gunkel, M., Schermelleh, L., Beichmanis, S., Neumann, J., Heidemann, M., Leonhardt, H., Eick, D., Cremer, C., Cremer, T., 2010. Functional nuclear organization of transcription and DNA replication: a topographical marriage between chromatin domains and the interchromatin compartment. Cold Spring Harb. Symp. Quant. Biol. 75, 475–92. doi:10.1101/sqb.2010.75.042

Matthews, H.R., 1993. Polyamines, chromatin structure and transcription. Bioessays 15, 561–6. doi:10.1002/bies.950150811

Misteli, T., Gunjan, a, Hock, R., Bustin, M., Brown, D.T., 2000. Dynamic binding of histone H1 to chromatin in living cells. Nature 408, 877–881. doi:10.1038/35048610

Moeller, B.J., Richardson, R.A., Dewhirst, M.W., 2007. Hypoxia and radiotherapy: Opportunities for improved outcomes in cancer treatment. Cancer Metastasis Rev. 26, 241–248. doi:10.1007/s10555-007-9056-0

Montavon, T., Soshnikova, N., Mascrez, B., Joye, E., Thevenet, L., Splinter, E., de Laat, W., Spitz, F., Duboule, D., 2011. A regulatory archipelago controls Hox genes transcription in digits. Cell 147, 1132–45. doi:10.1016/j.cell.2011.10.023

Mortensen, K.I., Churchman, L.S., Spudich, J.A., Flyvbjerg, H., 2010. Optimized localization analysis for single-molecule tracking and super-resolution microscopy. Nat. Methods 7, 377–81. doi:10.1038/nmeth.1447

Murphy, E., Steenbergen, C., Levy, L.A., Raju, B., London, R.E., 1989. Cytosolic free magnesium levels in ischemic rat heart. J. Biol. Chem. 264, 5622–7.

Nieuwenhuizen, R.P.J., Lidke, K. a, Bates, M., Puig, D.L., Grünwald, D., Stallinga, S., Rieger, B., 2013. Measuring image resolution in optical nanoscopy. Nat. Methods 10, 557–62. doi:10.1038/nmeth.2448

Njoh, K.L., Patterson, L.H., Zloh, M., Wiltshire, M., Fisher, J., Chappell, S., Ameer-Beg, S., Bai, Y., Matthews, D., Errington, R.J., Smith, P.J., 2006. Spectral analysis of the DNA targeting bisalkylaminoanthraquinone DRAQ5 in intact living cells. Cytom. Part A 69, 805–814. doi:10.1002/cyto.a.20308

Nowotarski, S.L., Woster, P.M., Casero, R.A., 2013. Polyamines and cancer: implications for chemotherapy and chemoprevention. Expert Rev. Mol. Med. 15, e3. doi:10.1017/erm.2013.3

Olins, D.E., Olins, A.L., 2003. Chromatin history: our view from the bridge. Nat. Rev. Mol. Cell Biol. 4, 809–14. doi:10.1038/nrm1225

Olivier, N., Keller, D., Gönczy, P., Manley, S., 2013. Resolution doubling in 3D-STORM imaging through improved buffers. PLoS One 8, e69004. doi:10.1371/journal.pone.0069004

P. Thévenaz, U.E. Ruttimann, M.U., 1998. A Pyramid Approach to Subpixel Registration Based on Intensity. IEEE Trans. Image Process. 7, 27–41.

Parkins, C.S., Dennis, M.F., Stratford, M.R., Hill, S. a, Chaplin, D.J., 1995. Ischemia reperfusion injury in tumors: the role of oxygen radicals and nitric oxide. Cancer Res. 55, 6026–9.

Patterson, G.H., Lippincott-Schwartz, J., 2002. A photoactivatable GFP for selective photolabeling of proteins and cells. Science 297, 1873–7. doi:10.1126/science.1074952

Pederson, T., 2014. Chapter One - The Nuclear Physique, in: Biology, R.H. and K.W.J.B.T.-I.R. of C. and M. (Ed.), New Models of the Cell Nucleus: Crowding, Entropic Forces, Phase Separation, and Fractals. Academic Press, pp. 1–13. doi:http://dx.doi.org/10.1016/B978-0-12-800046-5.00001-1

Persson, F., Bingen, P., Staudt, T., Engelhardt, J., Tegenfeldt, J.O., Hell, S.W., 2011. Fluorescence nanoscopy of single DNA molecules by using stimulated emission depletion (STED). Angew. Chem. Int. Ed. Engl. 50, 5581–3. doi:10.1002/anie.201100371

Pigram, W.J., Fuller, W., Davies, M.E., 1973. Unwinding the DNA helix by intercalation. J. Mol. Biol. 80, 361–365. doi:http://dx.doi.org/10.1016/0022-2836(73)90178-2

Pope, B.D., Ryba, T., Dileep, V., Yue, F., Wu, W., Denas, O., Vera, D.L., Wang, Y., Hansen, R.S., Canfield, T.K., Thurman, R.E., Cheng, Y., Gülsoy, G., Dennis, J.H., Snyder, M.P., Stamatoyannopoulos, J.A., Taylor, J., Hardison, R.C., Kahveci, T., Ren, B., Gilbert, D.M., 2014. Topologically associating domains are stable units of replication-timing regulation. Nature 515, 402–405. doi:10.1038/nature13986

Popken, J., Brero, A., Koehler, D., Schmid, V.J., Strauss, A., Wuensch, A., Guengoer, T., Graf, A., Krebs, S., Blum, H., Zakhartchenko, V., Wolf, E., Cremer, T., 2014. Reprogramming of fibroblast nuclei in cloned bovine embryos involves major structural remodeling with both striking similarities and differences to nuclear phenotypes of in vitro fertilized embryos. Nucleus 5, 555–89. doi:10.4161/19491034.2014.979712

Popken, J., Graf, A., Krebs, S., Blum, H., Schmid, V.J., Strauss, A., Guengoer, T., Zakhartchenko, V., Wolf, E., Cremer, T., 2015. Remodeling of the nuclear envelope and lamina during bovine preimplantation development and its functional implications. PLoS One 10, 1–22. doi:10.1371/journal.pone.0124619

Prakash, K., Fournier, D., Redl, S., Best, G., Borsos, M., Tiwari, V.K., Tachibana-Konwalski, K., Ketting, R.F., Parekh, S.H., Cremer, C., Birk, U.J., 2015. Superresolution imaging reveals structurally distinct periodic patterns of chromatin along pachytene chromosomes. Proc. Natl. Acad. Sci. U. S. A. 112, 14635–40. doi:10.1073/pnas.1516928112

Qian, T., Nieminen, A.L., Herman, B., Lemasters, J.J., 1997. Mitochondrial permeability transition in pH-dependent reperfusion injury to rat hepatocytes. Am. J. Physiol. 273, C1783–92.

Raffaghello, L., Lee, C., Safdie, F.M., Wei, M., Madia, F., Bianchi, G., Longo, V.D., 2008. Starvation-dependent differential stress resistance protects normal but not cancer cells against high-dose chemotherapy. Proc. Natl. Acad. Sci. 105, 8215–8220. doi:10.1073/pnas.0708100105

Rao, S.S.P., Huntley, M.H., Durand, N.C., Stamenova, E.K., Bochkov, I.D., Robinson, J.T., Sanborn, A.L., Machol, I., Omer, A.D., Lander, E.S., Aiden, E.L., 2014. A 3D map of the human genome at kilobase resolution reveals principles of chromatin looping. Cell 159, 1665–1680. doi:10.1016/j.cell.2014.11.021

Raul, F., 2007. Revival of 2-(difluoromethyl)ornithine (DFMO), an inhibitor of polyamine biosynthesis, as a cancer chemopreventive agent. Biochem. Soc. Trans. 35, 353–5. doi:10.1042/BST0350353

Reisner, W., Larsen, N.B., Silahtaroglu, A., Kristensen, A., Tommerup, N., Tegenfeldt, J.O., Flyvbjerg, H., 2010. Single-molecule denaturation mapping of DNA in nanofluidic channels. Proc. Natl. Acad. Sci. 107, 13294–13299. doi:10.1073/pnas.1007081107

Reymann, J., Baddeley, D., Gunkel, M., Lemmer, P., Stadter, W., Jegou, T., Rippe, K., Cremer, C., Birk, U., 2008. High-precision structural analysis of subnuclear complexes in fixed and live cells via spatially modulated illumination (SMI) microscopy. Chromosome Res. 16, 367–82. doi:10.1007/s10577-008-1238-2

Ricci, M.A., Manzo, C., García-Parajo, M.F., Lakadamyali, M., Cosma, M.P., 2015. Chromatin Fibers Are Formed by Heterogeneous Groups of Nucleosomes In Vivo. Cell 160, 1145–1158. doi:10.1016/j.cell.2015.01.054

Ries, J., Kaplan, C., Platonova, E., Eghlidi, H., Ewers, H., 2012. A simple, versatile method for GFP-based super-resolution microscopy via nanobodies. Nat. Methods 9, 582–584. doi:10.1038/nmeth.1991

Righolt, C.H., Guffei, A., Knecht, H., Young, I.T., Stallinga, S., van Vliet, L.J., Mai, S., 2014. Differences in nuclear DNA organization between lymphocytes, Hodgkin and Reed-Sternberg cells revealed by structured illumination microscopy. J. Cell. Biochem. 115, 1441–8. doi:10.1002/jcb.24800

Rust, M.J., Bates, M., Zhuang, X., 2006. Sub-diffraction-limit imaging by stochastic optical reconstruction microscopy (STORM). Nat. Methods 3, 793–5. doi:10.1038/nmeth929

Rye, H.S., Yue, S., Wemmer, D.E., Quesada, M. a, Haugland, R.P., Mathies, R. a, Giazer, A.N., 1992. bis-intercalating asymmetric cyanine dyes : properties and applications CO-. Nucleic Acids Res. 20, 2803–2812.

Sahl, S.J., Balzarotti, F., Keller-Findeisen, J., Leutenegger, M., Westphal, V., Egner, A., Lavoie-Cardinal, F., Chmyrov, A., Grotjohann, T., Jakobs, S., 2016. Comment on "Extended-resolution structured illumination imaging of endocytic and cytoskeletal dynamics." Science (80-.). 352, 527.

Sari, N., Antepli, E., Nartop, D., Yetim, N.K., 2012. Polystyrene Attached Pt(IV)–Azomethine, Synthesis and Immobilization of Glucose Oxidase Enzyme. Int. J. Mol. Sci. 13, 11870–11880. doi:10.3390/ijms130911870

Sauer, M., Hofkens, J., Enderlein, J., 2011. Handbook of Fluorescence Spectroscopy and Imaging, Handbook of Fluorescence Spectroscopy and Imaging. Wiley-VCH Verlag GmbH & Co. KGaA, Weinheim, Germany. doi:10.1002/9783527633500

Schermelleh, L., Carlton, P.M., Haase, S., Shao, L., Winoto, L., Kner, P., Burke, B., Cardoso, M.C., Agard, D. a, Gustafsson, M.G.L., Leonhardt, H., Sedat, J.W., 2008. Subdiffraction multicolor imaging of the nuclear periphery with 3D structured illumination microscopy. Science 320, 1332–6. doi:10.1126/science.1156947

Schoen, I., Ries, J., Klotzsch, E., Ewers, H., Vogel, V., 2011. Binding-Activated Localization Microscopy of DNA Structures. Nano Lett. 11, 4008–4011. doi:10.1021/nl2025954

Schwab, R.A.V., Niedzwiedz, W., 2011. Visualization of DNA Replication in the Vertebrate Model System DT40 using the DNA Fiber Technique. J. Vis. Exp. e3255. doi:10.3791/3255

Schweizer, S., Meisel, A., Marschenz, S., 2013. Epigenetic mechanisms in cerebral ischemia. J. Cereb. Blood Flow Metab. 33, 1335–1346. doi:10.1038/jcbfm.2013.93

Semenza, G., 2009. Regulation of Oxygen Homeostasis by Hypoxia-Inducible Factor 1. Physiol 24, 97–106. doi:doi:10.1152/physiol.00045.2008

Sharonov, A., Hochstrasser, R.M., 2006. Wide-field subdiffraction imaging by accumulated binding of diffusing probes. Proc. Natl. Acad. Sci. U. S. A. 103, 18911–18916. doi:10.1073/pnas.0609643104

Shcherbakova, D.M., Sengupta, P., Lippincott-Schwartz, J., Verkhusha, V. V, 2014. Photocontrollable Fluorescent Proteins for Superresolution Imaging. Annu. Rev. Biophys. 43, 303–329. doi:10.1146/annurev-biophys-051013-022836

Shlyueva, D., Stampfel, G., Stark, A., 2014. Transcriptional enhancers: from properties to genome-wide predictions. Nat. Rev. Genet. 15, 272–86. doi:10.1038/nrg3682

Shmakova, A., Batie, M., Druker, J., Rocha, S., 2014. Chromatin and oxygen sensing in the context of JmjC histone demethylases. Biochem. J. 462, 385–395. doi:10.1042/BJ20140754

Sibarita, J., Heilemann, M., 2012. Targeting, resolving and quantifying cellular structures by single-molecule localization microscopy. EMBO Rep. 13, 1043–1045. doi:10.1038/embor.2012.177

Smirnov, I. V, Dimitrov, S.I., Makarov, V.L., 1988. NaCl-induced chromatin condensation. Application of static light scattering at 90 degrees and stopped flow technique. J. Biomol. Struct. Dyn. 5, 1127–1134. doi:10.1080/07391102.1988.10506453

Smith, P.J., Blunt, N., Wiltshire, M., Hoy, T., Teesdale-Spittle, P., Craven, M.R., Watson, J. V., Brad Amos, W., Errington, R.J., Patterson, L.H., 2000. Characteristics of a novel deep red/infrared fluorescent cell-permeant DNA probe, DRAQ5, in intact human cells analyzed by flow cytometry, confocal and multiphoton microscopy. Cytometry 40, 280–291. doi:10.1002/1097-0320(20000801)40:4<280::AID-CYTO4>3.0.CO;2-7

Sorokin, V.A., Gladchenko, G.O., Valeev, V.A., 1986. DNA protonation at low ionic strength of solution. Die Makromol. Chemie 187, 1053–1063. doi:10.1002/macp.1986.021870502

Steinberg, D., Glass, C.K., Witztum, J.L., 2008. Evidence mandating earlier and more aggressive treatment of hypercholesterolemia. Circulation 118, 672–677. doi:10.1161/CIRCULATIONAHA.107.753152

Swoboda, M., Henig, J., Cheng, H.M., Brugger, D., Haltrich, D., Plumeré, N., Schlierf, M., 2012. Enzymatic oxygen scavenging for photostability without ph drop in single-molecule experiments. ACS Nano 6, 6364–6369. doi:10.1021/nn301895c

Takata, H., Hanafusa, T., Mori, T., Shimura, M., Iida, Y., Ishikawa, K., Yoshikawa, K., Yoshikawa, Y., Maeshima, K., 2013. Chromatin Compaction Protects Genomic DNA from Radiation Damage. PLoS One 8, 1–11. doi:10.1371/journal.pone.0075622

Tang, Z., Luo, O.J., Li, X., Zheng, M., Zhu, J.J., Szalaj, P., Trzaskoma, P., Magalska, A., Wlodarczyk, J., Ruszczycki, B., Michalski, P., Piecuch, E., Wang, P., Wang, D., Tian, S.Z., Penrad-Mobayed, M., Sachs, L.M., Ruan, X., Wei, C.L., Liu, E.T., Wilczynski, G.M., Plewczynski, D., Li, G., Ruan, Y., 2015. CTCF-Mediated Human 3D Genome Architecture Reveals Chromatin Topology for Transcription. Cell 163, 1611–1627. doi:10.1016/j.cell.2015.11.024

Thompson, R.E., Larson, D.R., Webb, W.W., 2002. Precise nanometer localization analysis for individual fluorescent probes. Biophys. J. 82, 2775–83. doi:10.1016/S0006-3495(02)75618-X

Traganos, F., Darzynkiewicz, Z., Sharpless, T., Melamed, M.R., 1975. Denaturation of deoxyribonucleic acid in situ effect of formaldehyde. J. Histochem. Cytochem. 23, 431–8.

Trembecka-Lucas, D.O., Dobrucki, J.W., 2012. A heterochromatin protein 1 (HP1) dimer and a proliferating cell nuclear antigen (PCNA) protein interact in vivo and are parts of a multiprotein complex involved in DNA replication and DNA repair. Cell Cycle 11, 2170–5. doi:10.4161/cc.20673

Trembecka-Lucas, D.O., Szczurek, A.T., Dobrucki, J.W., 2013. Dynamics of the HP1β-PCNA-containing complexes in DNA replication and repair. Nucleus 4, 74–82. doi:10.4161/nucl.23683

van de Linde, S., Krstić, I., Prisner, T., Doose, S., Heilemann, M., Sauer, M., 2011. Photoinduced formation of reversible dye radicals and their impact on super-resolution imaging. Photochem. Photobiol. Sci. 10, 499–506. doi:10.1039/c0pp00317d

Vanhaecke, T., Papeleu, P., Elaut, G., Rogiers, V., 2004. Trichostatin A-like hydroxamate histone deacetylase inhibitors as therapeutic agents: toxicological point of view. Curr. Med. Chem. 11, 1629–43.

Vardevanyan, P.O., Antonyan, a P., Parsadanyan, M. a, Davtyan, H.G., Karapetyan, a T., 2003. The binding of ethidium bromide with DNA: interaction with single- and double-stranded structures. Exp. Mol. Med. 35, 527–533. doi:10.1038/emm.2003.68

Vaughan, J.C., Dempsey, G.T., Sun, E., Zhuang, X., 2013. Phosphine quenching of cyanine dyes as a versatile tool for fluorescence microscopy. J. Am. Chem. Soc. 135, 1197–200. doi:10.1021/ja3105279

Vigne, P., Frelin, C., 2008. The role of polyamines in protein-dependent hypoxic tolerance of Drosophila. BMC Physiol. 8, 22. doi:10.1186/1472-6793-8-22

Visvanathan, A., Ahmed, K., Even-Faitelson, L., Lleres, D., Bazett-Jones, D.P., Lamond, A.I., 2013. Modulation of Higher Order Chromatin Conformation in Mammalian Cell Nuclei Can Be Mediated by Polyamines and Divalent Cations. PLoS One 8. doi:10.1371/journal.pone.0067689

Vivar, R., Humeres, C., Varela, M., Ayala, P., Guzman, N., Olmedo, I., Catalan, M., Boza, P., Munoz, C., Diaz Araya, G., 2012. Cardiac fibroblast death by ischemia/reperfusion is partially inhibited by IGF-1 through both PI3K/Akt and MEK-ERK pathways. Exp. Mol. Pathol. 93, 1–7. doi:10.1016/j.yexmp.2012.01.010

Vogelsang, J., Kasper, R., Steinhauer, C., Person, B., Heilemann, M., Sauer, M., Tinnefeld, P., 2008. A reducing and oxidizing system minimizes photobleaching and blinking of fluorescent dyes. Angew. Chemie - Int. Ed. 47, 5465–5469. doi:10.1002/anie.200801518

Vogelsang, J., Steinhauer, C., Forthmann, C., Stein, I.H., Person-Skegro, B., Cordes, T., Tinnefeld, P., 2010.

Make them blink: probes for super-resolution microscopy. Chemphyschem 11, 2475–90. doi:10.1002/cphc.201000189

Wang, S., Su, J.-H., Beliveau, B.J., Bintu, B., Moffitt, J.R., Wu, C. -t., Zhuang, X., 2016. Spatial organization of chromatin domains and compartments in single chromosomes. Science (80-.). 353, 598–602. doi:10.1126/science.aaf8084

Watson, J.D., Crick, F.H.C., 1953. Molecular Structure of Nucleic Acids: A Structure for Deoxyribose Nucleic Acid. Nature 171, 737–738. doi:10.1038/171737a0

Webster, A.L.H., Yan, M.S.-C., Marsden, P.A., 2013. Epigenetics and cardiovascular disease. Can. J. Cardiol. 29, 46–57. doi:10.1016/j.cjca.2012.10.023

Weis, S.M., Cheresh, D.A., 2011. Tumor angiogenesis: molecular pathways and therapeutic targets. Nat. Med. 17, 1359–1370. doi:10.1038/nm.2537

Weisblum, B., Haenssler, E., 1974. Fluorometric properties of the bibenzimidazole derivative Hoechst 33258, a fluorescent probe specific for AT concentration in chromosomal DNA. Chromosoma 46, 255–60.

Wojcik, K., Dobrucki, J.W., 2008. Interaction of a DNA intercalator DRAQ5, and a minor groove binder SYTO17, with chromatin in live cells - influence on chromatin organization and histone-DNA interactions. Cytometry. A 73, 555–62. doi:10.1002/cyto.a.20573

Wójcik, K., Zarębski, M., Cossarizza, A., Dobrucki, J.W., 2013. Daunomycin, an antitumor DNA intercalator, influences histone-DNA interactions. Cancer Biol. Ther. 14, 823–32. doi:10.4161/cbt.25328

Woringer, M., Darzacq, X., Izeddin, I., 2014. Geometry of the nucleus: A perspective on gene expression regulation. Curr. Opin. Chem. Biol. 20, 112–119. doi:10.1016/j.cbpa.2014.05.009

Yan, X., Habbersett, R.C., Yoshida, T.M., Nolan, J.P., Jett, J.H., Marrone, B.L., 2005. Probing the kinetics of SYTOX Orange stain binding to double-stranded DNA with implications for DNA analysis. Anal. Chem. 77, 3554–3562. doi:10.1021/ac050306u

Yan, X.M., Habbersett, R.C., Cordek, J.M., Nolan, J.P., Yoshida, T.M., Jett, J.H., Marrone, B.L., 2000. Development of a mechanism-based, DNA staining protocol using SYTOX orange nucleic acid stain and DNA fragment sizing flow cytometry. Anal Biochem 286, 138–148. doi:DOI 10.1006/abio.2000.4789

Yellon, D.M., Hausenloy, D.J., 2007. Myocardial Reperfusion Injury. N. Engl. J. Med. 357, 1121–1135. doi:10.1056/NEJMra071667

Zessin, P.J.M., Finan, K., Heilemann, M., 2012. Super-resolution fluorescence imaging of chromosomal DNA. J. Struct. Biol. 177, 344–8. doi:10.1016/j.jsb.2011.12.015

Zhao, H., Halicka, H.D., Li, J., Biela, E., Berniak, K., Dobrucki, J., Darzynkiewicz, Z., 2013. DNA damage signaling, impairment of cell cycle progression, and apoptosis triggered by 5-ethynyl-2'-deoxyuridine incorporated into DNA. Cytometry. A 83, 979–88. doi:10.1002/cyto.a.22396

Zhao, Y.J., Xu, C.Q., Zhang, W.H., Zhang, L., Bian, S.L., Huang, Q., Sun, H.L., Li, Q.F., Zhang, Y. qiao, Tian, Y., Wang, R., Yang, B.F., Li, W.M., 2007. Role of polyamines in myocardial ischemia/reperfusion injury and their interactions with nitric oxide. Eur. J. Pharmacol. 562, 236–246. doi:10.1016/j.ejphar.2007.01.096

Zhao, Z.W., Roy, R., Gebhardt, J.C.M., Suter, D.M., Chapman, A.R., Xie, X.S., 2014. Spatial organization of RNA polymerase II inside a mammalian cell nucleus revealed by reflected light-sheet superresolution microscopy. Proc. Natl. Acad. Sci. U. S. A. 111, 681–6. doi:10.1073/pnas.1318496111

Zheng, Y., John, S., Pesavento, J.J., Schultz-Norton, J.R., Schiltz, R.L., Baek, S., Nardulli, A.M., Hager, G.L., Kelleher, N.L., Mizzen, C.A., 2010. Histone H1 phosphorylation is associated with transcription by RNA polymerases I and II. J. Cell Biol. 189, 407–415. doi:10.1083/jcb.201001148

Zimmer, C., Luck, G., Venner, H., Fric, J., 1968. Studies on the conformation of protonated DNA. Biopolymers 6, 563–574. doi:10.1002/bip.1968.360060410

Żurek-Biesiada, D., Kędracka-Krok, S., Dobrucki, J.W., 2013. UV-activated conversion of Hoechst 33258, DAPI, and Vybrant DyeCycle fluorescent dyes into blue-excited, green-emitting protonated forms. Cytometry. A 83, 441–51. doi:10.1002/cyto.a.22260

Żurek-Biesiada, D., Waligórski, P., Dobrucki, J.W., 2014. UV-induced Spectral Shift and Protonation of DNA Fluorescent Dye Hoechst 33258. J. Fluoresc. doi:10.1007/s10895-014-1468-y

10. Associated publications

In the following, the publications related to this work released between September 2013 and December 2016 (P1 – P6), accepted articles (P7),and submitted manuscripts (P8) are listed:

[P-8] [*submitted*] MM. Kordon, **AT Szczurek**, K Berniak, O Szelest, K Solarczyk, M Tworzydło, S Wachsmann-Hogiu, A Vaahtokari, C Cremer, JW Dobrucki: *A distinct PML-like nuclear body juxtapositions the DNA repair protein XRCC1 to sites of single-strand breaks in replication foci.*

[P-7] [*Accepted manuscript*] **AT Szczurek**, L Klewes, J Xing, A. Gourrame, J Dobrucki, S Mai, C Cremer: *Imaging chromatin with binding activated localisation microscopy using DNA structure fluctuations*. Nucleic Acids Research, December 2016

[P-6] **AT Szczurek**, J Xing, U Birk, C Cremer: *Single Molecule Localization Microscopy of Mammalian Cell Nuclei*, Frontiers in Genetics, vol. 7/114, June 2016, doi: 10.3389/fgene.2016.00114

[P-5] A Pierzyńska-Mach, **AT Szczurek**, F Cella Zanacchi, F Pennacchietti, J Drukała, A Diaspro, C Cremer, Z Darzynkiewicz, JW Dobrucki: *Subnuclear localization, rates and effectiveness of UVC-induced unscheduled DNA synthesis visualized by fluorescence widefield, confocal and super-resolution microscopy*. Cell cycle, 04/2016; 15(8):1156-1167. DOI:10.1080/15384101.2016.1158377

[P-4] D Żurek-Biesiada, **AT Szczurek**, K Prakash, G Best, GK Mohana, H-K Lee, J-Y Roignant, JW Dobrucki, Christoph Cremer, Udo Birk: *Quantitative Super-Resolution Localization microscopy of DNA in situ using Vybrant® DyeCycle™ Violet Fluorescent Probe*. Data in Brief 01/2016; 7. DOI:10.1016/j.dib.2016.01.041

[P-3] I Kirmes[+], **AT Szczurek**[+], K Prakash, I Charapitsa, C Heiser, M Musheev, F Schock, K Fornalczyk, D Ma, U Birk, C Cremer, G Reid: *A transient ischemic environment induces reversible compaction of chromatin*. Genome Biology 11/2015;DOI:10.1186/s13059-015-0802-2 ([+]equal contribution)

[P-2] D Żurek-Biesiada, **AT Szczurek**, K Prakash, GK Mohana, H-K Lee, J-Y Roignant, U Birk, JW Dobrucki, C Cremer: *Localization microscopy of DNA in situ using Vybrant(®) DyeCycle™ Violet fluorescent probe: A new approach to study nuclear nanostructure at single molecule resolution*. Experimental Cell Research 09/2015;DOI:10.1016/j.yexcr.2015.08.020

[P-1] **AT Szczurek**[+], K Prakash[+], H-K Lee[+], D Zurek-Biesiada, G Best, M Hagmann, JW Dobrucki, C Cremer, U Birk: *Single molecule localization microscopy of the distribution of chromatin using Hoechst and DAPI fluorescent probes*. Nucleus, 06/2014; 5(4). DOI:10.4161/nucl.29564 ([+]equal contribution)

11. Appendix I: abbreviations

2D – two dimensional
3D – three dimensional
A – adenine
AA – ascorbic acid
Alexa – commercial fluorescent probe
ANC – active nuclear compartment
ATP – adenosine triphosphate
a.u. – arbitrary units
BALM – binding activated localisation microsocpy
BME – β-mercapthoethanol
BrU – bromouridine
bp – basepair
BSA – bovine serum albumin
C – cytosine
CAT – catalase
CCD – charge coupled device
CDC – chromatin dense cluster
CHD – coronary heart disease
ChIA-PET – chromatin interaction analysis by pair-tag sequencing
ChIP-seq – chromatin immunoprecipitation DNA sequencing
CTCF – CCCTC-binding factor
Da – dalton
DAPI - 4',6-diamidyno-2-fenyloindol
DFMO – difluoromethylornithine
DMEM – Dulbecco's Modified Eagle's Medium
DNA – deoxyribonucleic acid
dSTORM – direct stochastic optical reconstruction microscopy
EDTA – ethylendiaminetetraacetic
EdU – 5-ethynyl-2'-deoxyuridine
FACS – fluorescence activated cell sorting
*f*BALM – DNA structure fluctuation assisted binding activated localisation microscopy
FBS – fetal bovine serum
FISH – fluorescence in situ hybridisation
FLIM – fluorescence lifetime imaging
FP – fluorescent protein
FRAP – fluorescence recovery after photobleaching
FRET – Foerster resonance energy transfer
g – gravitational acceleration
G – guanine
GFP – green fluorescent protein
GOX – glucose oxidase
GP – glucose pyranose
GSDIM – ground state depletion microscopy followed by individual molecule return
H1 – histone H1
H2A – histone H2A

H3 – histone H3
H4 – histone H4
HAT – histone acetyltransferase
HCl – hydrochloric acid
HEPES – 4-(2-hydroxyethyl)-1-piperazineethanesulfonic acid
HDAC – histone deacetylase
Hoechst – 4-[5-(4-methyl-1-piperazinyl)[2,5'-bi-1H-benzimidazol]-2'-yl]-, trihydrochloride
HOMO – highest occupied molecular orbital
INC – inactive nuclear compartment
IR – ischemia-reperfusion
LDL – low density lipoprotein
LUMO – lowest unoccupied molecular orbital
MEA – β-mercapthoethylamine, cysteamine
mCherry – monomeric Cherry, fluorescent protein
MLE – maximum likelihood estimation
MV – methyl viologen
NA – numerical aperture
nm – nanometre
NMR – nuclear magnetic resonance
ODC – ornithine decarboxylase
PA-FP – photoactivatable fluorescent protein
PAINT – point accumulation for imaging in nanoscale topography
PALM – photoactivated localisation microscopy
PBS – phosphate buffered saline
PicoGreen – commercial name for monomeric DNA dye
Pol II – RNA polymerase II
PSF – point spread function
ROI – region of interest
SIM – structured illumination microscopy
SMLM – single molecule localisation microscopy
SPDM – spectral precision distance microscopy
SPT – single particle tracking
STED – stimulated emission depletion microscopy
STORM – stochastic optical reconstruction microscopy
Redox – reduction-oxidation
RNA – ribonucleic acid
RT – room temperature
T – thymidine
TAD – topologically associated domain
TCEP – tris(2-carboxyethyl)phosphine
TOTO-1 – thiazole orange dimer
TSA – trichostatin A
TX – trolox
UT – untreated
YO-PRO-1 – oxazole yellow
YOYO-1 – {1,1'-(4,4,8,8-tetramethyl-4,8-diazaundecamethylene)bis[4-[(3-methylbenzo-1,3-oxazol-2-yl)methylidene]-l,4-dihydroquinolinium] tetraiodide}

12. Eidesstattliche Erklärung

Hiermit versichere ich, Aleksander Szczurek, geboren am 31.10.1989 in Krakau, die vorliegende Dissertation „*Single molecule localisation microscopy by photoconversion and dynamic labelling using DNA-binding dyes resolves chromatin compaction in model ischemia*“ selbstständig und ausschließlich unter Verwendung der angegebenen Quellen und Hilfsmittel verfasst zu haben.

Mainz, den 20. Dezember 2016

Aleksander Szczurek